CONFORMATIONAL STUDIES ON MUONIC FREE RADICALS.

Submitted to the University of Glasgow in partial fulfilment of the requirements for the degree of Doctor of Philosophy in the Faculty of Science.

by

Roderick Malcolm Macrae

Chemistry Department

February 1990

ProQuest LLC.
789 East Eisenhower Parkway
P.O. Box 1346
Ann Arbor, MI 48106 – 1346

To K.

ACKNOWLEDGEMENTS.

I wish to thank my supervisor, Dr Brian Webster, for his cheerful encouragement during the three years of this work and especially the months of writing, for his advice and guidance, and for at all times lighting for me the path where common sense lay.

I am in debt to Professor Hanns Fischer for making available to me the facilities of the University of Zürich and the Paul Scherrer Institute. For his help and advice during times spent in Switzerland I warmly thank Dr Emil Roduner. I am also grateful to Dr Ivan Reid, Dr Christopher Rhodes, and Dr Toshiyuki Azuma for their practical assistance during the experimental runs.

My thanks go to Dr Stephen Cox for enlightening scientific discussion and to Mr David Buttar for furnishing me with the results of his μSR experiments.

I would also like to thank Professor Laurence Barron, on whose laser printer this thesis was produced, and Mr Robert Munro, the departmental photographer, for his assistance in the creation of some of the diagrams.

My fondest thanks are due to my parents for their faith in me, and for a quarter century of encouragement and tolerance.

I would like to thank all my friends and colleagues for their forbearance with me through my moods and caprices over the last years.

Finally I thank the SERC for a studentship, and for the generous travel grants with which I was enabled to undertake work in Switzerland.

CONTENTS

"What do I know of man's destiny? I could tell you more about radishes."

Samuel Beckett

Prefatory Remarks.

The study by the technique of muon spin rotation spectroscopy of organic free radicals in which a hydrogen atom has been substituted by its short-lived light isotope muonium has now been under way for more than a decade, and many intriguing insights into radical structure and properties gained[1] . This thesis extends these enquiries into the domain of temperature and solvent dependence studies of α-muoxyalkyl radicals produced by muon irradiation of carbonyl compounds in the liquid phase. Parallel investigations of the conformations and properties of several α-hydroxyalkyl radicals using the methods of *ab initio* molecular quantum mechanics are described. A confluence of these twin streams is hoped for.

The first, introductory chapter describes in some detail the principles and tenets of the methods used. Properties of the muon are enumerated and compared with those of other fundamental particles in order to illustrate the unique features of μ^+ which make μSR possible. The theoretical and practical details of the general μSR experiment are discussed, noting the states of the muon implanted in condensed matter which are distinguishable by the technique, and with particular regard to the theory governing the observation of muonium-substituted radicals. A relationship is drawn between the dependence upon temperature of the isotropic β-hyperfine coupling constant measured by μSR spectroscopy and the internal dynamics of the free radical observed, concentrating primarily upon torsional motions. In this context the theory of rotational averaging is presented, by means of which potential barriers to internal rotation can be extracted from temperature-dependent μSR data. The domains of usefulness of *ab initio* quantum chemical techniques in calculating the structures and properties of organic radicals are commented upon.

The remainder of the thesis concerns the application of the ideas embodied in the introduction to various genera of free radical. Chapter two reviews the revealing study of the muonic isotopomers of the ethyl radical, and presents several SCF calculations which shed some light on the conformational properties of this relatively simple radical. In the first part of Chapter 3 past studies of α-hydroxyalkyl radicals by paramagnetic resonance spectroscopy are examined with a view towards understanding the gradual way in which their properties were revealed by techniques of increasing sophistication. In the latter section of the chapter a fairly comprehensive μSR study of the 2-muoxyprop-2-yl radical formed in pure propan-2-one and various binary aqueous solutions of propan-2-one is described. In the succeeding chapter further novel results on α-muoxyalkyl radicals are presented. The radicals are enumerated according to the substrates in which they are formed, namely 1,1,1-trifluoropropan-2-one, ethanal, 2,5-hexanedione, and *trans*-but-2-enal. Chapter 5 contains a set of *ab initio* quantum mechanical calculations upon several α-hydroxyalkyl and related radicals including the 2-hydroxyprop-2-yl radical and the hydroxyethyl radical. The effect of functional groups upon equilibrium conformation and spin density distribution is considered.

Further μSR studies not easily integrated into the body of the text are contained in an Appendix.

CHAPTER 1

Introduction.

"Through their whole logical apparatus the physical laws still speak of the objects of the world."

L. Wittgenstein

1.1 Towards Muon Chemistry.

1.1.1 Properties of the Muon.

The positive muon, μ^+, is a member of that category of fundamental particles called leptons, which also includes μ^-, the antiparticle of μ^+, together with electrons (e^+, e^-), the neutrinos corresponding to particles of both types (ν_e, $\bar{\nu}_e$, ν_μ, $\bar{\nu}_\mu$), and the tau-particles (τ^+, τ^-). Some of the physical properties of μ^+ are presented in **Table 1.1**, with the corresponding properties of p^+ and e^+ also displayed for the purpose of comparison.

Produced through the parity-violating weak pion decay process (1.1), μ^+ itself ends its short lifespan through the three-body decay mechanism described by equation (1.2) to generate a positron, an electron-neutrino and a muon-antineutrino.

$$\pi^+ \longrightarrow \mu^+ + \nu_\mu \qquad (1.1)$$

$$\mu^+ \longrightarrow e^+ + \nu_e + \bar{\nu}_\mu \qquad (1.2)$$

Because ν_μ is left-handed[3], having spin parallel to its momentum, the principle of angular momentum conservation requires that μ^+ be polarised in a left-handed sense also, considered in the rest frame of the pion, with helicity H=-1. The muon decay process is also spatially asymmetric, with the majority of positrons being emitted in a direction parallel to the μ^+ spin axis[4]. In principle these asymmetries allow the evolution with time of the muon spin direction to be monitored, and make possible a variety of spectroscopic methods.

Table 1.1 Selected physical properties of μ^+, p^+, and e^+ [(a)].

Property	μ^+	p^+	e^+
mass m/m_e	206.76865	1836.1515	1
charge	+1	+1	+1
spin/$\hbar$	1/2	1/2	1/2
magnetic moment:			
μ/JT^{-1}	4.490474×10^{-26}	1.410617×10^{-26}	9.284832×10^{-24}
μ/μ_p	3.1833	1	658.21
Nuclear, or Bohr			
magneton μ_n/JT^{-1}	4.485244×10^{-26}	5.050824×10^{-27}	9.274078×10^{-24}
g	2.002331848	5.585690	2.0023192
gyromagnetic			
ratio $\gamma_\mu/2\pi$ $MHzT^{-1}$	135.5374	42.5771	28024.71
lifetime τ/s	2.19714×10^{-6}	–	–

(a) Fundamental constants are taken from Cohen and Taylor[2].

1.1.2 Muon Beams and Muon Spectroscopy.

These forms of spectroscopy concern themselves with the fate of positive muons implanted in matter, usually in the condensed phases. They depend upon the availability of a beam of spin-polarised muons, so that on entry into the sample all muons have the same initial spin orientation. Such beams are generated by directing protons of energy several times higher than the pion rest mass (180MeV) into a target consisting of a light element such as Be or C, whereupon the resulting nuclear processes lead to multiple pion production. At this stage two options present themselves. In the first, low-energy π^+ which have come to rest in the vicinity of the primary production target are used. The helicity characteristics of the decay of stationary pions ensure that a beam created by collection of muons of a given momentum direction has a degree of spin polarisation near 100%. A beam of this kind is called a surface muon beam, and has the additional property of low muon momentum, leading to a very short range in matter. In the second option, pions of higher energy are collected using quadrupole magnets and decay in flight in a long superconducting solenoid, whereupon further dipole and quadrupole magnets train this diffuse muon source upon the sample target. In this instance muon spin polarisation can be chosen by selecting muon momentum using the final dipole magnet; in practice, since maximal polarisation is desired, selection is generally either of forward emitted ($\mathbf{p}_\mu \| \mathbf{p}_\pi$) or backward emitted ($\mathbf{p}_\mu$ and $\mathbf{p}_\pi$ antiparallel) muons. The attainable polarisation is reduced by limited momentum resolution in the beam line optics, together with a spread in beam angle around $\vartheta = 0^\circ$ (resulting in a projection factor of $\cos\vartheta$), to $P_\mu \approx 60$-80%. Muon beams are further distinguished in being either continuous (DC) or pulsed. The main proton accelerators around the world which are or have been associated

with muon spectroscopy are PSI (Switzerland, formerly known as SIN), TRIUMF (Canada), and CERN (France/Switzerland)of the former type, and LAMPF (USA), KEK/BOOM (Japan), and RAL (UK), of the latter.

The acronym μSR describes three distinct spectroscopic methods: muon spin rotation, muon spin relaxation, and muon spin resonance. In the first of these, the most commonly used μSR technique and that which will form the basis of the experimental observations contained in this thesis, a static magnetic field **B** is applied such that $\mathbf{B} \perp \mathbf{p}_\mu$ under the influence of which the muon spin vector precesses. In the relaxation experiment $\mathbf{B} \parallel \mathbf{p}_\mu$ and the relaxation with time of the muon spin is measured. In the third type of experiment a longitudinal field $\mathbf{B}_o$ is again used, while a radiofrequency field $\mathbf{B}_1$ is simultaneously applied in the transverse direction. Positron counters are placed in the forward (F) and backward (B) positions, and the variation of the time-integrated difference $N_F - N_B$ with $|\mathbf{B}_o|$ yields the resonance signal.

A more youthful, but highly useful, mode of muon spectroscopy is found in (Avoided) Level Crossing Resonance (ALC or LCR). First suggested by A. Abragam[5], and later applied with considerable success both at PSI[6] and TRIUMF[7], this technique, which has its antecedents in atomic spectroscopy and nuclear quadrupole resonance[8,9], uses an approach similar to that of muon spin resonance, with a time-integrated difference counting system and a longitudinally applied field; in this case, however, no RF field need be present, and the resonance signal arises when the longitudinal field is tuned so that a Zeeman transition of the muon energetically matches some other transition within the sample, leading to a nonlinearity in the field dependence of the muon Zeeman states, and therefore in the counted forward-backward asymmetry.

1.1.3 Transverse Field μSR at PSI.

All the experiments described in this work were undertaken at the Paul Scherrer Institute (PSI), Villigen, Switzerland, formerly the Swiss Institute of Nuclear Physics. At PSI protons are accelerated in a two-stage process to energies of the order of 590 MeV and directed onto a Be target to yield a pion flux of $2 \times 10^9 \pi^+ s^{-1}$. Some of the pions thus produced are used directly for pion research or medical applications, but the remainder decay in flight with lifetime 26ns leading to a total muon flux of $10^7 \mu^+ s^{-1}$.

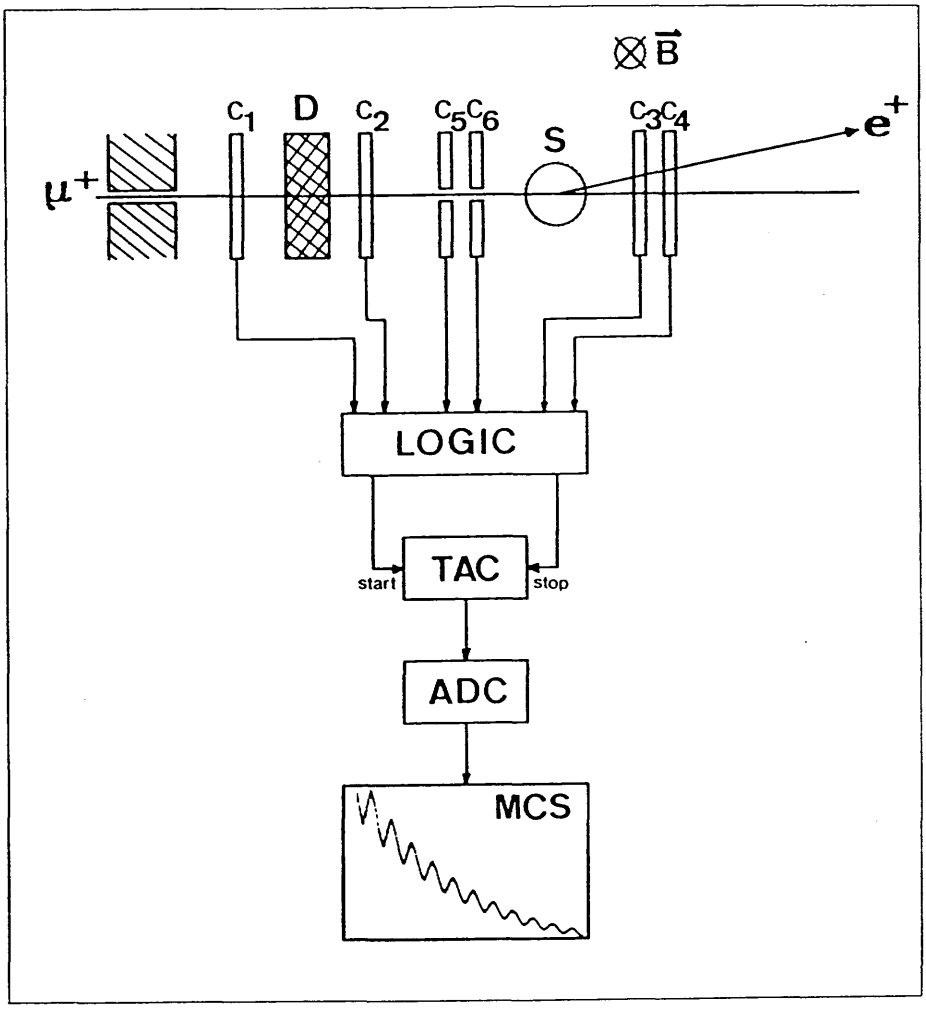

Figure 1.1 Schematic representation of TFμSR apparatus at PSI.

The experimental TFμSR apparatus at PSI is represented schematically in **Figure 1.1.**

The sample (S) is set centrally between a pair of Helmholz coils producing a magnetic field **B** of strength variable between zero and 0.6 T. In low-field and zero-field experiments three additional, mutually orthogonal, smaller pairs of coils surrounding the sample are used to compensate for the Earth's magnetic field and any accidental local fields which might influence the measurement.

Muons with momentum of around 115 MeV/c and typically 70% forward spin polarisation are stopped in the sample where they decay according to equation (1.2). The requirements for conservation of spin and momentum lead to an anisotropy in the decay process, yielding an e^+ emission probability proportional to $1 + a\cos\vartheta$, where ϑ is the angle between the muon spin and the positron momentum and a is the coefficient of decay asymmetry for which the average value over all e^+ energies is $\frac{1}{3}$. Any evolution with time of the muon's spin orientation (as a result of interactions both with the applied field and with local fields intrinsic to the sample) is reflected in a modulation in the rate at which decay positrons are counted in any fixed direction.

The experiment proceeds as follows. Passage through a lead collimator reduces the beam diameter to 15-20 mm, whereupon the muons are slowed down, first by polyethylene in the collimator exit hole, then in a water degrader (D). The latter is of continuously controllable thickness and is used to select muon momenta such that the number of μ^+ stopping in the sample is maximised. The transit of charged particles through the μSR apparatus is registered by plastic scintillators. The incident muon passes through counters C_1 and C_2 and stops in the sample. Decay positrons pass through counters C_3 and C_4 in the forward position, or through counters C_5 and C_6 in the

backward position (through which a hole has been cut in order that the beam pass unimpeded), or through one of two sets of counters located above and below the sample (not illustrated). The electronic pulses thus created are analysed using a coincidence method whereby a certain characteristic signature of pulses is associated with an "event" in which a decay positron can be traced to its progenitor muon; electronic logic discards spurious events. (A consequence of this single-counting technique is that no more than one muon is permitted to be in the sample at any time.) The time intervals (between μ^+ and e^+ detection) corresponding to such events are then supplied sequentially to a time-to-amplitude converter (TAC), an analogue-to-digital converter (ADC), and finally to a multichannel storage device in which a separate histogram is accumulated for each set of positron detectors. The histograms are, in effect, representations of the relation between the number of events collected (H) and the time interval between the detection of the muon and of its corresponding decay positron.

In the absence of an applied field each μSR histogram shows the exponential form of the muon decay curve, $H(t) \alpha e^{-t/\tau}$, with τ the muon lifetime. However, when a magnetic field **B** is applied transverse to the initial muon trajectory z the spin vector of the muon in the sample precesses at its Larmor frequency, $\nu = 135.537\,\mathrm{MHz\,T^{-1}}$, and the temporal distribution of decay positrons arriving at each scintillator is thus modulated. The histograms so generated show the muon precession frequency superimposed upon the decay curve, with a phase dependent upon the counter position. An example is given in **Figure 1.2.** Other sample-dependent factors also affect the nature of the modulation. The general form of a μSR histogram is[10,11]

$$H(t) = N_o \{B_o + e^{-t/\tau}[1 + F(t)]\} \qquad (1.3)$$

where N_o is a normalisation factor dependent only on the total number

of counts, B_o is the accidental background fraction, usually small and roughly constant, and F(t) is the form of the time dependence of the muon spin polarisation, contingent upon the number and type of muon environments present in the sample, and the number of frequencies associated with each. Its general expression is

$$F(t) = \sum_i F_i(t) = \sum_i A_i e^{-\lambda_i t}(\cos \omega_i t + \varphi_i) \qquad (1.4)$$

where ω_i is the precession frequency, φ_i is the initial phase, a function of the spatial relation between the initial muon spin polarisation direction and the axis of the e^+ counter "telescope", A_i is the asymmetry, dependent upon the beam polarisation P, the anisotropy coefficient a in the positron distribution, and other factors, and λ_i is the depolarisation rate (or damping constant), related inversely to the

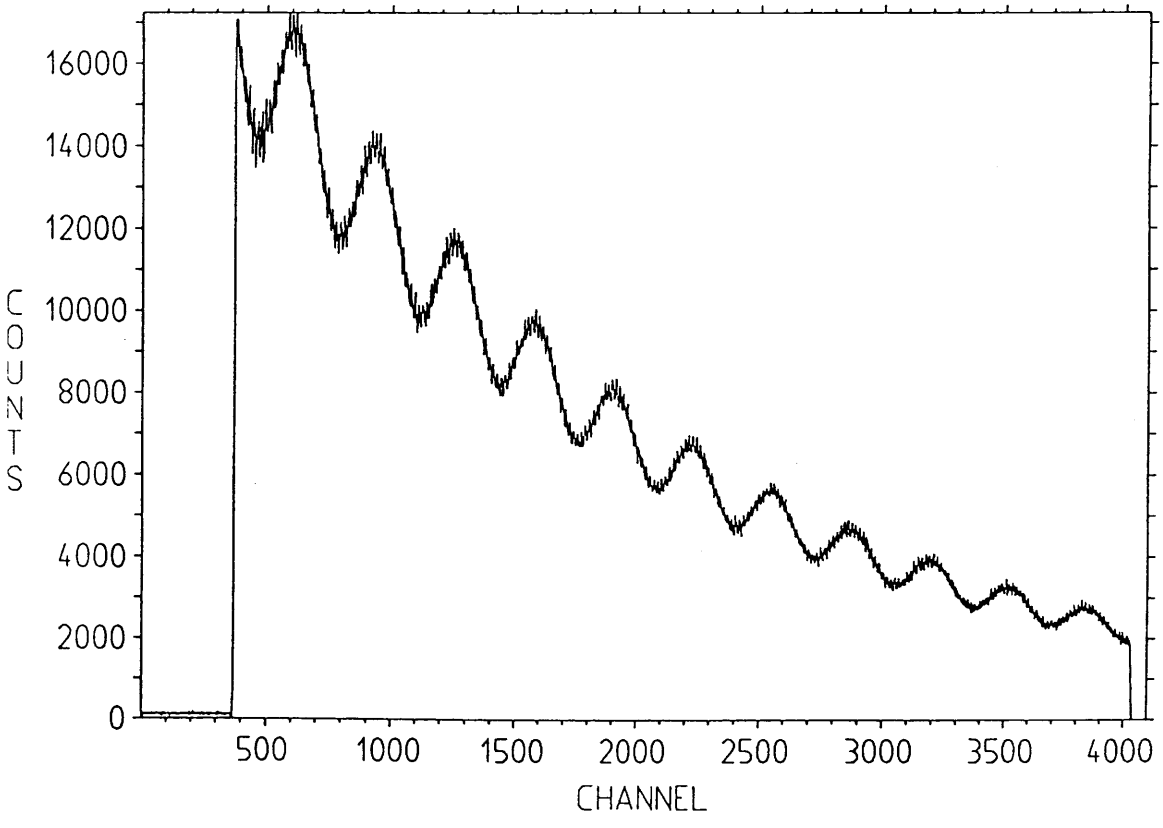

Figure 1.2 Sample μSR histogram (H_2O at 18mT).

spin-spin relaxation time, and reflecting relaxation or reaction processes.

At PSI a total of 8K channels (or "bins") are divided equally among the four telescopes typically used for an experiment. Bin width is chosen to suit the frequency range under examination, but is typically around 875 ps, leading to an upper limit of observable frequency in the region of 575 MHz. For the experiments described in this work the average number of events collected per temperature studied was about 5×10^7, depending on the strength and number of signals of interest. Experiments at temperatures other than room temperature were carried out in a sealed insulated cryostat in which cooling was produced by means of the flow of cold N_2 gas, heating generated by an electrical resistance, and the sample temperature monitored using two thermocouples attached to the exterior of the sample bulb. Samples were, where possible, of commercial origin, and of the highest grade of purity available. In order that the liquid samples be rendered free of dissolved oxygen, which reacts very efficiently with paramagnetic muonic species, each was subjected to a set of freeze-pump-thaw cycles on a vacuum line. Thereupon, the liquids were sealed into spherical thin-walled glass vessels of 35mm diameter (slightly larger than the beam diameter) if sufficient material was available; otherwise, of 25mm diameter.

At all stages the experiments were controlled using a DEC-based computer system, most recently of the MICROVAX type. Data files were subsequently transferred to a DEC VAX 8650 for further processing, including transformation of the μSR histograms into Fourier space leading to clear peaks at the precession frequencies, followed by lineshape analysis of these signals using an iterative least-squares program[12] to yield best-fit frequencies, phases, and other properties.

Several books now exist in which the μSR method is well described, notably those by Schenck[4] and Walker[13], and that edited by Chappert

and Grynszpan[14]; these have been freely consulted in the composition of this introductory section. Among other texts so used are papers by Brewer, Fleming, and Percival[15], Roduner and Fischer[16], and Webster[17].

1.1.4 Muon States in Matter.

1.1.4.1 Muonium.

When positive muons thermalise in matter, some degree of interaction is inevitable, and several distinct possible states exist which can be studied by μSR spectroscopy. In electron-rich substrates which are chemically unreactive, the simplest muonic species is formed. This is the "atom" muonium, μ^+e^-, first proposed by Friedman and Telegdi[18] as an explanation of losses observed in the polarisation attributable to μ^+ in early experiments. Regarded as a two-body system in which a negatively charged particle of small mass experiences the electrostatic "central field" of a positively charged particle of much larger mass, it is clear that muonium thus closely resembles atomic hydrogen, and may reasonably be considered as a unique isotope with approximately one ninth of the mass of common H. Substantiating evidence for this statement is presented in **Table 1.2**, in which certain of the properties of muonium and protium are compared. (As an isotope of H, muonium is considered to merit a chemical symbol, expressly Mu.)

Table 1.2 Some physical properties of Mu and H[2,16,19].

property	Mu	H
atomic mass/a.m.u.	0.11403	1.007825036
Bohr radius /pm	53.17	52.9917706
ionisation potential/J	2.169×10^{-18}	2.179×10^{-18}
hyperfine splitting/MHz	4463.30235	1420.4057517662
reduced mass/m_e	0.9952	0.9995

The electrostatic properties, and therefore the chemical properties (neglecting vibrational effects), are identical but for a small variation due to centre-of-mass differences, which are present in any case to a smaller extent in any pair of isotopes. The magnetic properties of muonium might therefore also be expected to be analogous to those of atomic H, with a hyperfine interaction larger by the ratio of the muon and proton magnetic moments, $\mu_\mu/\mu_H \approx 3.1833$. The theory of this interaction will be treated further in a succeeding section. At this stage it suffices to say that in the presence of a transverse magnetic field the triplet state of muonium is resolved into three levels, leading to four possible transitions, of which two are at frequencies too high for practical observation while the other two (ν_{12} and ν_{23}) are essentially degenerate at low fields, only being resolved at $|\mathbf{B}| \gtrsim 1\,\mathrm{mT}$[20].

1.1.4.2 Diamagnetic States.

In molecular matter chemical reaction is possible involving either μ^+ or Mu. In some cases reaction leads to diamagnetic muonic molecules or ions. For example, equation (1.5) shows the reaction of a muon with a water molecule to form a species analogous to the conventional hydroxonium ion H_3O^+.

$$\mu^+ + H_2O \longrightarrow H_2OMu^+ \qquad (1.5)$$

Very often in molecular liquids the majority of implanted muons pass into diamagnetic states. At present, unfortunately, these diamagnetic environments are indistinguishable by μSR, due to the inability of the technique to discern the small chemical shifts familiar from proton NMR. Consequently, no detailed consideration of diamagnetic states will be found in this work.

1.1.4.3 Muonic Radicals.

When positive muons are implanted into chemical substrates containing one or more canonical double bonds per molecule (especially C=C or C=O

bonds, although there have been some results for others such as C=S[21]) the formation of muonium-substituted free radicals is possible. The process of radical formation is described by net addition of atomic Mu at the double bond, although several possible mechanistic routes exist[22,23]. For example, the first step in the process might be either the formation of muonium itself (which then adds to the substrate like a hydrogen atom) or of a positively-charged diamagnetic intermediate (which then abstracts an electron from its surroundings). Some experimental work has been directed towards assessing the relative importance of the various precursors in certain radical formation reactions. Since the earliest identification of these species by μSR[24,25,26], this area of research has progressed vastly in depth and extent, leading to some major reviews[17,27,28] and one book[1]. The reason for this is that in general not only can muonic radicals be distinguished from one another by μSR techniques, but detailed information on coupling constants and their temperature-dependences, radical kinetics (involving the muon as an active probe in the study of Mu/H isotope effects) and radical conformations can also be gained. Indeed the creation by means of the μSR technique of unique radicals for which no H analogue exists is also a possibility[21].

Muonic radicals are multispin systems possessing, in the presence of an external magnetic field, a complex set of Zeeman states. However, when a sufficiently strong magnetic field ($|\mathbf{B}| \geq 0.02\,\mathrm{T}$) is applied in the transverse direction, the evolution of states is such that the coupling of the muon to all the other nuclei becomes very small, and only those transitions involving the muon and the electron remain at energies easily observed; the nuclear spins are effectively decoupled. The hyperfine coupling constants of muonic radicals are smaller by some orders of magnitude than that of Mu.

Some further theory underlying the experimental study of muonic radicals by transverse field μSR spectroscopy will be found in the following section.

1.1.5 Some Theoretical Principles of TFμSR.

1.1.5.1 The Hamiltonian Operator.

The evolution of the spin polarisation of muons implanted in matter is dependent upon the presence and nature of magnetic interactions, either with local fields generated by nearby electrons and nuclei, or with an external magnetic field, or both. The bulk of the experimental work contained in this thesis deals with situations where Mu has reacted with a substrate in the liquid phase by bonding chemically to a molecule to form a radical. To a first approximation, then, the muon can be considered to be a member of a small ensemble of particles constituting a single molecule, with all "intermolecular" interactions neglected; also, due to rapid reorientational motions present in the low viscosity liquids studied, direct dipole contributions to the hyperfine interaction average to zero, and only Zeeman and Fermi contact terms need be considered in the Hamiltonian operator. The form of the relevant operator is

$$\hat{H} = \hat{H}_Z^{\mu} + \hat{H}_Z^{e} + \hat{H}_Z^{N} + \hat{H}_{\mu e} + \hat{H}_{\mu N} + \hat{H}_{eN} \qquad (1.5)$$

where the first three terms describe the Zeeman interaction of each of the three types of particle with the external field, respectively, and the last three describe intramolecular interactions of muons with electrons, muons with nuclei, and electrons with nuclei, respectively. The negligibly small internuclear coupling terms are omitted. The Zeeman term for a particle i under a magnetic field **B** in the direction z, expressed in terms of its Larmor precession frequency ν_i and its spin operator $\hat{S}_i$ takes the form

$$\hat{H}_Z^i = \nu_i \hat{S}_z^i \qquad (1.6)$$

while the magnetic interactions $\hat{H}_{ij}$ which couple the magnetic moments of paricles i and j are expressed

$$\hat{H}_{ij} = \sum_i A_i \hat{S}^j . \hat{I}^i \qquad (1.7)$$

where A_i is the isotropic Fermi contact hyperfine coupling constant representing the spin density contributed by particle i measured at the site of particle j, $\hat{S}^j$ is the spin operator of particle j and $\hat{I}^i$ is the spin operator of particle i. The relevant Hamiltonian for singly muonium-substituted monoradicals in a low-viscosity fluid substrate under an applied magnetic field **B** along an arbitrary direction z is then

$$\hat{H} = \nu_e \hat{S}^e_z - \nu_\mu \hat{I}^\mu_z - \sum_k \nu_k \hat{I}^k_z + A_\mu \hat{S}^e . \hat{I}^\mu + \sum_k A_k \hat{S}^e . \hat{I}^k \qquad (1.8)$$

The couplings between the electron and the various nuclei are very much smaller than that between the muon and the electron (ie $A_k << A_\mu \; \forall k$) and can be neglected at fields greater than about 0.02 T[16].

1.1.5.2 Muon Spin Polarisation under Transverse Fields.

The general theory of the evolution with time of the polarisation of muon spin under an applied magnetic field was developed by degrees during the latter half of the 1970s by Schenck, Percival, Roduner, Fischer, and other workers[16,29,30,31]. Only the transverse field case will be considered here, and only the briefest treatment given. The muon spin polarisation at time t=0 is (the beam polarisation) P.

Consider the evolution with time of the muon spin polarisation observed in an arbitrary direction q defined by the observation axis of the positron detector. Given by the expectation value of the Pauli spin operator $\hat{\partial}^\mu_q$ [32], that is to say,

$$P^\mu_q(t) = \langle \hat{\partial}^\mu_q \rangle \qquad (1.9)$$

this quantity may be expressed either in the Schrödinger representation

$$P^\mu_q(t) = \mathrm{Tr}\{\hat{\rho}(t) . \hat{\partial}^\mu_q\} \qquad (1.10)$$

with $\hat{\rho}(t)$ the system density function, or in the Heisenberg notation

$$P^\mu_q(t) = \mathrm{Tr}\{\hat{\rho}(0) . \hat{\partial}^\mu_q(t)\} \qquad (1.11)$$

where $\hat{\sigma}_q^{\mu}(t)$ has the form

$$\hat{\sigma}_q^{\mu}(t) = \exp(i\hat{H}t/\hbar)\,\hat{\sigma}_q^{\mu}\exp(-i\hat{H}t/\hbar) \qquad (1.12)$$

and $\hat{H}$ is as defined in equation (1.8).

Taking a basis set of product spin functions

$$|\chi_i\rangle = |\chi_i^{\mu}\rangle|\chi_i^{e}\rangle\prod_k|\chi_i^{k}\rangle \qquad (1.13)$$

the eigenkets of $\hat{H}$ can be expressed in the form

$$|n\rangle = \sum_i c_{ni}|\chi_i\rangle \qquad (1.14).$$

With the unpaired electron and the nuclear spins initially unpolarised, and no evolution of the spin before formation of the chemical species, the formalism of Roduner and Fischer[16] (which essentially omits the electron and nuclear polarisations from the analysis) can be employed in order to derive a clear expression for $P_q^{\mu\,33}$. Firstly, $\hat{\rho}(0)$ is most conveniently expressed in the above basis set with quantisation of spins along the direction b of beam polarisation.

$$\hat{\rho}(0) = \hat{\rho}^{\mu}(0) \times \hat{\rho}^{e}(0) \times \prod_k \hat{\rho}^{k}(0) = \frac{1}{2}\begin{pmatrix} 1+P & 0 \\ 0 & 1-P \end{pmatrix} \times \frac{1}{2}1^{e} \times \prod_k \frac{1}{2I^k+1}1^{k} \qquad (1.15)$$

whereas $\hat{\sigma}_q$ is most easily expressed such that quantisation is along the axis of observation q,

$$\hat{\sigma}_q = \hat{\sigma}_q^{\mu} \times \hat{\sigma}_q^{e} \times \prod_k \hat{\sigma}_q^{k} = \begin{pmatrix} 1 & 0 \\ 0 & -1 \end{pmatrix} \times 1^{e} \times \prod_k 1^{k} \qquad (1.16).$$

Rewriting (1.15) as

$$\hat{\rho}(0) = N^{-1}\{1^{\mu} + \mathbf{P}.\hat{\sigma}_b\} \times 1^{e} \times \prod_k 1^{k} \qquad (1.17),$$

where

$$\hat{\sigma}_b = \begin{pmatrix} 1 & 0 \\ 0 & -1 \end{pmatrix} \qquad (1.18)$$

and

$$N = 4\prod_k(2I^k + 1) \qquad (1.19),$$

then inserting (1.17) into (1.11), noting meanwhile that $\mathrm{Tr}(\hat{\sigma}_q) = 0$, the expression

$$P_q(t) = \mathrm{Tr}\{N^{-1}\hat{\sigma}_q(t) + N^{-1}P\hat{\sigma}_b\hat{\sigma}_q(t)\}$$

$$= \frac{P}{N}\mathrm{Tr}\{\hat{\sigma}_b\hat{\sigma}_q(t)\} \qquad (1.20)$$

is obtained. In general (1.20) need only be evaluated for the case b=q=z (longitudinal field) or b=q=x (transverse field). Here only the latter is considered. For b=q,

$$P_q(t) = \frac{P}{N}\mathrm{Tr}\{\hat{\sigma}_q\hat{\sigma}_q(t)\}$$

$$= \frac{P}{N}\sum_m\sum_n\langle m|\hat{\sigma}_q\hat{\sigma}_q(t)|n\rangle$$

where $|m\rangle$ and $|n\rangle$ are orthonormal eigenvectors of $\hat{H}$ with energies $h\omega_m$ and $h\omega_n$ respectively. Since $\hat{\sigma}_q$ and $\hat{H}$ are Hermitian

$$P_q(t) = \frac{P}{N}\sum_m\sum_n\langle m|\hat{\sigma}_q\exp(i\hat{H}t/\hbar)\hat{\sigma}_q\exp(-i\hat{H}t/\hbar)|n\rangle$$

$$= \frac{P}{N}\sum_m\sum_n|\langle m|\hat{\sigma}_q|n\rangle|^2\exp(i\omega_{nm}t) \qquad (1.21),$$

and since $P_q(t)$ is a real dynamical variable

$$P_q(t) = \frac{P}{N}\sum_m\sum_n|\langle m|\hat{\sigma}_q|n\rangle|^2\cos(\omega_{nm}t) \qquad (1.22).$$

Expanding the eigenfunctions $|n\rangle$ in terms of the basis set defined by (1.14), the expression for P(t) in the case of a transverse magnetic field (q=b=x) can be obtained.

$$\langle m|\hat{\sigma}_x|n\rangle = \sum_i\sum_j c^*_{mi}c_{nj}\langle\chi_i|\hat{\sigma}_x|\chi_j\rangle$$

$$= \sum_i\sum_j c^*_{mi}c_{nj}\langle\chi^\mu_i\chi^e_i\prod_k\chi^k_i\,|\hat{\sigma}_x|\,\chi^\mu_j\chi^e_j\prod_k\chi^k_j\rangle$$

which, since $\hat{\sigma}_x$ is a muon spin operator,

$$= \sum_i\sum_j c^*_{mi}c_{nj}\langle\chi^\mu_i|\hat{\sigma}_x|\chi^\mu_j\rangle\,\delta^e_{ij}\prod_k\delta^k_{ij} \qquad (1.23).$$

The final expression is obtained by inserting (1.23) into (1.22).

$$P_x(t) = \frac{P}{N}\sum_m\sum_n\Big|\sum_i\sum_j c^*_{mi}c_{nj}\langle\chi^\mu_i|\hat{\sigma}_x|\chi^\mu_j\rangle\,\delta^e_{ij}\prod_k\delta^k_{ij}\Big|^2\cos(\omega_{nm}t) \qquad (1.24).$$

For several years transverse field μSR studies have suggested that not all of the initial spin polarisation is transferred into the chemical states finally observed, but that a certain fraction, designated P_L, is lost[34,35,36,37]; that is,

$$P_L = 1 - P_D - \sum_R P_R\,; \qquad (P=1) \qquad (1.25)$$

Efforts have been made to address the problem of P_L, and for aqueous systems it has been suggested[34,38,39] that the lost polarisation originates in muonium formed soon after the muon enters the sample (within 1ps) which loses approximately one half of its polarisation by spin exchange processes (on a timescale of ~1ns) during unreactive encounters with paramagnetic species present at the end of the radiolytical track caused by the passage of the energetic muon through the condensed medium. This in turn has given rise to debate on the processes occurring at the end of the radiation spur[22,23,40].

Recent results[41] using the new technique of muon level crossing resonance spectroscopy on the benzene derivatives allylbenzene, styrene, and toluene, compounds belonging to a class in which TFμSR studies had indicated the existence of a "missing fraction", have accounted for the full original polarisation among the product radical and diamagnetic states. The importance of this result with regard to the interpretation of existing TFμSR data is not yet fully understood.

1.1.5.3 Allowed μSR Transitions; Selection Rules.

For q=x, that is, the case of a transverse magnetic field **B** of low to intermediate strength the Hamiltonian (1.8) mixes product kets $|\chi_i\rangle$ given by equation (1.13) in accordance with equation (1.24). The intensity of a μSR transition, being the amount of muon polarisation located at frequency ω_{nm}, is proportional to the transition moment $|\langle m|\hat{\sigma}_q|n\rangle|^2$ between eigenstates $|m\rangle$ and $|n\rangle$.

With the total magnetic moment given by $M = m^{\mu} + m^{e} + \sum_k m^{k}$ (this is exactly true for the zero-field case only), it follows that

$$\hat{\sigma}_x = \frac{1}{2}(\hat{\sigma}^+ + \hat{\sigma}^-) \qquad (1.26)$$

giving a non-zero transition moment only when $\Delta m = \pm 1$ in experiments under low transverse field. At higher fields ($|\mathbf{B}| \geqslant 0.02$T) the spins are decoupled and the eigenstates become pure product functions. They

are characterised by the z-components of individual angular momenta m^{μ}, m^{e}, m^{k}. The transition operator $\hat{\partial}_q$ acts upon the muon wavefunction only, and the high field selection rules

$$\Delta m = \pm 1, \quad \Delta m^{e} = \Delta m^{k} = 0 \qquad (1.27)$$

are obtained.

Explicit results follow for (a) muonium and (b) the general case of a paramagnetic muonic species, both evaluated in the high field regime in which the eigenstates are pure products.

(a) Muonium.

With the appropriate Hamiltonian operator (derived from equation (1.8)) in its slightly altered form (the transverse field is here considered to be in the direction z)

$$\hat{H} = \nu_e \hat{S}_z - \nu_\mu \hat{I}_z + A_\mu [\tfrac{1}{2}(\hat{S}^+ \hat{I}^+ + \hat{S}^- \hat{I}^-) + \hat{S}_z \hat{I}_z] \qquad (1.28)$$

where

$$\left.\begin{aligned} \hat{S}^+ &= \hat{S}_x + i\hat{S}_y \\ \hat{S}^- &= \hat{S}_x - i\hat{S}_y \end{aligned}\right\} (1.29)$$

and

$$\left.\begin{aligned} \hat{I}^+ &= \hat{I}_x + i\hat{I}_y \\ \hat{I}^- &= \hat{I}_x + i\hat{I}_y \end{aligned}\right\} (1.30),$$

and the eigenvectors of the spin operators $\hat{S}_z$ and $\hat{I}_z$, namely

$$|\alpha_\mu \alpha_e\rangle, |\alpha_\mu \beta_e\rangle, |\beta_\mu \alpha_e\rangle, |\beta_\mu \beta_e\rangle, \qquad (1.31)$$

after some algebra the eigenvalues

$$\left.\begin{aligned} E_1 &= \nu_- + A_\mu/4 \\ E_2 &= (\nu_+^2 + A_\mu^2/4)^{1/2} - A_\mu/4 \\ E_3 &= -\nu_- + A_\mu/4 \\ E_4 &= -(\nu_+^2 + A_\mu^2/4)^{1/2} - A_\mu/4 \end{aligned}\right\} (1.32)$$

are obtained, where

$$\nu_{\pm} = \frac{1}{2}(\nu_e \pm \nu_\mu) \qquad (1.33).$$

The frequencies of the transitions allowed by the selection rules (1.27)

are then

$$\left.\begin{aligned} \nu_{12} &= E_1 - E_2 = \nu_- - (\nu_+^2 + A_\mu^2/4)^{1/2} + A_\mu/2 \\ \nu_{23} &= E_2 - E_3 = \nu_- - (\nu_+^2 + A_\mu^2/4)^{1/2} + A_\mu/2 \\ \nu_{14} &= E_1 - E_4 = \nu_- - (\nu_+^2 + A_\mu^2/4)^{1/2} + A_\mu/2 \\ \nu_{34} &= E_3 - E_4 = \nu_- - (\nu_+^2 + A_\mu^2/4)^{1/2} + A_\mu/2 \end{aligned}\right\} \quad (1.34)$$

The Breit-Rabi diagram[42] for muonium (**Figure 1.3**) is a good illustration of the interplay of Zeeman and hyperfine effects upon the energy levels of the atom as the external field is increased. The field is given in units of the parameter $\nu_o = 2\nu_+/A_\mu$. The energy levels and transitions are labelled for clarity. At low fields only the transitions ν_{12} and ν_{23} are observed, and for $|\mathbf{B}|$ sufficiently small these are effectively degenerate. (An example of this phenomenon is found in the studies on the catalytic material EUROPT-1 in the Appendix.) A good exploration of the Breit-Rabi diagram for Mu is found in Schenck[4].

(b) General Paramagnetic Species - High Field Perturbation Treatment[16].

At high transverse fields hyperfine interactions become very small in comparison with the electron Zeeman interaction, and a perturbation treatment can be introduced in which the zeroth-order Hamiltonian

$$\hat{H}^{(0)} = \nu_e \hat{S}_z - \nu_\mu \hat{I}_z + A_\mu \hat{I}^\mu . \hat{S} - \sum_k \nu_k \hat{I}_z^k \quad (1.35)$$

is perturbed at first order by the nuclear-electronic hyperfine terms

$$\hat{H}^{(1)} = \sum_k A_k \hat{I}^k . \hat{S} \quad (1.36)$$

Following this procedure, the first-order energies are given by

$$\left.\begin{aligned} E_1^{(1)} &= \frac{1}{2}\sum_k A_k M_k \\ E_2^{(1)} &= \frac{1}{2}\sum_k A_k M_k (c^2 - s^2) \\ E_3^{(1)} &= \frac{-1}{2}\sum_k A_k M_k \\ E_4^{(1)} &= \frac{-1}{2}\sum_k A_k M_k (c^2 - s^2) \end{aligned}\right\} \quad (1.37)$$

where

$$c = \frac{1}{\sqrt{2}}\left(1 - \frac{\nu_o}{\sqrt{1+\nu_o^2}}\right)^{1/2} \quad (1.38)$$

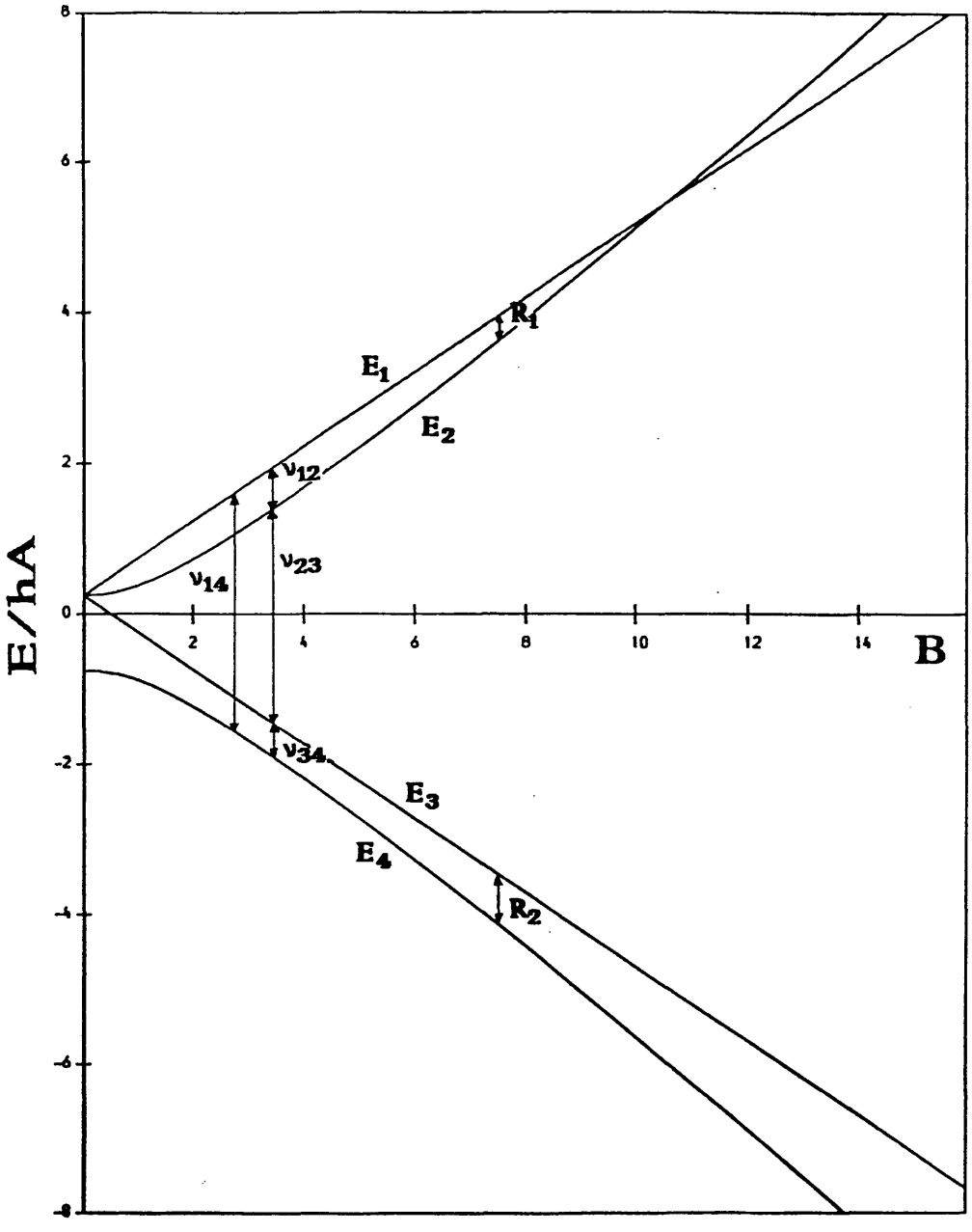

Figure 1.3 Breit-Rabi diagram for Muonium, scaled for pictorial clarity.

$$s = \frac{1}{\sqrt{2}}\left(1 + \frac{\nu_o}{\sqrt{1+\nu_o^2}}\right)^{1/2} \qquad (1.39),$$

$$c^2 + s^2 = 1 \qquad (1.40),$$

and M_k is the quantum number of the spin operator $\hat{F}_z$ for nucleus k. The first-order transition frequencies are then (in terms of the corresponding transition frequencies for Mu, given by equations (1.34),

$$\left.\begin{aligned} \nu_{12} &= \nu_{12}^{Mu} + s^2\sum_k A_k M_k \\ \nu_{23} &= \nu_{23}^{Mu} + c^2\sum_k A_k M_k \\ \nu_{14} &= \nu_{14}^{Mu} + c^2\sum_k A_k M_k \\ \nu_{34} &= \nu_{34}^{Mu} - s^2\sum_k A_k M_k \end{aligned}\right\} (1.41).$$

Roduner and Fischer[16] find that second-order corrections to the energies and transition frequencies are insignificant for $|\mathbf{B}| \geq 0.02$T.

At high fields such as those used in the work on free radicals described here, the Breit-Rabi diagram for a muonic radical resembles that for muonium in the number of energy levels, although the separations are considerably different. Only the transitions at ν_{12} and ν_{34} are actually observed (these are marked on the high field part of the Breit-Rabi diagram shown in **Figure 1.3** as R_1 and R_2), the intensities of the others being weakened due to the conditions $c \to 1$ and $s \to 0$ as $|\mathbf{B}| \to \infty$. The muon-electron hyperfine coupling constant A_μ is then given in terms of the transition frequencies by

$$|A_\mu| = |\nu_{12}| \pm |\nu_{34}| \qquad (1.42).$$

The sign change is in the direction - to + with increasing $|\mathbf{B}|/|A_\mu|$ and occurs at $|\mathbf{B}| = 3.672 \cdot |A_\mu|$ mT[33] due to the crossing of the levels E_1 and E_2. Since in this work it is important to compare the muon-electron hyperfine coupling constants obtained in studies of muonic radicals with the corresponding ^{1}H couplings appropriate to their hydrogenic analogues, the concept of the reduced muon coupling constant A'_μ is

used throughout. This is defined as

$$A'_{\mu} = A_{\mu} \cdot {}^{\mu_P}/_{\mu_\mu} \qquad (1.43)$$

where μ_p and μ_μ are the proton and muon magnetic moments, respectively.

1.2 Radicals in the Liquid Phase.

1.2.1 Internal Dynamics.

The concept of the liquid state implicit within past μSR studies, and indeed suggested by the μSR spectra obtained from liquids, has been that intermolecular (radical-solvent) interactions are small relative to intramolecular interactions and therefore that the single radical generated in a given event by the continuous beam technique can be regarded as a self-contained entity. The sum of the series of sequentially existing transient radicals is effectively equivalent to the standard canonical ensemble. Reorientational motions average the anisotropic (dipole-dipole) contributions to the hyperfine coupling tensor to zero; only the isotropic Fermi contact term remains, and this is measured as the muon-electron hyperfine coupling constant A_μ . At experimental temperatures there is a Boltzmann distribution among the states in the radical's vibrational manifold; motional co-ordinates of both small and large amplitude are excited. Vibrational transitions are rapid on the μSR timescale, so the measured values of radical properties are averages over all the populated vibrational states. The Born-Oppenheimer approximation[43] is assumed to hold. In order that the μSR results presented later in this work be fully appreciated it is first essential to explore the theory governing the internal motions in small molecules to some extent.

The general expression for the potential energy of a molecule in curvilinear internal co-ordinates, disregarding terms above the quadratic, is[44,45]

$$V = 1/2 \sum_{rs} f_{rs} \mathcal{R}_r \mathcal{R}_s + 1/6 \sum_{rst} f_{rst} \mathcal{R}_r \mathcal{R}_s \mathcal{R}_t + 1/24 \sum_{rstu} f_{rstu} \mathcal{R}_r \mathcal{R}_s \mathcal{R}_t \mathcal{R}_u + \ldots \quad (1.44)$$

where, expressed in terms of cartesian co-ordinates x_n,

$$\mathcal{R}_s = \sum_m B^s_m x_m + 1/2 \sum_{mn} B^s_{mn} x_m x_n + 1/6 \sum_{mnp} B^s_{mnp} x_m x_n x_p + \ldots \quad (1.45).$$

The internal co-ordinates $\mathcal{R}_s$ describe motions of the molecule such as bond stretching, angle bending, and internal rotation. The terms B^s_m are the appropriate partial derivatives of the internal co-ordinates with respect to the cartesian co-ordinates. The coefficients f_{rs} in equation (1.44) are the internal co-ordinate force constants; they are partial derivatives of V with respect to the internal co-ordinates $\mathcal{R}_s$. For example,

$$f_{rs} = \left(\frac{\partial^2 V}{\partial \mathcal{R}_r \partial \mathcal{R}_s} \right)_0 \quad (1.46).$$

Curvilinear internal co-ordinates are useful in that they relate molecular properties to readily understandable chemical concepts of molecular structure. They fall naturally into two classes. Those which experience large displacements from their equilibrium value at ambient temperatures are known as large amplitude co-ordinates; this category includes motions such as torsion and inversion. Bond stretching and angle bending fall into the class of small amplitude co-ordinates, experiencing on the whole only relatively small displacements from their equilibrium values. It is likely that a physical property of a molecule which shows a strong dependence on temperature is closely related to one or more large amplitude motions of that molecule.

1.2.2 Relation to Temperature Studies of Radicals.

Studies on free radicals either muonic by μSR or otherwise by ESR have shown the isotropic hyperfine coupling constant in certain cases to be a temperature dependent phenomenon. This is clearly a result of changes in the average radical structure with temperature due to changes in the populations of vibrational states.

All muonic radicals produced by muonium addition to unconjugated

π-systems have Mu in the β-position with respect to the unpaired electron. In simple cases (for example the ethyl radical – see Chapter 2) changes in the muon-electron hyperfine coupling can be attributed to changes in a single large amplitude co-ordinate – the torsional angle γ around the bond axis joining the atoms α- and β- to Mu (usually C and C or O and C). The angle γ, as illustrated in **Figure 1.4**, in a system of axes in which the C-C or C-O bond is parallel to the y-axis, and the axis of the p-orbital notionally containing the unpaired electron is the z-axis, is defined as the angle between the z-axis and the projection of the C-Mu or O-Mu bond onto the xz plane.

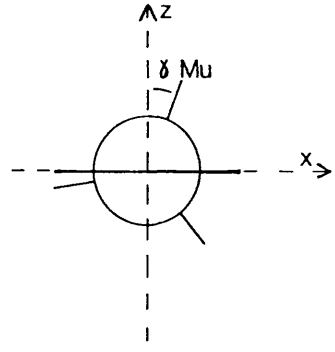

Figure 1.4 Newman projection of a general unconjugated muonic radical.

In a radical with some degree of conjugative delocalisation in the π-system the p-orbital axis under consideration is that passing through C_β which is perpendicular to the nodal plane of the π-system.

The dependence of the coupling between a β-nucleus X (X=H or Mu) and an unpaired electron contained in an orbital of π-symmetry on the torsional angle γ can be expressed as a Fourier expansion of even terms

$$A_\beta^X(\gamma) = A_0 + A_2\cos 2\gamma + A_4\cos 4\gamma + \ldots \qquad (1.47)$$

In simple cases it is reasonable to neglect terms higher than the second and rewrite the series in the form

$$A_\beta^X(\gamma) = A + B\cos^2\gamma \qquad (1.48)$$

due to Heller and McConnell[46], in which the first, angle-independent term, A, can be considered to originate in angle-independent spin polarisation processes, while the second represents the change with

γ in the interaction between the nucleus X and the unpaired π-electron density.

When the change with temperature of the β-hyperfine coupling constant can be related in such a straightforward way with a single internal co-ordinate it is simple to obtain information regarding that portion of the total molecular potential energy which varies with the co-ordinate in question. Here, the quantum-mechanical theory of rotational averaging[47,48,49,50,51,52] can be used in order to determine the form of the appropriate one-dimensional potential energy function, and to extract insights relating to the equilibrium conformation and the factors influencing it. (For more complex species, or in a more sophisticated treatment, the possibility of coupling of several large amplitude motions must be considered.)

1.2.3 Theory of Rotational Averaging for Torsional Processes having Periodic Barriers.

The one-dimensonal Hamiltonian operator for internal rotation can be written

$$\hat{H} = \frac{-\hbar^2}{2I}\frac{\partial^2}{\partial\vartheta^2} + V(\vartheta) \qquad (1.49)$$

where I, the reduced moment of inertia for internal rotation, defined as

$$I = \frac{I_T I_F}{I_T + I_F} \qquad (1.50)$$

is related to the ratio of the moments of inertia I_T and I_F of the two contra-rotating groups (the *top*, T, and the *frame*, F, designated arbitrarily) about the torsional axis.

Regarding the torsional Hamiltonian as a perturbation of the zeroth-order free internal rotation Hamiltonian, that is,

$$\hat{H} = \hat{H}^0 + \hat{H}^1 \qquad (1.51)$$

where

$$\hat{H}^0 = \frac{-\hbar^2}{2I}\frac{\partial^2}{\partial\vartheta^2} \qquad (1.52)$$

and

$$\hat{H}^1 = V(\vartheta) \qquad (1.53),$$

the free internal rotation wavefunctions

$$\psi_n = \frac{1}{\sqrt{2\pi}} e^{\pm in\vartheta} \qquad (1.54)$$

(for which the corresponding energy levels are $E_n = n^2$, $n=0, \pm1, \pm2, \ldots, \pm n$) can be used can be used as a set of basis functions from which the wavefunctions corresponding to the hindered internal rotation Hamiltonian (1.49) may be constructed. These are

$$\psi_j = \frac{1}{\sqrt{2\pi}} \sum_n c_n e^{\pm in\vartheta} \qquad n = -\infty, \ldots, \infty \qquad (1.55).$$

$$j = 1, \ldots, 2n+1$$

For a general periodic barrier it is assumed that the potential energy can be expanded as a Fourier cosine series about the equilibrium value of the torsional angle ϑ, that is,

$$V(\vartheta) = \sum_m \frac{V_m}{2}(1 - \cos m\vartheta) \qquad (1.56).$$

From $\langle \psi_k | \hat{H} | \psi_j \rangle$ the terms of the secular determinant are obtained in their general form

$$\left.\begin{aligned} H_{nn} &= \frac{\hbar^2}{2I} n^2 + \sum_m \frac{V_m}{2} \\ H_{nn'} &= -V_m/4 \qquad ; \; n' = n+m, n-m \\ H_{nn'} &= 0 \qquad ; \; n' \neq n+m, n-m \end{aligned}\right\} (1.57),$$

For example, if the torsional potential is purely twofold,

$$V(\vartheta) = \frac{V_2}{2}(1 - \cos 2\vartheta) \qquad (1.58),$$

the diagonal elements of the secular determinant are given by

$$H_{nn} = \frac{\hbar^2}{2I} n^2 + \frac{V_2}{2} \qquad (1.59),$$

while the non-zero off-diagonal elements are

$$H_{nn'} = -V_2/4 \qquad ; \; n' = n+2, n-2 \qquad (1.60).$$

Where the timescale of the experiment is such that transitions between individual torsional states cannot be distinguished, the observed splitting is given by a population-weighted average of $\langle A_\beta^\chi(\gamma) \rangle_i$ over all (2m+1) values of i. With

$$\langle\cos^2\gamma\rangle_i = \langle i|\cos^2\gamma|i\rangle \qquad (1.61)$$

where γ, as previously defined, is related to ϑ by the equation $\gamma=\vartheta+\vartheta_o$, ϑ_o being the value of the dihedral angle between the axis of the p-orbital and the bond to the coupling nucleus evaluated at the potential minimum, the Heller-McConnell equation (1.48) can be rewritten

$$\langle A_\beta^X(\gamma)\rangle_i = A + B\langle\cos^2\gamma\rangle_i \qquad ;i = 1,\ldots,2n+1 \quad (1.62).$$

Some elementary but tedious algebra yields the following general expression for $\langle\cos^2\gamma\rangle_i$.

$$\langle\cos^2\gamma\rangle_i = \frac{1}{2}\sum_n c_n[c_n + \frac{1}{2}c_{n+2}(\cos 2\vartheta_o - \sin 2\vartheta_o) + \frac{1}{2}c_{n-2}(\cos 2\vartheta_o + \sin 2\vartheta_o)] \quad (1.63)$$

For the two special cases $\vartheta_o=0^\circ$ and $\vartheta_o=90^\circ$ which encompass most of the examples discussed here, the above expression simplifies to

$$\langle\cos^2\gamma\rangle_i = \frac{1}{2}\sum_n c_n(c_n + \frac{1}{2}c_{n+2} + \frac{1}{2}c_{n-2}) \quad ; \vartheta_o = 0^\circ \qquad (1.64a)$$

and

$$\langle\cos^2\gamma\rangle_i = \frac{1}{2}\sum_n c_n(c_n - \frac{1}{2}c_{n+2} + \frac{1}{2}c_{n-2}) \quad ; \vartheta_o = 90^\circ \qquad (1.64b).$$

Within a Boltzmann distribution of the ensemble among the torsional states i of energy E_i, the β-hyperfine coupling constant expressed as a function of temperature is

$$A_\beta^X(T) = \frac{\sum_i \langle A_\beta^X\rangle_i \exp(-E_i/kT)}{\sum_i \exp(-E_i/kT)} \qquad (1.65)$$

where k is Boltzmann's constant ($=1.380662\times10^{-23}\,JK^{-1}$ [2]).

For low barriers, approaching the limiting case of free internal rotation, the appropriate quantum numbers are those of free internal rotation, and the energy levels show the characteristics of double degeneracy for $n\neq0$ and quadratic dependence on n. For high barriers the limiting case is that of the one-dimensional harmonic oscillator, with quantum numbers ν and eigenvalues

$$E_\nu = (\nu + \tfrac{1}{2})\,h\omega \qquad (1.66)$$

where ω is the frequency of the oscillator. The correlation between

these two extreme cases with increasing barrier is exemplified (for the case of a twofold barrier) in **Figure 1.5**.

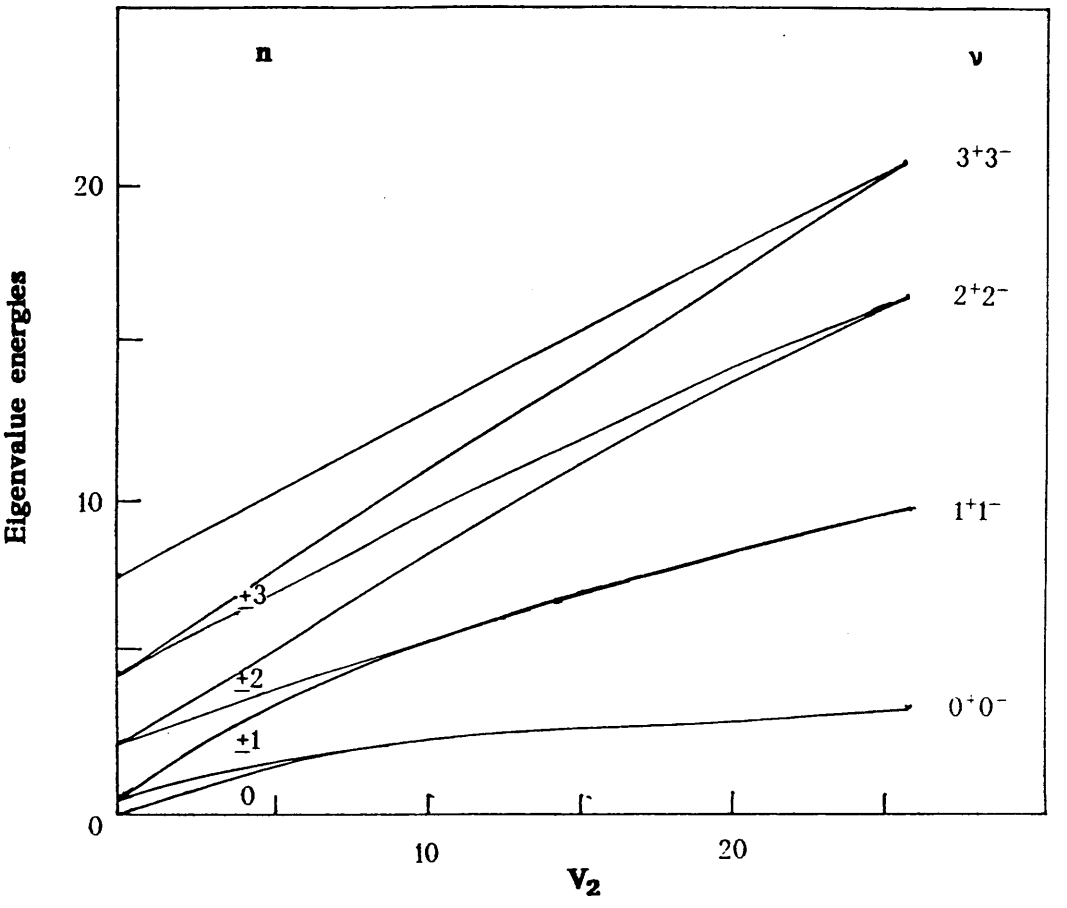

Figure 1.5 Correlation of energy levels associated with a twofold potential function V_2, indicating that for low V_2 the appropriate quantum numbers are those of free internal rotation, whereas simple harmonic oscillator quantum numbers are appropriate for very high V_2. (The units on both axes are arbitrary.)

In the limit of high temperature, the occupation numbers of the torsional states become equal; the situation is analogous to classical free rotation. The limiting value of $A_\beta^X(T)$ is given by

$$\lim_{T\to\infty} A_\beta^X(T) = A + B\,\frac{\sum_i \langle\cos^2\gamma\rangle_i}{2m+1} \qquad (1.67)$$

and, since $\sum_i \langle \cos^2\gamma \rangle_i = \frac{2m+1}{2}$ (1.68),

this reduces to the well-known expression

$$\lim_{T\to\infty} A_\beta^X(T) = A + B/2 \qquad (1.69).$$

In other words, the high temperature limit of the average over all values of i of the expectation value of $\cos^2\gamma$ is equal to the average over 2π radians of the function $f(\gamma)=\cos^2\gamma$.

The concepts and formulations sketched above form the basis for the analysis of the μSR data presented in the following chapters.

1.3 The Use of *Ab Initio* Techniques in the Calculation of Free Radical Properties.

A concept familiar from many texts on molecular quantum mechanics is the "difficulty diagram", or "accuracy diagram"[52], in which on one axis the number of functions in the basis set increases, while on the other what is varied is the number of electronic configurations. In the bottom left-hand corner lie the easy (but inaccurate) single determinantal calculations which use a minimal basis set. In the top right-hand corner it is common for the words "Exact Solution" to be placed, implying that with a saturated basis set in which core orbitals, the valence shells, localised wavefunctions of higher angular momentum, and diffuse Rydberg functions are all included, and with a total wavefunction of multi-determinantal character embodying all conceivable substitutions (single, double, triple, and so forth) in addition to the ground state configuration, in principle the exact solution of the molecular Schrödinger equation can be achieved.

This view does not take into account relativistic corrections, in the case of which it is the molecular Dirac equation which is being numerically approximated. Only for molecules containing atoms of high nuclear charge ($Z \gtrsim 40$) is this level of theory a necessity in order to calculate molecular properties to a high level of accuracy. At least

two other assumptions of a more fundamental nature, however, are also tacitly made.

Firstly, it is assumed that in the construction of a wavefunction the molecule may be isolated. On a philosophical level, it is well understood that the only system for which the Schrödinger equation has "absolute" validity is the universe itself, that all subsystems of the universe of necessity interact with one another, and that under the influence of even only very weak interactions the relevant eigenstates are not pure products, but rather are non-trivial linear combinations of product states[53]. This "entanglement" of systems is nevertheless casually ignored by theoretical chemists using the *ab initio* method as a practical tool. To some extent this behaviour is justifiable as the extent of interaction is not of chemical importance unless the intermolecular distance is very short (compare, for example, the relative strengths of the interactions involved in chemical bonding, hydrogen bonding, and van der Waals' bonding).

The second implicit approximation is the fundamental principle to which virtually all quantum concepts of molecular chemistry owe their existence, namely the postulate of Born and Oppenheimer[43] that, due to the large difference in scale between nuclear and electronic masses, the two classes of particle may be considered separately when solving the Schrödinger equation. The succinct mathematisation of this principle is found in the partitioned molecular Hamiltonian operator

$$\hat{H} = \hat{T}_n + \hat{T}_e + \hat{V}_n + \hat{V}_e \qquad (1.70)$$

where $\hat{T}_n$ is the kinetic energy operator of the nuclei and $\hat{T}_e$ that of the electrons. The assumption here is that the motion of the electrons can be considered in the context of the fixed Coulomb field of the nuclei; in the electronic Schrödinger equation the nuclei are considered stationary, and their kinetic energy is omitted from the Born-Oppenheimer

electronic Hamiltonian

$$\hat{H} = \frac{-1}{2}\sum_{i=1}^{n}\nabla_i^2 - \sum_{i=1}^{n}\sum_{I=1}^{N}\frac{Z_I}{|\mathbf{R}_I-\mathbf{r}_i|} + \sum_{i>j}^{n}\sum_{j=1}^{n}\frac{1}{|\mathbf{r}_i-\mathbf{r}_j|} + \sum_{I>J}^{N}\sum_{J=1}^{N}\frac{Z_I Z_J}{|\mathbf{R}_i-\mathbf{R}_j|} \qquad (1.71)$$

where lower-case indices refer to electrons, upper-case indices to nuclei, and the molecule contains n electrons and N nuclei respectively. The Born-Oppenheimer approximation thus introduces a paradoxical dichotomy between the treatments afforded nuclei and electrons in quantum chemistry; in the conceptual language of Primas[53], it is considered meaningful (if not correct) to say that the three nuclei of C_3 form an equilateral triangle, yet a parallel proposition describing the disposition of the three electrons of an atom of Li is universally recognised as meaningless. Techniques exist by means of which the Born-Oppenheimer approximation can be transcended (for example, the Generator Co-ordinate Method of Van Leuven and Lathouwers[54]); at such levels it is difficult to speak of molecular structure. Methods of this degree of sophistication, however, are not in general use in the hands of chemists, as chemical meaning and chemical concepts are lost. In muonic species the mass ratio of the nucleus to the electron is less than in any other chemical situation; effects beyond the Born-Oppenheimer Approximation might therefore be expected to manifest themselves most strongly in such cases. Very accurate calculations by McKenna and Webster[55] upon all the possible isotopomers of the hydrogen molecule-ion (including muonic species) have indicated that any such effects are extremely small. In this thesis they are neglected.

The necessity or apposition of the technique of Configuration Interaction (CI)[56], applied either directly or through an indirect approach such as Møller-Plesset perturbation theory[57] or the Coupled Cluster method[58], is contingent upon the degree of electron correlation present within the species studied. This in turn is related to the presence

and number of electronically excited states having geometries close to that of the ground state. In the ethyl radical (the subject of Chapter 2 of this thesis) for example, recent studies[59] have shown that the lowest-lying excited states are Rydberg states which are either dissociative or predissociative in nature. Hence the use of CI is not considered necessary in the calculations presented here. However, it is possible that in radicals containing oxygen (see Chapter 5) the delocalisation of unpaired spin density into orbitals centred on the O nucleus indicates the presence of a delocalised π-system with accompanying low-lying antibonding σ^* and π^* orbitals transitions into which should be considered in the calculation. Nevertheless, largely in the face of computational expense, such excitations are not employed here. It is also worthy of comment that the usefulness of non-CI calculations is drastically diminished on parts of the potential energy hypersurface outside the immediate vicinity of the equilibrium geometry.

At the single-configuration SCF level used here some recognisable trends exist in the dependence of geometrical and other properties upon the size and character of the basis set of atomic functions. The erratic and unpredictable effects of basis set superposition error mitigate against the use of minimal basis sets (such as STO-3G). Since what is generally sought after in *ab initio* calculations is a good description of chemical bonding, the dictum guiding the selection of larger basis sets is the quality of representation of the valence region. An economical means of obtaining an accurate description of the valence electrons is the use of a split-valence basis set such as 3-21G, 4-31G, or 6-31G[60]; while these basis sets give only a minimal account of core electrons, their depiction of the valence shells is of a quality comparable to that of the double or triple zeta basis sets of Dunning[61]. Bond lengths obtained using these basis sets are usually quite accurate. Enlargement

of the basis set beyond (and sometimes, indeed, as far as) triple zeta level without including the effects of electron correlation tends to worsen structural predictions, producing bonds which are too short. This phenomenon derives from the coupled facts that at the Hartree-Fock limit single configuration SCF overestimates electron density in bonding regions, thus drawing nuclei together, while at the same time it neglects instantaneous interelectronic repulsions. The inclusion of polarisation functions in a basis set can have quite a considerable effect on molecular geometry, since small contributions from higher-order hybridisation structures can influence bond angles by a matter of some degrees.

The calculation of the isotropic hyperfine coupling constant at a given nucleus N by *ab initio* techniques is possible. This property is related to the molecular electronic wavefunction Ψ by the equation

$$A_N = \frac{8\pi}{3} g\beta g_N\beta_N \langle \Psi | \hat{\rho}(\mathbf{r}_N) | \Psi \rangle \qquad (1.72)$$

where g and g_N are the g-factors for the electron and the nucleus, and β and β_N are the Bohr magneton and the nuclear magneton, respectively, and the quantity $\langle \Psi | \hat{\rho}(\mathbf{r}_N) | \Psi \rangle$ is the expectation value of the spin density evaluated at nucleus N. In the LCAO approximation, equation (1.72) becomes

$$A_N = \frac{8\pi}{3} g\beta g_N\beta_N \sum_i \sum_j \rho_{ij}^{spin} \varphi_i^*(\mathbf{r}_N) \varphi_j(\mathbf{r}_N) \qquad (1.73)$$

where ρ_{ij}^{spin} is the ij^{th} element of the spin density matrix $\boldsymbol{\rho}^{spin}(\mathbf{r})$ given, for a wavefunction which is an unrestricted single determinant corresponding to p electrons of spin α and q(<p) of spin β, by

$$\rho_{ij}^{spin} = \sum_s^p c_{is}^{\alpha *} c_{js}^{\alpha} - \sum_s^q c_{is}^{\beta *} c_{js}^{\beta} \qquad (1.74).$$

While an unrestricted single determinant wavefunction yields a better value for the total energy of a doublet state than does a half-open shell restricted Hartree-Fock wavefunction, it is not an exact eigenfunction of $\hat{S}^2$, experiencing contamination from higher-order

multiplets, principally the quartet. Various projection techniques (UHF-ASA[62], UHF-AA[63], PUHF[64,65]) exist whereby these contaminants may be eliminated. In general UHF wavefunctions give hyperfine coupling constants the absolute values of which are larger than those determined experimentally, while the projection techniques give results smaller than experiment.

The field of *ab initio* quantum chemistry is flourishing, and many reviews are published each year, embodying many diverse and intriguing schools of thought. A reasonable acquaintance with the state of the art can be achieved by perusal of two books. The first of these, by Dykstra[66], is a monograph dealing very lucidly with the descriptive concepts of quantum chemistry, while the second, by McWeeny[67], is a detailed high-level textbook which explores thoroughly the mathematical principles of advanced quantum chemistry, taking the reader to the frontiers of the discipline.

CHAPTER 2

The Ethyl Radical and its Muonium-Substituted Isotopomers.

"The Magical Universe, MU, is a universe of many gods, often in conflict."

William S. Burroughs

2.1 Introduction.

2.1.1 First Experimental Observations on the Ethyl Radical and its Deuterium Isotopomers.

The ethyl radical $\dot{C}_2H_5$ is an "unconjugated π-radical"[68], having an unpaired electron localised in a π-orbital considered largely to consist of a 2p orbital centred on a single sp^2 carbon atom. A system of 7 nuclei and 17 electrons, the second-simplest alkyl radical, it has for many years offered itself to spectroscopists and theoreticians alike through its electronic structure and dynamical behaviour as a stimulating example of a species with a doublet electronic ground state.

The earliest spectroscopic studies of the ethyl radical were by ESR,[69,70,71,72] and revealed two separate proton couplings, one corresponding to three identical protons, the other to an identical pair, yielding a total of twelve lines in the spectrum. These were measured and assigned as follows: A_H^{α} = 62.7 MHz, A_H^{β} = 75.3 MHz, where the subscripts α and β refer to the positions of the protons with respect to the radical centre. The couplings were found to be virtually invariant with temperature over the range 93 K to 298 K. The same independence of temperature was found to hold for the β-deuterium coupling constant in the perdeuterated ethyl radical, $\dot{C}D_2CD_3$[47]. However, in cases where the radical possesses two different hydrogen isotopes the β-couplings cease to be temperature-independent.

In $CHD_2\dot{C}D_2$ the β-proton splitting was found[47] to decrease with temperature from 83.4 MHz at 98 K to 79.5 MHz at 188 K, and to exhibit a larger β-proton coupling constant than does $\dot{C}_2H_5$ and a smaller

β-deuterium coupling (equivalent proton splitting 70.8 MHz) than does $\dot{C}_2D_5$ (equivalent proton splitting 74.5 MHz). These observations suggest that the mean torsional angle $\langle\gamma\rangle$ in the CHD_2 group is different for H and D (i.e. $\langle\gamma_H\rangle \neq \langle\gamma_D\rangle$), with conformations of higher coupling favoured for H while those of lower coupling are favoured for D. Within the Heller-McConnell relation[46], this is consistent with preferred radical geometries of type (A).

(A)

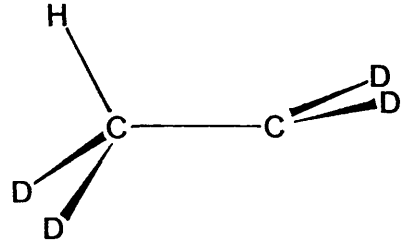

(The non-planar rendition of the CD_2 group in this figure is based upon SCF calculations of the geometry of the ethyl radical[73,74].) The mean value of the β-proton and scaled β-deuteron couplings is, however, very close to the value of A_H^β in $\dot{C}_2H_5$ or of the equivalent scaled coupling in $\dot{C}_2D_5$. It is therefore clear that there exists some difference between a C-H bond and a C-D bond which results in a breakdown of free torsional averaging around C-C. Concomitant with this breakdown is the loss of sixfold symmetry in the barrier to internal rotation. Fessenden's analysis of his ESR results within a theory of rotational averaging similar to that discussed in Chapter 1 found the data to be consistent with a twofold potential barrier of around 385 $J\,mol^{-1}$ [47].

Studies of this radical by Pacansky and Coufal[75] using the technique of infrared spectroscopy and an approach based upon the "deuterium isolation" method of McKean *et al.*[76] led them to conclude from their observation of only a single methyl C-H stretch that the barrier to internal rotation was very low or nonexistent. It therefore seems fair to state that the temperature-dependent ESR experiment is a superior method of evaluating small barriers to internal rotation in free radicals,

despite the "better" timescale of infrared spectroscopy.

The radical $CDH_2\dot{C}H_2$ was studied by McKenna and co-workers[77,78] using ESR spectroscopy at temperatures ranging from 163 K to 273 K and the α-proton, β-proton, and β-deuteron coupling constants measured. While A_H^α showed little variation with temperature, a temperature dependence was found to obtain both in A_H^β and A_D^β, the former coupling being larger, with a negative coefficient of temperature, the latter (scaled) coupling smaller, with a positive coefficient of temperature.

It has been stated by Ramos *et al.*[78] that the temperature dependences of A_H^β and A_D^β in this radical are consistent with an equilibrium conformation such that $\vartheta_0(D) = 90^\circ$. Such a "staggered" conformation is in contradistinction to the SCF minimum energy geometry of $\dot{C}_2H_5$[73], which is of the "eclipsed" type (the terms "eclipsed" and "staggered" here referring to whether or not a C-H or C-D bond eclipses the axis of the 2p orbital on the radical centre carbon atom in which the unpaired electron notionally resides), and implies that for this radical the total vibrational zero-point energy is so much lower in this staggered form than in any of the eclipsed forms that the electronic energy barrier generally thought to favour the eclipsed form is overcome. Consideration of **Figure 2.1** shows that the above assumption is not a necessary condition for the observed behaviour of the H and D coupling constants.

Figure 2.1

(I) 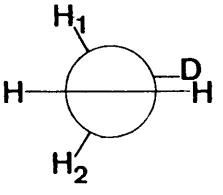

(II) 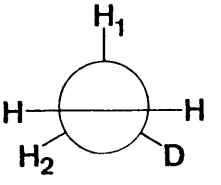

Figure 2.1(I) shows the staggered conformation of the monodeuterated ethyl radical which has been described above. **Figure 2.1**(II) shows one of

the three possible eclipsed conformations. It will be demonstrated that the observed behaviour of the coupling constants can be accounted for if the minimum energy conformation is an eclipsed conformation, but not that in which it is the C-D bond that eclipses the 2p orbital.

First of all note that in the high temperature limit of free internal rotation the average torsional angle

$$\langle\gamma(H)\rangle = \langle\gamma(D)\rangle = \pi/4 \qquad (2.1).$$

In cases where $\vartheta(H)$ or $\vartheta(D)$ is less than $\pi/4$ in the conformation of least energy (for the sake of convenience, and without loss of generality, ϑ will be measured such that $0 \leq \vartheta \leq \pi/2$ for the duration of this argument), within the Heller-McConnell relationship the corresponding H or D β-hyperfine coupling constant is expected to decrease monotonically towards its infimum. Conversely, where $\vartheta_0(H)$ (or $\vartheta_0(D)$) $> \pi/4$, A^{β}_{H} (or A^{β}_{D}) is expected to increase with temperature towards its supremum. Concisely expressed,

$$\vartheta_0(X) < \pi/4 \Rightarrow dA^{\beta}_{X}/dT < 0 \qquad (2.2a)$$

$$\vartheta_0(X) > \pi/4 \Rightarrow dA^{\beta}_{X}/dT > 0 \qquad (2.2b)$$

where X is H or D. Since in this radical there exist situations where the torsional angles of the two methyl protons are unequal, the quantity

$$\overline{\vartheta_0(H)} = \cos^{-1}[(\cos^2\vartheta_0(H_1) + \cos^2\vartheta_0(H_2))/2]^{1/2} \qquad (2.3)$$

is introduced.

Within the model depicted in **Figure 2.1**(I), $\overline{\vartheta_0(H)} = \pi/6$ and $\vartheta_0(D) = \pi/2$, and the experimentally observed behaviour is anticipated. In the case of a minimum energy geometry which is eclipsed, as in **Figure 2.1**(II), and where the total conformational energy is the same regardless of whether it is H_1, H_2, or D that eclipses the 2p orbital, it is found that $\overline{\vartheta_0(H)} = \pi/4$ and $\vartheta_0(D) = 2\pi/9$. The temperature dependences associated with such a situation are different from those observed. However, in a model which recognises that a conformational energy difference exists

between those geometries in which a proton eclipses the 2p orbital and those in which the deuteron does so, and favours the former situation (**Figure 2.1**(II)), it is then true that $\overline{\vartheta_0(H)} \approx \pi/5$ and $\vartheta_0(D) = \pi/3$, which again reproduces the experimental behaviour. In neither of the possible valid models is the barrier to internal rotation well represented by a single twofold term.

The high temperature limit of the β-proton (or scaled β-deuteron) hyperfine coupling constant, given by equation (1.69) in cases where a fit to the experimental data is possible, represents a situation of free torsional averaging around the C-C bond, a situation equivalent to that inferred to prevail in the unsubstituted ethyl radical $\dot{C}_2H_5$ and in the perdeuteroethyl radical $\dot{C}_2D_5$. This is the value towards which the temperature-dependent proton (and scaled deuteron) couplings tend both in $CHD_2\dot{C}D_2$ and in $CDH_2\dot{C}H_2$.

2.1.2 Muonium-Substituted Ethyl Radical Isotopomers.

The likely conditions of formation of paramagnetic muonic species together with a method for their observation were put forward by Brodskii in 1963[79], but it is probable that the first intentional laboratory generation of a muonic ethyl radical was in the seminal muonium chemistry experiments of Mobley in 1966[24], in which the chemical reaction of Mu with a substrate - in this case ethene - was measured by the removal of the former from resonant states. At this time no study was made of the product formed. It was over a decade later that the advent of μSR spectroscopy made possible the detection and study of many novel isotopomers of the ethyl radical each containing a single atom of the light hydrogen isotope muonium.

As noted in Chapter 1, at least two distinct mechanisms can be postulated for the formation of muonic radicals in unsaturated materials, but the net effect of each may be described as the addition of an atom

of muonium to the carbon-carbon double bond. In the case of ethene

$$Mu^{\cdot} + CH_2{=}CH_2 \longrightarrow CMuH_2{-}\dot{C}H_2 \qquad (2.4).$$

The first published report of the detection of the muonic ethyl radical (along with 43 other muonic radicals) was by Roduner and co-workers[80], who measured the muon-electron hyperfine coupling constant at six temperatures within the liquid range of ethene. The temperature dependence of A'_{μ}, found to be much stronger than that of the β-proton coupling constant in $CHD_2\dot{C}D_2$, indicates the influence of a strong isotope effect, occasioned by the large mass ratio Mu:H, upon the dynamics of the radical, and hence the possible existence of a large twofold term in the potential barrier to internal rotation. By use of the method of rotational averaging, Ramos *et alia*[81,82] calculated a torsional barrier of 2845 $Jmol^{-1}$ for this radical, a figure seven times greater than that found by Fessenden[47] in the radical $CHD_2\dot{C}D_2$. Webster, Ramos, and Roduner continued this fascinating study by examining the paramagnetic products obtained by muon irradiation of several deuterium isotopomers of ethene[78,80,82,83]. The isotopomers and corresponding product radicals are shown below.

$$CH_2{=}CH_2 \longrightarrow CH_2Mu{-}\dot{C}H_2$$

$$CHD{=}CH_2 \begin{cases} \longrightarrow & CHDMu{-}\dot{C}H_2 \\ \longrightarrow & CH_2Mu{-}\dot{C}HD \end{cases}$$

$$CHD{=}CD_2 \begin{cases} \longrightarrow & CHDMu{-}\dot{C}D_2 \\ \longrightarrow & CD_2Mu{-}\dot{C}D_2 \end{cases}$$

$$CD_2{=}CD_2 \longrightarrow CD_2Mu{-}\dot{C}D_2$$

In their subsequent analysis of the temperature-dependent hyperfine coupling in these radicals they assumed a dominant twofold term in the barrier to internal rotation, with potential minima at $\vartheta(Mu)=0$ and $\vartheta(Mu)=\pi$. This view is consistent with the sign of dA'_{μ}/dT. The values extracted from this analysis for the potential barrier V_2 in each of

the muonic isotopomers studied, together with the hyperfine parameters A and B corresponding to these solutions and the high temperature limit of the hyperfine coupling, given by A + B/2, are shown in **Table 2.1**.

Table 2.1 Twofold barriers to internal rotation and corresponding hyperfine coupling parameters for muonic ethyl radical isotopomers[82]. V_2 is in $J mol^{-1}$; A, B, and A+B/2 are in MHz.

Radical	V_2	A	B	A+B/2
CH_2MuCH_2	2845	-16.3	191.0	79.2
$CHDMuCH_2$	2704	-13.1	190.6	82.2
CH_2MuCHD	2483	-17.6	198.9	81.9
$CHDMuCD_2$	2927	-20.0	201.7	80.9
CD_2MuCHD	2898	-20.0	200.7	80.4
CD_2MuCD_2	3452	-23.4	197.1	75.2

Re-examination of the data using a different fitting algorithm, based upon the simplex method of Nelder and Mead[84], yielded results which in the majority of cases differ from those tabulated by less than 1%.

In the **Discussion** section of his 1964 paper, Fessenden[47] suggests that it may be valid to partition the potential barrier to internal rotation in ethyl radical isotopomers into a series of pairwise interactions between a substituent on C_α and one on C_β.

$$V = \sum_i \sum_j V^{ij} \qquad (2.5)$$

Ramos *et al.* employ this approach in their study of the muonic isotopomers. By expressing each pairwise interaction as a Fourier series of even terms truncated at the twofold term and considering the case

of the radical $CXYZ\dot{C}A_2$ (X,Y,Z,A≡ Mu,H,D) they obtain the following equation

$$V = V_{max} - V_{min}$$
$$= [(2V_2^{XA}\cos 2\vartheta_o^X + 2V_2^{YA}\cos 2\vartheta_o^Y + 2V_2^{ZA}\cos 2\vartheta_o^Z)^2$$
$$+ (2V_2^{XA}\sin 2\vartheta_o^X + 2V_2^{YA}\sin 2\vartheta_o^Y + 2V_2^{ZA}\sin 2\vartheta_o^Z)^2]^{1/2} \quad (2.6)$$

Hence they derive the values of V_2^{DH}, V_2^{HH}, V_2^{MuD} and V_2^{MuH} with respect to V_2^{DD}, and from these reconstruct calculated barriers to internal rotation both in those radicals studied experimentally and in those derived from $CH_2{=}CD_2$, yet to be studied. With one exception (the relative placement of $CD_2Mu\dot{C}HD$ and $CHDMu\dot{C}D_2$) the trend experimentally observed is correctly reproduced by this method, although the numerical values calculated for V_2 differ from those obtained directly from the experimental data by up to about 10%. It is likely that one of the factors contributing to the inaccuracy of the decomposition-reconstruction method is the assumption of a twofold overall barrier in the initial analysis of the experimental data. While the very large isotope effect raising the twofold term in the potential barrier in $CH_2Mu\dot{C}H_2$ by a factor of seven with respect to that in $CHD_2\dot{C}D_2$ can be simply accounted for (in the first instance, at any rate) by the difference between the isotopic mass ratios Mu/H (≈1:9) and H/D (≈1:2) it is probably unreasonable to expect that the subtle interplay of essentially twofold pairwise interactions between substituents on C_α and C_β can be adequately understood through the variation in a twofold overall potential barrier. The inclusion of a sixfold term in the initial analysis to derive the barrier might improve the results of such a decomposition-reconstruction procedure.

Although the above technique does not of itself consider the physical origin of the pairwise terms, Ramos *et al.*[82] note that the

results of their analysis point towards an explanation of the barrier through the concept of differential steric hindrance between lighter and heavier isotopes, the lighter experiencing the effect to a greater extent than the heavier, this in turn being accounted for in terms of an interaction radius which is greater for the lighter isotope than for the heavier. With the assumption that the rest of the molecule is a rigid structure of "infinite" mass, Cox *et al.*[85] estimate the ratio of Mu and H covalent radii to be 1.7:1 (from $(m_H/m_{Mu})^{1/4}$). (Indeed, viewed within a simplistic framework in which there is a driving force for every vicinal pair of substituents to adopt a mutually *transoid* geometrical relationship, it can be seen that the experimental results bear out a situation in which the steric repulsion is greatest between the C_β-substituents and Mu.)

2.1.3 Physical Models of the Vicinal Interactions.

More recent studies hae attempted to assign physical interpretations to the pairwise vicinal interactions. Claxton and Graham[86] have employed a model in which the individual C-X bonds (X= Mu, H, D) are regarded as independent oscillators making separate, additive contributions to the zero-point vibrational energies of the staggered and eclipsed conformations in order to extract favoured conformations and barriers to internal rotation in ethyl radical isotopomers both known and unknown. Their equation

$$\begin{aligned}\Delta\Xi &= \Xi_E - \Xi_S \\ &= 227.84 + 1031/m_X^{1/2} - 336\,[(1/m_Y)^{1/2} + (1/m_{Y'})^{1/2}] \\ &\quad - 233\,[(1/m_Z)^{1/2} + (1/m_{Z'})^{1/2}] \qquad (2.7)\end{aligned}$$

(where X is the substituent on C_α which takes the $\vartheta=0$ position in the eclipsed conformation and the $\vartheta=\pi/2$ position in the staggered conformation, Y and Y' are the other two substituents on C_α, and Z and Z' are the substituents on C_β), obtained using UHF-SCF

calculations of conformational energies and vibrational zero-point energies, reproduces experimental trends well for cases in which the geometry of minimum energy is thought to be of the eclipsed type, but fails for $CDH_2\dot{C}H_2$, which is usually considered to have a staggered minimum energy conformation in which $\vartheta(D)=\pi/2$. These authors find that the assumption of a conformation of minimum total energy which is of the staggered type but has $\vartheta(D)=\pi/6$ yields a "better" value for the barrier. However, it should be noted that such a preferred conformation does not yield the correct temperature dependence of A_H and A_D. (In a short communication published at about the same time[87], the same authors, using an argument in which isotopically dependent vibrational zero-point energies obtained from finite perturbation SCF force constant calculations are simply added on to conformational energies obtained at the UHF-SCF level with a medium-sized basis set, calculate the favoured conformation of $CDH_2\dot{C}H_2$ to be that in which $\vartheta(D)=\pi/2$.)

Recent work at Glasgow has adopted an approach superficially similar to that of Claxton and Graham, yielding a set of equations in which the isotopomeric conformational energy differences are again expressed in terms related to the masses of the substituents[88]. In this method the assembly of independent oscillators is taken as the zeroth-order approximation in a perturbative scheme based upon the work of Bartell[89].

2.1.4 Perturbation Approach to Isotopomeric Variations in Conformational Energy.

In the unperturbed state there is no interaction between the oscillators. The assumption is made that the motions of the interacting substituents about their equilibrium positions can be treated as the superposition of two oscillators, one describing the motion of the

substituent relative to the carbon atom to which it is bonded, the other describing the accompanying motion in the remainder of the molecule. (The first of these depends on the mass of the substituent; the second, to a first approximation, does not.) A time-average probability distribution

$$P(x) = (2\pi\overline{x^2})^{-1/2} \exp(-x^2/2\overline{x^2}) \qquad (2.8)$$

(where x is the displacement from the equilibrium internuclear distance) describes the separation of the atoms. This can be factorised into components corresponding to the two oscillators.

$$P_m(x_m) = (2\pi\overline{x_m^2})^{-1/2} \exp(-x_m^2/2\overline{x_m^2}) \qquad (2.9a)$$

$$P_s(x_s) = (2\pi\overline{x_s^2})^{-1/2} \exp(-x_s^2/2\overline{x_s^2}) \qquad (2.9b)$$

(The x_m component corresponds to the mass-dependent oscillator.) In these equations $\overline{x_m^2}$ and $\overline{x_s^2}$ are the mean-square values of the component displacements x_m and x_s. They sum to give the mean-square value of the total displacement x.

$$\overline{x^2} = \overline{x_m^2} + \overline{x_s^2} \qquad (2.10)$$

Now the non-bonded interaction of the oscillators is introduced in the form of the potential function V(r), where r is the distance between interacting atoms. With V(r) a weak coupling between nearly independent oscillators of amplitudes respectively x_m and x_s, the average non-bonded potential is described by equation (2.11).

$$\overline{V}(r_g) = \int_{-\infty}^{\infty}\int_{-\infty}^{\infty} V(r)\, P_m(x_m)\, P_s(x_s)\, dx_m dx_s \qquad (2.11)$$

This is the average first-order perturbation energy. In order to obtain a useful expression for V(r) a Taylor expansion about the equilibrium separation r_g is carried out to yield

$$V = \sum V_{ij}(r_g) + \sum x_{ij}\left(\frac{\partial V}{\partial r_{ij}}\right)_{r_g} + \frac{1}{2}\sum\sum x_{ij}x_{rl}\left(\frac{\partial V}{\partial r_{ij}\partial r_{rl}}\right)_{r_g} + \ldots \qquad (2.12).$$

Using this expression for V, and within the harmonic approximation with additive pairwise potentials, integration of equation (2.12) according to equation (2.11) produces an expression for the average first-order

perturbation energy $\overline{V}$ in terms of the mean-square total displacements $\overline{x^2}$.

$$\overline{V}(r_g) = V(r_g) + \tfrac{1}{2}\overline{x^2}\,V''(r_g) + \tfrac{1}{8}(\overline{x^2})^2\,V''''(r_g) + \ldots \qquad (2.13)$$

Hence it is seen that the first-order perturbation energy increases with the total mean-square displacement. Equation (2.13) can be used directly to assess the effect of isotopic substitution upon the first-order energy. As an example, the perturbation energy difference incurred by an isotopic substitution of H for D is shown in equation (2.14).

$$[\overline{V}(r_g)]_H - [\overline{V}(r_g)]_D = \tfrac{1}{2}[\overline{x^2_H} - \overline{x^2_D}]\,V''(r_g) + \tfrac{1}{8}[(\overline{x^2_H})^2 - (\overline{x^2_D})^2]\,V''''(r_g) + \ldots$$
$$= \tfrac{1}{2}(\overline{x^2_H} - \overline{x^2_D})[V''(r_g) + \tfrac{1}{4}(\overline{x^2_H} + \overline{x^2_D})V''''(r_g)] + \ldots \qquad (2.14)$$

Neglecting all terms but the first, this becomes

$$[\overline{V}(r_g)]_H - [\overline{V}(r_g)]_D = \tfrac{1}{2}(\overline{x^2_H} - \overline{x^2_D})[V''(r_g)] \qquad (2.15).$$

Treating the C-H and C-D oscillators as diatomic vibrators the mean-square displacement $\overline{x^2_m}$ is inversely proportional to the square root of the reduced mass of the oscillator. That is,

$$\overline{x^2_{mH}} \propto \mu_{CH}^{-1/2} \qquad (2.16a)$$

$$\overline{x^2_{mD}} \propto \mu_{CD}^{-1/2} \qquad (2.16b)$$

and the mean-square displacements of the two oscillators have the following relation.

$$\frac{\overline{x^2_{mD}}}{\overline{x^2_{mH}}} = \left(\frac{\mu_{CH}}{\mu_{CD}}\right)^{1/2} \qquad (2.17)$$

Substituting (2.17) into (2.14) an expression for the non-bonded interaction in terms of $\overline{x^2_{mH}}$ is obtained.

$$[\overline{V}(r_g)]_H - [\overline{V}(r_g)]_D = \tfrac{1}{2}(\overline{x^2_{mH}} - (\mu_{CH}/\mu_{CD})^{1/2}\,\overline{x^2_{mH}})[V''(r_g)] \qquad (2.18)$$

In order to solve this equation it is next necessary to obtain a value for the mean-square displacement of the carbon-hydrogen oscillator. Within the model of the vibrating diatomic this quantity is related to the vibrational frequency of the oscillator through the equation

$$\overline{x^2_{mH}} = h/(8\pi^2\mu_{CH}\nu) \qquad (2.19).$$

Using values for ν obtained from the infrared spectrum of the ethyl

radical[90], the individual pairwise potentials can be calculated. From these the barriers to internal rotation in the various isotopomers of the ethyl radical can be reconstructed in a manner analogous to that of Ramos *et al*[82]. For the case of the radical CXYZ$\dot{C}$AB, where X, Y, Z, A and B are all isotopes of H, and X is the substituent eclipsing the 2p orbital of C_β, Buttar[88] obtains the general equation

$$V_2 = \frac{1333.64}{\sqrt{\mu_{CX}}} - 649.01\left[\frac{1}{\sqrt{\mu_{CY}}} + \frac{1}{\sqrt{\mu_{CZ}}}\right] - 312.415\left[\frac{1}{\sqrt{\mu_{CA}}} + \frac{1}{\sqrt{\mu_{CB}}}\right] + \frac{624.83}{\sqrt{\mu_{CA}}} \qquad (2.20)$$

and using this equation generates a set of barriers to internal rotation for the various muonic ethyl radical isotopomers on which experimental data exist. The experimental trends are found to be reproduced.

While it is the case that the technique described above as it has been applied so far involves several levels of approximation which impair its quantitative accuracy, it is also noteworthy that in principle all these approximations can be overcome, and higher levels of sophistication can be incorporated, such as the inclusion of anharmonicity in the description of the oscillators, or the use of higher terms in the perturbation energy difference equation (2.14).

2.1.5 The Potential Well and the Torsional Eigenvalues.

It is instructive to consider the quantum-mechanical eigenvalues of the torsional Hamiltonian corresponding to the solutions for A, B, and V_2 obtained by fitting of the experimental data on those ethyl radical isotopomers for which the barrier to internal rotation is largely twofold. Special attention will be given to the radicals $CMuD_2\dot{C}D_2$ and $CHD_2\dot{C}D_2$, which will serve to illustrate the similarities and differences between the situations engendered by addition of Mu to CD_2=CD_2 (perdeuteroethene) and by addition of H to the same olefin.

For the non-muonic radical the twofold barrier to internal rotation

was recalculated using the simplex method of function minimisation[84], to yield a value of 363 $J\,mol^{-1}$ for V_2. The angle-independent hyperfine parameter A was assumed to be zero. The difference between this result and that of Ramos *et al.*[82] lies primarily in the fact that in both cases the data points were physically measured from the graphically displayed results of Fessenden[47]. These measurement errors are assumed to be random. Using this value of V_2 and with a basis set of 21 torsional wavefunctions the secular problem for internal rotation hindered by a small periodic potential barrier was solved in the manner described in Chapter 1. Three torsional levels were found to lie within the potential well, located at $E_1 = 142\,J\,mol^{-1}$, $E_2 = 176\,J\,mol^{-1}$, and $E_3 = 355\,J\,mol^{-1}$. The situation is depicted in **Figure 2.2**. If the populations of the torsional states are presumed to follow a Boltzmann distribution, then at 150 K, a typical experimental temperature for liquid ethene, 45% of the radicals in the ensemble will lie in energy states within the torsional potential well.

In the case of the muonic radical the recalculated value of V_2 (3452 $J\,mol^{-1}$) agrees exactly with that of Ramos *et al.* Upon solving the secular problem, seven torsional eigenvalues were found to lie within the well, at $E_1 = 568\,J\,mol^{-1}$, $E_2 = 568\,J\,mol^{-1}$, $E_3 = 1643\,J\,mol^{-1}$, $E_4 = 1647\,J\,mol^{-1}$, $E_5 = 2556\,J\,mol^{-1}$, $E_6 = 2608\,J\,mol^{-1}$, and $E_7 = 3214\,J\,mol^{-1}$. The barrier and eigenvalues are shown in **Figure 2.4**. At 150 K 91% of the radicals have energies which place them within the well.

The Boltzmann distribution of radicals among the energy levels within the twenty-one wavefunction expansion is shown for $CHD_2\dot{C}D_2$ in **Figure 2.4** (a) and for $CMuD_2\dot{C}D_2$ in **Figure 2.4** (b). In $CHD_2\dot{C}D_2$ the barrier to internal rotation is sufficiently low that the eigenvalue pairing characteristic of free internal rotation is seen above E_3. In the muonic radical the situation is somewhat different.

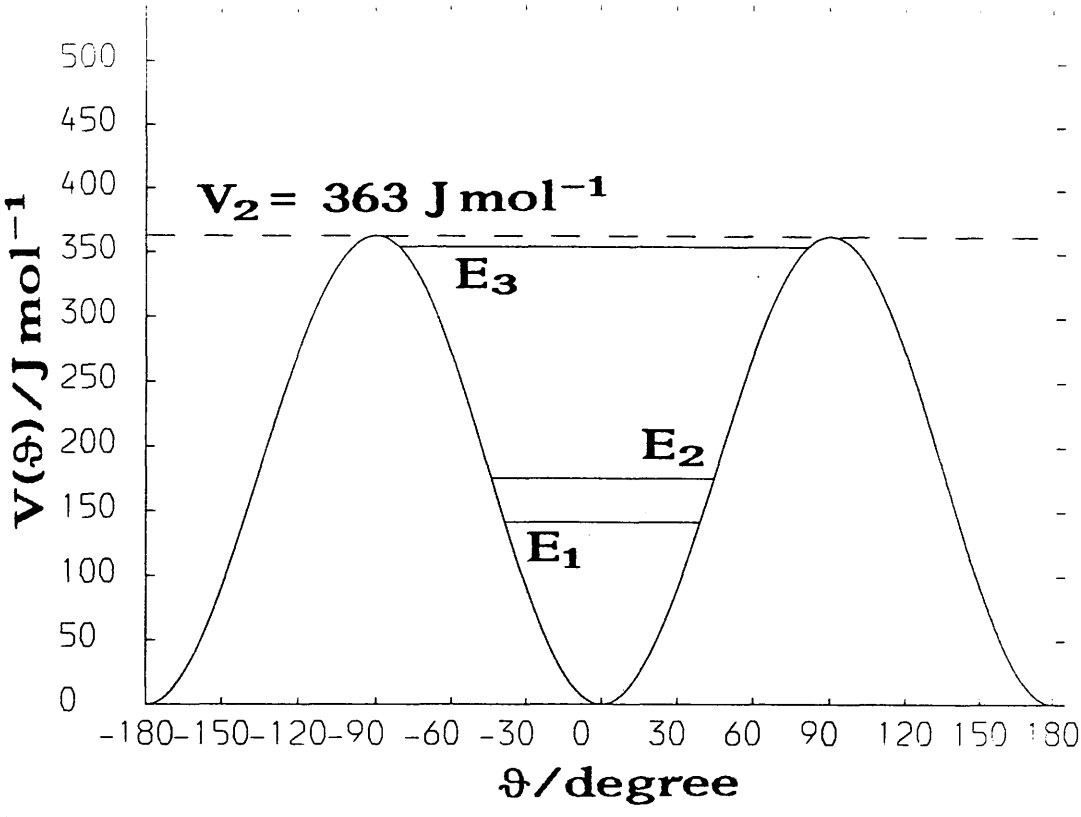

Figure 2.2 The twofold barrier to internal rotation in $CHD_2\dot{C}D_2$ showing the torsional levels lying within the barrier.

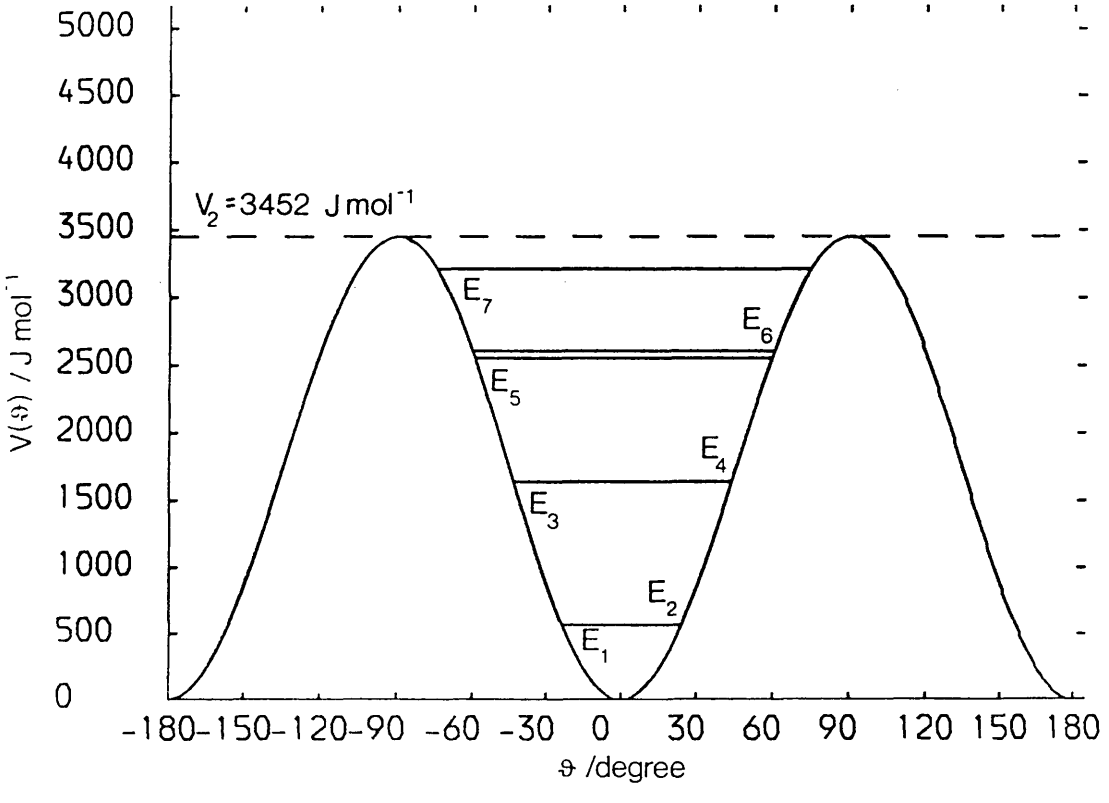

Figure 2.3 Twofold barrier and torsional levels for $CMuD_2\dot{C}D_2$.

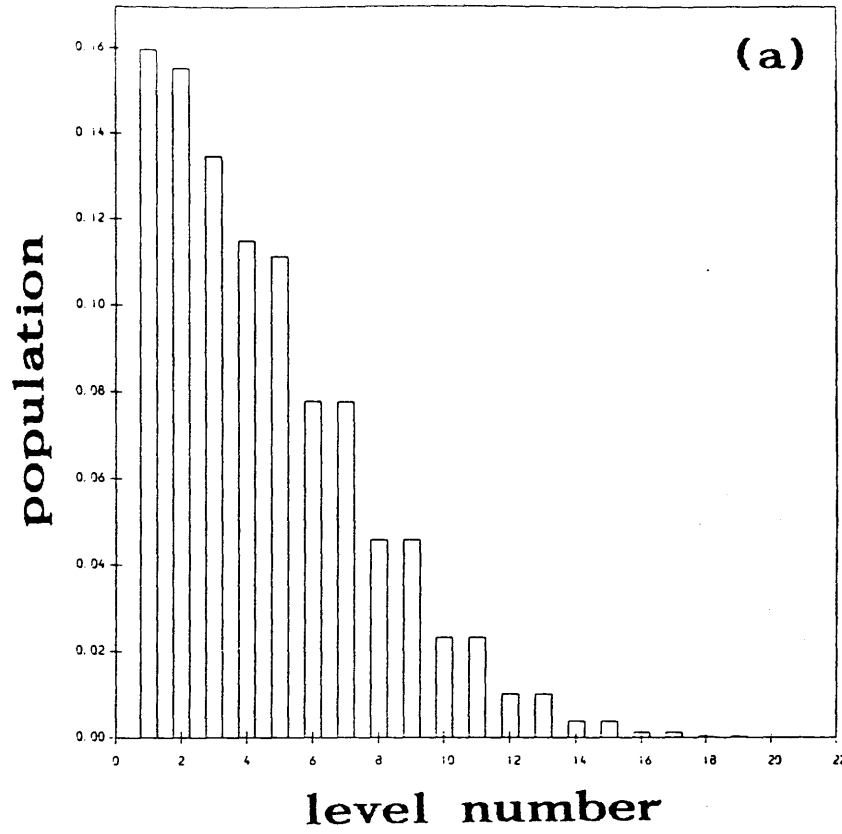

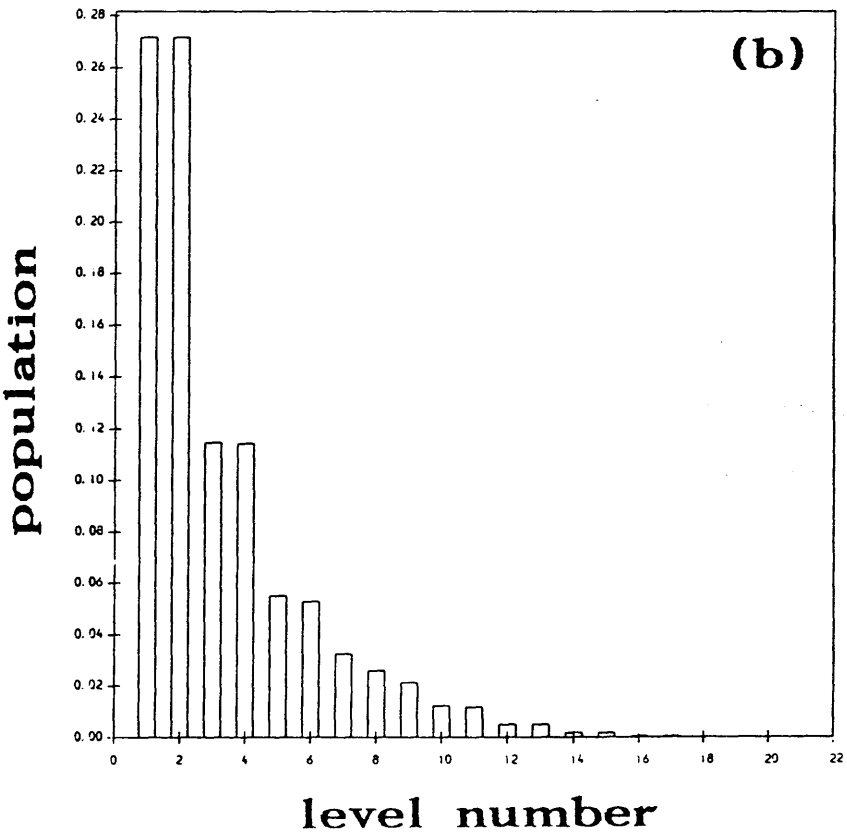

Figure 2.4 Boltzmann distributions among the torsional states at 150 K in (a) $CHD_2\dot{C}D_2$ and (b) $CMuD_2\dot{C}D_2$.

With hindered internal rotation considered as intermediate between free internal rotation (quadratically dependent eigenvalues, doubly degenerate for $m \neq 0$) and one-dimensional harmonic oscillatory motion around the equilibrium position (evenly spaced levels), as illustrated in the correlation diagram in Chapter 1 (**Figure 1.5**), it can be seen that while in $CHD_2\dot{C}D_2$ behaviour characteristic of free internal rotation is seen even in the lowest energy levels, in $CMuD_2\dot{C}D_2$ the lowest levels (up to about E_6) are paired in accordance with simple harmonic oscillator behaviour in the torsional co-ordinate. The characteristic frequency associated with this oscillator is approximately $90\,cm^{-1}$, and the corresponding zero-point frequency about $45\,cm^{-1}$.

In the other muonic ethyl radical isotopomers, which in general have shallower torsional potential wells containing fewer energy levels (five in the case of the muonic ethyl radical itself, $CMuH_2\dot{C}H_2$), the distinctive pattern of energy levels characteristic of simple harmonic oscillator behaviour is not so clearly apparent. Evidently the very large mass ratio D:Mu ($\approx$18:1) is a critical influence upon the dynamics of the radical and the *sine qua non* of vibrationally induced simple harmonic oscillator behaviour in the torsional co-ordinate.

2.1.6 The Hyperfine Parameters A and B.

For the non-muonic isotopomers of the ethyl radical analyses of the experimental ESR data within the theory of rotational averaging carried out by Fessenden[47] , Ramos[82] , and others, have consistently yielded near-zero values for A (always of negative sign), and values for B in the region of 150 MHz. The high temperature limit of the β-hyperfine coupling constant, given by A+ B/2, is in each of these radicals about 75 MHz, very close to the temperature-independent figure for A_H^β obtained in studies of the unsubstituted ethyl radical[47].

Values of A, B, and A + B/2 for the muonic ethyl radical isotopomers,

presented in **Table 2.1**, differ from those of their non-muonic counterparts in some rather interesting ways. The parameter A is now in each case a significantly negative number, and inferences made on the basis that A=0 are hence questionable[91]. The parameter B is again positive, now with a somewhat higher value than before (in the region of 200 MHz), and is found to have changed in concert with A with the net result that the quantity A + B/2 remains largely unaltered. In fact, some slight variation in A + B/2 with isotopic substitution is apparent in the various muonic ethyl radical isotopomers, with only $CMuD_2\dot{C}D_2$ yielding exactly the value of the temperature-independent ethyl β-proton coupling. The largest of the deviations (which are all in the positive sense) are found in the radicals $CMuD_2\dot{C}HD$ and $CMuH_2\dot{C}HD$, in which the C_s symmetry of the methylene group is broken, and it is possible that the large values of the high temperature limit of A'_μ in these radicals are simply products of the fact that this reduction in symmetry is not taken into account in the theoretical analysis. The high value of A + B/2 found for the muonic ethyl radical itself, $CMuH_2\dot{C}H_2$, expressly 79.2 MHZ, seemingly belies such a view. Using a different set of data more recently obtained for the muonic ethyl radical[92], however, a slightly higher value for V_2 results (3024 $J\,mol^{-1}$), together with a somewhat lower value for A + B/2 (77.3 MHz), indicating that the effect of random experimental errors on the calculated high temperature limit may be quite large. Attempts at combination of the two data sets were carried out which led to large fitting errors and a considerably smaller barrier. This suggests that some degree of systematic error exists in one or both of the data sets. Possible sources of such error could lie in the calibration of the cryostat, or in a variation in the energies of the incident muons. In any μSR experiment, thermalisation of muons in the bulk of the sample is certain to lead to a systematic error in

temperature measurement as a result of local thermal excitation in the vicinity of the muon. This systematic error is likely to depend on the average energy of the muons impinging upon the sample, which varies from one experimental facility to another.

Some authors[85] have suggested a "residual" isotope effect, present after correction for the proton:muon magnetic moment ratio, and still present when angular preferences have been accounted for, to exist in the muonic ethyl radical, which increases the muon coupling by a factor of about 1.2 with respect to A^{β}_{H} in $CH_3\dot{C}H_2$. The arguments initially presented in support of this view were based upon consideration of the angle-dependent hyperfine parameter B in isolation from its angle-independent partner A and from the overall hyperfine coupling constant A'_{μ} or A^{β}_{H}. In the muonic radicals B is in the range 190-200 MHz; in isotopomers not containing Mu, the proton couplings yield values of B in the range 150-160 MHz. Such arguments must be regarded with some caution. In the absence of an angle-independent term these observations would indeed suggest the existence of a residual isotope effect. However, the parameter A takes a significantly negative value in the muonic radicals, while in those from which Mu is absent it is approximately zero, and this fact virtually cancels the effect of the weighting of B on the overall hyperfine coupling constant. While considerations of the residual isotope effect are therefore somewhat inconclusive, they are of interest in that they introduce the "hyperconjugative" theory of conformational preference in the muonic ethyl radical.

2.1.7 The Muonic Ethyl Radical and Hyperconjugation.

The term "hyperconjugation" was coined by Mulliken, Rieke, and Brown[93] in 1941 with reference to C-H electron delocalisation effects, in a piece of quantum-mechanical work intended to explore the processes underlying the "Baker-Nathan Order"[94] of the relative electron-releasing

strengths of different alkyl groups, and, in general, the effect of different alkyl substituents upon reaction rates. It fell into general use in the ensuing two decades, and in 1958 inspired a conference in its honour[95]. As the term originated in attempts to describe the reactivities of species in electronic singlet states, a degree of imprecision is introduced when its use is extended to free radicals. In this context it is generally understood[96] to describe delocalisation of electronic spin density through space between nuclei non-adjacent along the canonical bonding pathway (although this definition itself admits of multiple interpretations, depending on whether or not this delocalisation of spin density is accompanied by a release of overall charge density). The relevance of the concept of hyperconjugation to the work presented here derives from its employment as a device to explain the "unexpectedly" high values obtained for β-proton coupling constants in unconjugated π-radicals such as ethyl[48].

In species of this kind the theoretical view of hyperconjugation hinges on the overlap between electronic systems of p and π symmetry. For the ethyl radical a simple, if rather extreme molecular orbital approach is as follows[97]. The three methyl hydrogen 1s orbitals a, b, and c are reformulated into a set of orthogonal group orbitals.

$$\psi_1 = \frac{1}{\sqrt{3}}(a + b + c) \qquad (2.21a)$$

$$\psi_2 = \frac{1}{\sqrt{2}}(b - c) \qquad (2.21b)$$

$$\psi_3 = \frac{1}{\sqrt{6}}(2a - b - c) \qquad (2.21c)$$

While ψ_1 is approximately of threefold symmetry about the C-C internuclear axis, ψ_2 and ψ_3 have nodal planes intersecting this axis, the result of which is that they resemble a pair of p_y and p_z orbitals. If the methyl C atom forms two sp_x hybrid orbitals along the C-C direction, then one of these can be regarded as forming the C-C bond while the other joins with ψ_1 to generate a single C-H_3 bond. The

remaining p_y and p_z orbitals on the methyl carbon atom can overlap ψ_2 and ψ_3, and the p_z orbital can also overlap with C_α. The unpaired electron can then conceptually occupy a molecular π-orbital comprising contributions from the p_z orbitals of both carbon atoms and the methyl hydrogen group orbital ψ_3.

It is well known that hyperconjugative effects are most significant in cationic systems, where the overlap between a vacant p-type function, ψ_p, and a filled orbital of π-symmetry, ψ_π, is strong and stabilising[98]. At the level of second-order perturbation molecular orbital theory the stabilising two-electron interaction energy between such a pair of orbitals is given by[99]

$$\delta = \frac{[\int \psi_p \hat{H} \psi_\pi d\tau]^2}{|E_p - E_\pi|} \qquad (2.22)$$

Within the Wolfsberg-Helmholtz approximation[100] equation (2.22) can be simplified to yield an expression describing the energy of hyperconjugation in terms of the overlap between the interacting orbitals.

$$\delta = \frac{[\int \psi_p \psi_\pi d\tau]^2}{|E_p - E_\pi|} \qquad (2.23)$$

As the overlap shows an angular dependence related directly to the cosine of the angle γ between the interacting functions, it is clear that the hyperconjugative energy is correctly represented by a $\cos^2\gamma$ relationship. Theoretical studies on the conformational dependence of secondary β-deuterium isotope effects[98,99] have borne out the veracity of this relationship, while confirming the much greater significance of hyperconjugative effects in cationic species (in which the interacting p-orbital is empty) than in neutral radical species (in which the p-orbital is half-filled). This latter is a consequence of the relative weakness of 1-electron and 3-electron interactions as compared to

2-electron interactions.

Fessenden[47], in his analysis of ESR results, describes the hyperfine parameter A as a term arising from spin polarisation processes, and simply ascribes B to the dependence on γ of the spin density at the β-nucleus. Krusic *et alia*[48] elaborate upon this by stating that B arises from hyperconjugative delocalisation. Indeed, the angular dependence of B suggests that this is the case. It is, however, possible that the parameter conceals a variety of mechanisms for the transmission of spin density which share this angular dependence. In the remainder of this work, the use of terminology such as "hyperconjugation" will be kept to a minimum. Rather, an attempt will be made to account for the hyperfine coupling phenomena found in muonic radicals using less ambiguous ideas often based upon molecular orbital theory.

2.2 Five Self Consistent Field Geometry Calculations.

2.2.1 Preamble.

In order to test theories of the electronic structure of the ethyl radical, and in an attempt to account for some of the properties of its muonic isotopomers, a series of calculations were carried out at UHF-SCF level using the GAMESS package of *ab initio* molecular orbital programs as implemented upon the CYBER 205 supercomputer at UMRCC. The basis set chosen was as follows. Dunning's [5s4p] contraction[61] of Huzinaga's (10s6p) primitive basis set for first row atoms[101] was used for each carbon atom, together with the corresponding [3s] set, contracted from (5s), for each hydrogen atom. This set was supplemented with polarisation functions[102], consisting of a single set of d-functions centred on each carbon atom and a set of p-functions at each hydrogen atom. Dunning states that when augmented with suitable polarisation functions in this way, this basis should yield wavefunctions of near Hartree-Fock accuracy.

In the calculation by *ab initio* methods of hyperfine coupling constants in free radicals containing first row atoms, it is generally found[74,103] that a wavefunction from which the contaminating spin multiplets have not been removed overestimates with respect to experiment, while a spin-projected wavefunction underestimates. This is in accordance with perturbation theory arguments[104]. Since in the first instance it was the purpose of these calculations to determine the energies corresponding to various geometries of the ethyl radical, rather than to evaluate the hyperfine coupling constants to a high level of numerical accuracy, the unprojected UHF technique was considered sufficiently precise. In any case, the degree of higher multiplet contamination of the resulting wavefunctions was estimated to be about 1%. SCF convergence was considered to have been achieved when the change in elements of the density matrix was less than 10^{-5} in a single SCF iteration. The criteria for convergence of the geometrical optimisation algorithm were as follows.

maximum change in geometrical variables < 1×10^{-3} bohr

average change in geometrical variables < 6.7×10^{-4} bohr

maximum gradient < 4.4×10^{-4} hartree/bohr

average gradient < 3.0×10^{-4} hartree/bohr

2.2.2 Full Geometry Optimisation.

A calculation was performed on the ethyl radical in which the fifteen independent geometrical parameters were allowed to optimise freely. The resulting conformation was found to be of the "eclipsed" type, in common with the results of other *ab initio* calculations on this radical[73,74,86]. The corresponding total energy, nuclear energy, and electronic energy are reproduced below, together with a pictorial representation of the converged geometry (**Figure 2.5**).

E_{total} = -78.625718 hartree

E_{el} = -115.635706 hartree

E_{nuc} = 37.009987 hartree

Figure 2.5 Fully optimised eclipsed geometry of the ethyl radical (Conformer (I)).

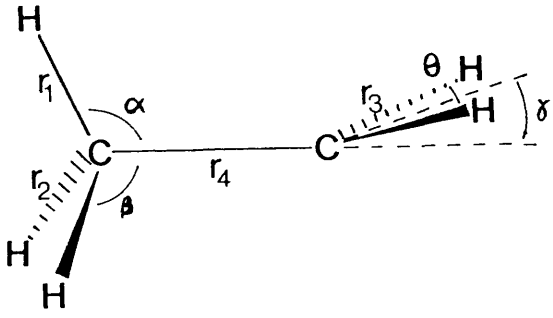

r_1 = 109.0 pm ; r_2 = 108.4 pm;

r_3 = 107.4 pm ; r_4 = 149.8 pm;

α = 111.54° ; β = 111.34° ;

ϑ = 117.57° ; γ = 11.8°.

In terms of bond angles the methyl group is not significantly distorted from a tetrahedral sp^3 arrangement, although the eclipsing methyl C-H bond is noticeably longer than the other two. The methylenic moiety, however, is considerably displaced from a planar trigonal sp^2 arrangement. In future discussion of these calculations the geometry obtained in this instance will be referred to as Conformer (I).

2.2.3 Eclipsed Geometry with Planar Methylene Group and all Methyl C-H Bond Lengths Held Equal.

The orientation of the methylenic segment has long been an object of contention among those who have performed quantum chemical calculations on the ethyl radical. While Pacansky and Coufal[75] , having obtained a conformation of least energy in which the methylenic protons are several degrees out of the plane, note that the SCF energy difference between the staggered and eclipsed forms (which they calculate at 0.83 kJ mol^{-1}) vanishes if the methylenic moiety is forced to be planar, Feller and Davidson[104] comment that the force in stringent SCF-CI calculations is always towards a planar methylene group. Verification

of the truth of the latter statement is outwith the scope of this thesis, but in order to explore the effect of a planar methylene group on the conformational energy and other properties, two further calculations were performed on eclipsed conformers of the ethyl radical. In the first of these the additional condition was placed upon the molecule that all the C-H bonds of the methyl group should be equal in length. The total molecular energy is shown below, along with its nuclear and elactronic components, and the converged geometry is displayed in **Figure 2.6**.

E_{total} = -78.625477 hartree

E_{el} = -115.635306 hartree

E_{nuc} = 37.009829 hartree

Figure 2.6 An eclipsed conformer of the ethyl radical having the methylene part constrained planar and all methyl C-H bonds equal in length (Conformer (II)).

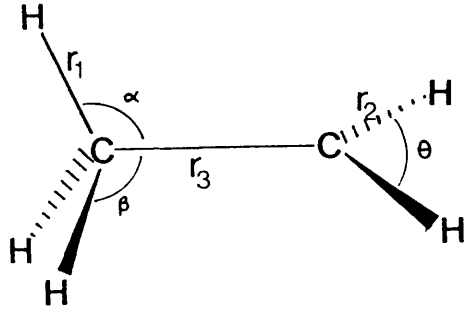

r_1 = 108.6 pm ; r_2 = 107.3 pm ;

r_3 = 149.7 pm ; α = 111.78° ;

β = 111.22° ; ϑ = 117.72° .

The "hybridisation" of the methyl group is not greatly altered from Conformer (I), but the C-H bond lengths are found to be intermediate between the freely optimised value for the long eclipsing bond and those for the two shorter bonds. The C-C and methylene C-H internuclear distances are virtually unaltered. Probably the most significant difference is in the energy of the radical, which is increased by several hundreds of $J mol^{-1}$ with respect to the freely optimised

conformation. This has its origin entirely in a destabilisation of the electronic component, the classical internuclear repulsion energy having in fact decreased slightly.

2.2.4 Eclipsed Geometry with Planar Methylene Group, all other parameters free.

In this, the last geometry optimisation to be performed upon an eclipsed conformation of the ethyl radical, the planarity of the methylene group was retained, but the methyl group was allowed to relax. The resulting energies appear below, and the geometry is presented pictorially in **Figure 2.7.**

E_{total} = -78.625486 hartree

E_{el} = -115.633330 hartree

E_{nuc} = 37.007843 hartree

Figure 2.7 An eclipsed conformer of the ethyl radical with the methylenic moiety constrained to planarity (Conformer (III)).

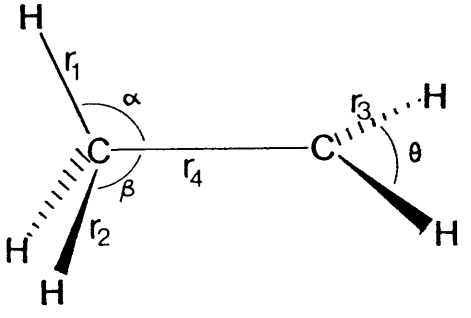

r_1 = 108.9 pm ; r_2 = 108.5 pm ;

r_3 = 107.3 pm ; r_4 = 149.7 pm ;

α = 111.74° ; β = 111.19° ;

ϑ = 117.71° .

Relaxation of the methyl group brings about little change in bond angles or internuclear distances, and little improvement in the total energy. The length of the eclipsed bond, r_1, increases by 0.3 pm to a value just short of that obtained in the unconstrained optimisation (I), while there is a corresponding slight diminution of r_2. There is a very slight "opening out" of the methyl group, characterised by small decreases in both α and β. Comparing the orientation of the methyl group in these last

two calculations with that found in Conformer (I), it can be seen that the upward tilt of the methylene group in the unconstrained geometry is accompanied by a slight upward tilt in the methyl moiety, a lengthening of r_1, and a shortening of r_2. It is possible to view this as a very small step away from the conventional representation of an sp^3 methyl group joined to an sp^2 methylene group in the direction, not of a bridged structure such as that of $C_2H_5^+$ [105], but of a structure more typical of the ethyl anion $C_2H_5^-$ [106], or its isoelectronic congener methylamine CH_3NH_2 [107], in which each first row atom is at the centre of a distorted tetrahedral or pyramidal arrangement.

2.2.5 Staggered Geometry.

Two calculations were also performed near the geometry corresponding to the torsional barrier (related to the equilibrium conformation by a twist of $\pi/6$ around the C-C bond). The first of these calculations, in which all the geometrical degrees of freedom except for the torsional angles were optimised, represents a search for the torsional saddle point (accurate for this basis set and level of computation) at which forces on all internal co-ordinates except the torsional co-ordinate are zero. The energies resulting from this calculation are shown below, and the converged geometry appears in **Figure 2.8**.

E_{total} = -78.625494 hartree

E_{el} = -115.631814 hartree

E_{nuc} = 37.006320 hartree

Here the geometry of the methyl group has changed, albeit only slightly. The C-H bond in the plane of the methylene group is shorter than the others, and the angle made by this bond with the C-C axis is smaller than the other H-C-C angles. This is a reversal of the situation in the eclipsed geometries, but in all cases both staggered and eclipsed the deviation of the symmetry of the methyl group from

Figure 2.8 The torsional saddle-point geometry of the ethyl radical (Conformer (IV)).

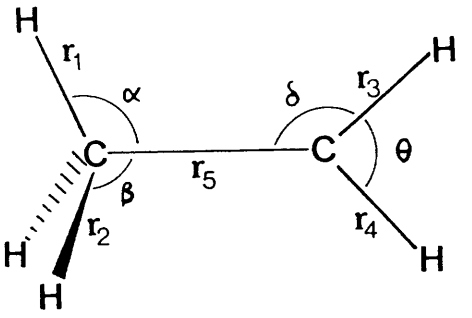

r_1 = 108.3 pm ; r_2 = 108.8 pm;
r_3 = 107.3 pm ; r_4 = 107.4 pm;
r_5 = 149.8 pm ; α = 111.38° ;
β = 111.44° ; δ = 121.48° ;
ϑ = 117.95° .

C_{3V} is slight. The methylenic group has also lost its mirror plane passing through the axis of the p-orbital containing the unpaired electron, but again the deviation is small. The total energy corresponding to this geometry is 587 $J mol^{-1}$ greater than that of the freely optimised eclipsed conformation (I), but is on a parallel with the partially constrained eclipsed geometries (II) and (III) in which the methylene group is held planar. On analysis of the total energy into its nuclear and electronic components, it is seen that the classical energy of internuclear repulsion is lower for this conformation than for (I) (indeed, than for any of the eclipsed conformations) and that the raising of the overall energy arises through the electronic term. It seems, then, that the SCF barrier to internal rotation in the ethyl radical originates largely in the need to flatten the CH_2 part of the radical in order that such a motion can occur.

2.2.6 Staggered Geometry with all Methyl C-H Bond Lengths Equal.

A second calculation was carried out on the "staggered" (or "barrier") conformation of the ethyl radical in which, this time, all the methyl C-H bonds were constrained to be equal in length, as in the eclipsed conformer (II). In the converged geometry residual non-zero forces exist on the following internal co-ordinates: torsion about the C-C

bond, and stretches and compressions in the methyl C-H bonds. The energies resulting from this calculation are shown below.

E_{total} = -78.625486 hartree

E_{el} = -115.634653 hartree

E_{nuc} = 37.009166 hartree

Details of the converged geometrical parameters are displayed in **Figure 2.9.**

Figure 2.9 Constrained saddle-point geometry of the ethyl radical (Conformer (V)).

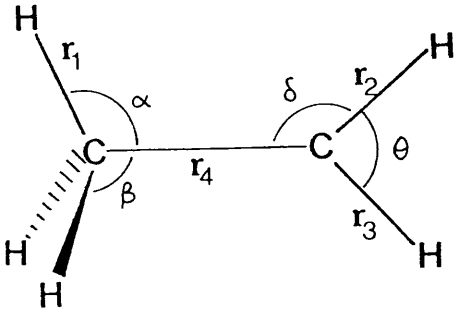

r_1 = 108.6 pm ; r_2 = 107.3 pm;

r_3 = 107.4 pm ; r_4 = 149.8 pm;

α = 111.38° ; β = 111.44° ;

δ = 121.48° ; ϑ = 117.95° .

Except for a small change in the methyl C-H bond lengths, necessitated by the requirement that all three H nuclei be equidistant from C, in which the two long bonds shorten and the short bond lengthens, the geometrical parameters remain virtually unaltered from those of Conformer (IV). The total energy of this conformer is identical with that of Conformer (III). Analysis of this energy into its electronic and nuclear components reveals that the small increase in energy compared to Conformer (IV) is due to an increase in the nuclear repulsion term, for which a lowering of the electronic component narrowly fails to compensate.

In consideration of the five calculations described above, in particular those yielding conformers (I) and (IV), it is worthy of note that the equilibrium conformation is determined by a minimum in the electronic energy while the torsional saddle-point conformation is determined by a minimum in the internuclear repulsion energy.

Table 2.2 *Ab initio* molecular orbital calculations of differences in total energy, electronic energy, and nuclear energy for conformations of the ethyl radical, expressed relative to those of Conformer (I). The internuclear distance C-H_x, H_x being the hydrogen nucleus which eclipses the p_z orbital in conformers (I), (II) and (III), and falls into its nodal plane in conformers (IV) and (V), is also listed.

Conformer	R(C-H_x) /pm	ΔE_{nuc} /kJmol^{-1}	ΔE_{el} /kJmol^{-1}	ΔE_{total} /Jmol^{-1}
(I)	108.98	0	0	0
(II)	108.62	-0.416	1.048	632
(III)	108.92	-5.629	6.237	608
(IV)	108.27	-9.629	10.216	587
(V)	108.59	-2.155	2.763	608

2.2.7 Further Considerations.

The trends in energy and internuclear distance discussed above are exhibited quantitatively in **Table 2.2**. Turning attention to analysis of the molecular orbital populations, it is found that the population of the $2p_z$ orbital located at the methylenic carbon atom is lower in the least energy conformer (I) (where it takes a value of 0.974) than in either of the other eclipsed conformers (in each of which it is 0.983). The s-population of the eclipsing methyl H atom shows a complementary small increase from 0.465 to 0.468. Consideration of these observations in conjunction with the increased C-H_x distance in (I) leads to an understanding of the conformational preference displayed by the ethyl radical in terms similar to the Brunck-Weinhold hypothesis[108,109], in which

torsional barriers in ethane-like molecules are attributed to vicinal interactions between orbitals of bonding and antibonding type. Strikingly, the SOMO in (I) is more stable than those in (II) or (III) by 6.42 kJ mol^{-1}, and possesses a larger component deriving from s-functions centred on the methylenic H atoms. The SCF barrier to internal rotation in the ethyl radical, as measured by the energy difference between conformations (I) and (IV), is 587 J mol^{-1}. If the methylene group is constrained to planarity, however, the barrier vanishes.

Table 2.3 Calculated atom spin densities for conformers of $\dot{C}_2H_5$. (H_x, H_y, H_z are the methyl H atoms; H_a and H_b are the H atoms of the methylenic group.)

Atom	Conformer				
	(I)	(II)	(III)	(IV)	(V)
C_{CH_3}	-0.094	-0.097	-0.097	-0.097	-0.097
C_{CH_2}	0.251	0.232	0.232	0.232	0.232
H_x	0.045	0.044	0.044	0.003	0.003
H_y, H_z	0.013	0.014	0.014	0.034	0.034
H_a	-0.039	-0.040	-0.040	-0.040	-0.040
H_b	-0.039	-0.040	-0.040	-0.039	-0.039

Table 2.3 gives the atomic spin densities corresponding to these calculated conformations. The proton (or reduced muon) coupling constants, expressed in MHz, may be obtained from the H spin densities by multiplication by 1420. Little change in the spin densities is seen within a set of conformations of a given type, except that the methylenic

carbon atom has a higher spin density in Conformer (I) than in either of the constrained eclipsed conformers. **Figure 2.10** shows the dependence of the methyl H spin density - directly related to the coupling constant - on the torsional angle γ. The conformers used to generate this diagram were (I), (IV), and a further conformer in which all parameters were freely optimised except for γ, which was constrained in such a way that a geometry produced from (IV) by a 10° twist around C-C was the result. The solid curve is $0.0034 + 0.042\cos^2\gamma$, obtained by a least-squares fit.

Recent results by Percival and co-workers[110] using the technique of muon Level Crossing Resonance spectroscopy have shown that at around room temperature $\overline{A} = \frac{1}{3}(A'_{\mu} + 2A_H^{Me})$ is significantly greater than the temperature-independent methyl proton hyperfine coupling constant in $\dot{C}H_3CH_2$. This is not surprising, as at this temperature the methyl H atoms are predominantly sampling conformations near the equilibrium torsional geometry (with $\gamma(Mu) = 0°$). This "residual isotope effect" might be expected to diminish with increasing temperature as free internal rotation is approached. Interestingly, Percival *et al.* obtain a ratio of $|A^{\alpha}(^{13}C)|:|A^{\beta}(^{13}C)|$ of 0.34, less than that corresponding to Conformer (I) above (which, in turn, is less than those corresponding to any of the other calculated conformers). It might therefore be inferred that the vibrationally-induced lengthening of the mean C-Mu bond encourages non-planarity at the methylene carbon to the extent that the overall conformation is yet more extremely distorted from the conventional picture in the direction of a methylamine-like geometry.

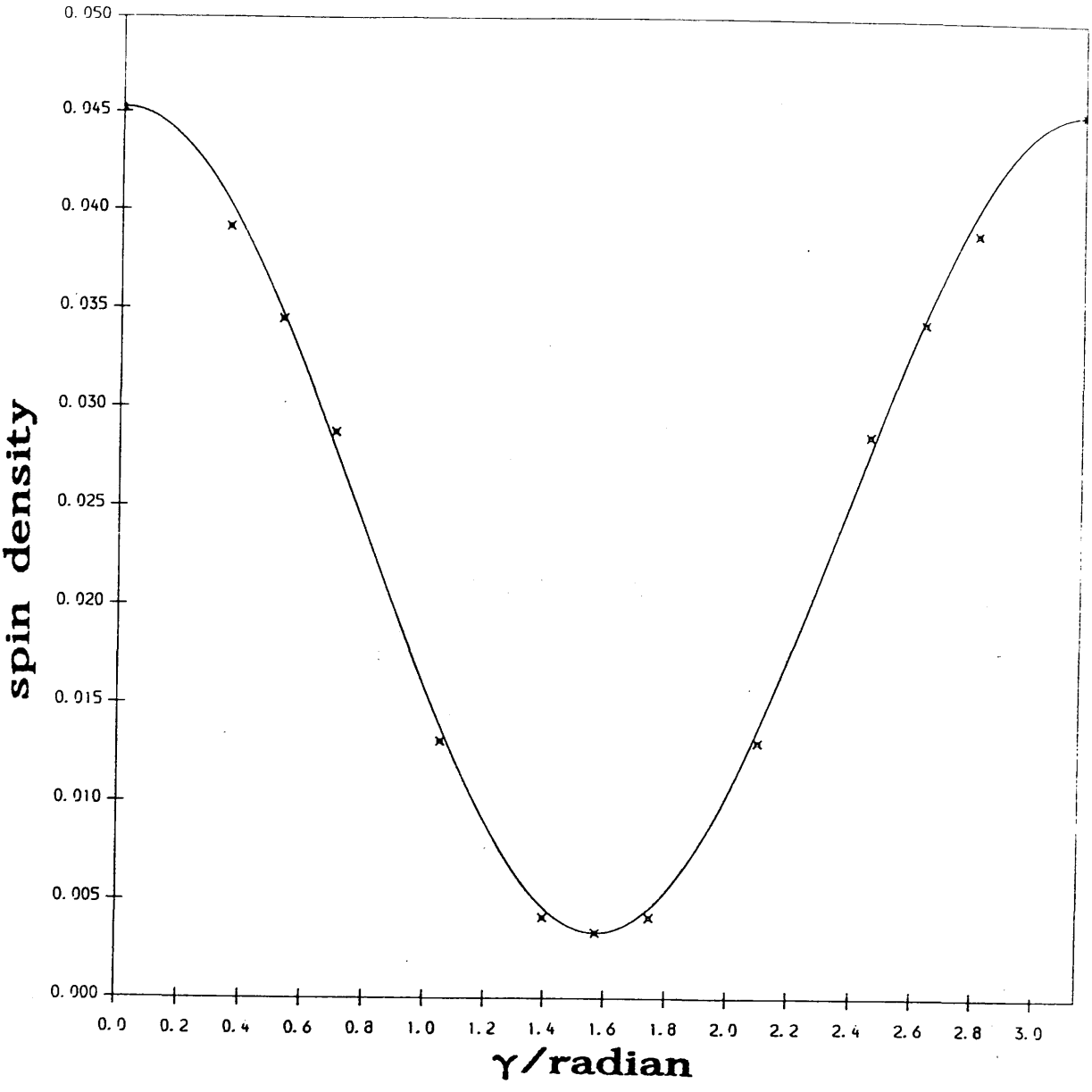

Figure 2.10 *Ab initio* methyl proton spin density (at the TZVP level) against torsional angle.

CHAPTER 3

Experimental Studies on α-Muoxyalkyl Radicals.

"Theory is grey, but the golden tree of life is green."

J. W. von Goethe.

3.1 Historical Perspective — α-Hydroxyalkyl Radicals.

Electron spin resonance studies upon α-hydroxyalkyl radicals (A) began with the work of Gibson *et alia*[111] over thirty years ago. Much

(A) 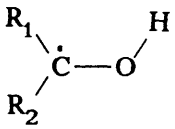

interest was shown in radicals of this type in the decades that followed, and many ESR studies were undertaken. These experiments were characterised by a variety of research motivations and methods of radical production. Typically the radicals were generated *in situ* by photochemical or radiochemical means. Structural information yielded by these studies challenged some traditionally held views regarding free radical conformation.

The earliest ESR studies on the hydroxymethyl radical $\dot{C}H_2OH$[112] revealed a slightly distorted three line spectrum; it was inferred that the cause of the distortion was the presence of another spectrum having a different g-value and five lines. The triplet, with a coupling constant of about 47.6 MHz at 300 K, was assigned to the coupling of the unpaired electron with the α-protons, that is to say, the protons directly attached to the radical centre. Further investigation and improved resolution[113,114] revealed that each line in the triplet forming the main feature of the spectrum was in fact a poorly resolved doublet. Clearly, then, a small amount of electronic spin density is delocalised over a greater distance and experienced by the proton at the β-position (or, in other words, attached to the oxygen atom). The coupling of this hydroxylic proton was measured to be 6.05 MHz[48],

showing some variation with temperature[115]. Further ESR experiments on the fully deuterated isotopomer of the hydroxymethyl radical[48], by consideration of the deviation of multiplet height ratios from those expected on the basis of the coupling of two identical I = 1 nuclei, indicated the inequivalence of the α-deuterons, and therefore, by logical extension, of the α-protons in the protonic analogue. The α-couplings also showed a small temperature dependence; with $A = (A^1_\alpha + A^2_\beta)/2$, it was found that $dA/dT \approx 13.2\,kHz/^oC$, assuming a linear relationship. This effect is thought to be vibronic in origin.

Within a notional framework of ideal orbital hybridisation, and from consideration of the nonequivalence of the two α-protons and the small hyperfine coupling constant of the β-proton, the conformational situation prevailing in this radical may be considered in its simplest form as a slow interchange between the two equivalent planar conformations (I) and (II) depicted in **Figure 3.1** below.

Figure 3.1 Conformational interchange in the hydroxymethyl radical.

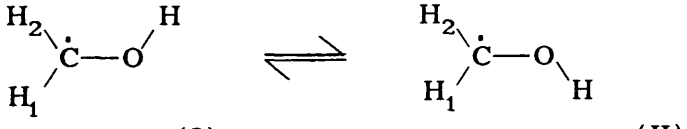

(I) (II)

These two conformations are interconverted by internal rotation around the C-O bond. Krusic *et alia* have calculated the activation barrier for this exchange to be $E_o = 19\,kJ\,mol^{-1}$, with a corresponding frequency parameter of $\nu_o = 3.98 \times 10^{12}\,s^{-1}$, using a density matrix method. This is somewhat larger than their value for the static potential barrier to internal rotation, $V_2 = 17\,kJ\,mol^{-1}$, obtained through a combination of INDO calculations (to determine "suitable" parameter values) and least-squares fitting methods similar to those employed in this work.

(Use of a classically modelled static barrier led Krusic *et al.* to values of V_2 which were larger than those produced from their quantum mechanical calculation; a large barrier and small moment of inertia mitigate against the accuracy of the classical approximation.)

The absolute values of the α-H coupling constants in α-hydroxyalkyl radicals are found to be "anomalously" low when compared, for example, to those in $\dot{C}H_2COCH_3$, and this observation is usually explained by assuming some nonplanarity at the radical centre, allowed (in terms of canonical bonding schemes) by a lack of double bond character in the C-O bond, related to a lack of conjugation in the π-system. However, some contribution from a π-bonded canonical form must be inferred to be present in order to explain the barrier to internal rotation in the hydroxymethyl radical, considerably larger than those found in unconjugated π-radicals such as ethyl.

Some diminution of the couplings of α-protons in α-hydroxyalkyl radicals compared to those in alkyl radicals might in any case be expected as a consequence of spin delocalisation onto oxygen.

In paramagnetic resonance studies by Krusic *et alia*, the homologous methoxymethyl radical ($\dot{C}H_2OCH_3$), produced in solution by chemical reaction of t-butoxy radicals with diethyl ether, showed similar spectral properties to hydroxymethyl, the principal difference being the replacement of the hydroxylic proton doublets by methoxylic proton quartets. A somewhat higher activation barrier to the exchange between symmetry-related conformers was obtained but, despite the existence of a variation with temperature in the methoxylic proton couplings, no static torsional barrier was determined.

The first paramagnetic resonance studies of the hydroxyethyl radical ($CH_3\dot{C}HOH$) were conducted by Smaller and Matheson[69], but it was not until the advent of the mixed flow method of Dixon and Norman[113]

that reasonably accurate measurements of the proton couplings became available. These authors determined $A_H^{CH_3}$ to be 61.6 MHz and A_H^{CH} to be 42.0 MHz from a spectrum consisting of a 1:3:3:1 quartet of 1:1 doublets. The hydroxylic proton coupling was not observed due to the fact that Dixon and Norman's experiment was carried out in an acidified aqueous solution (a feature of the rapid mixing technique), and consequently fast exchange processes with protons in solution could occur[116]. The photolytic method of Zeldes and Livingston[117], in which a solution of up to approximately 1% hydrogen peroxide in the alcohol to be studied was subjected to intense ultraviolet irradiation, overcame this obstacle and, in addition to obtaining more accurate values for $A_H^{CH_3}$ and A_H^{CH}, they obtained A_H^{OH}, the hydroxylic proton coupling, together with the temperature dependences of all three coupling constants. $A_H^{CH_3}$ and A_H^{CH} show the expected small vibronic temperature variation; A_H^{OH} shows a pronounced dependence, stronger than that of the analogous coupling in hydroxymethyl. Although Zeldes and Livingston did not obtain sufficiently many temperature points on the hydroxylic proton coupling for a comprehensive analysis, they noted a decrease in the absolute value of the coupling with increasing temperature, until at room temperature it could no longer be resolved, and inferred a negative sign for this coupling constant, passing through zero in the vicinity of room temperature, and becoming positive at higher temperatures. In a much more recent, more accurate, and considerably more comprehensive study by Cirelli and co-workers[118], all three proton coupling constants in this radical were reported over ten temperature values spanning the range 153 K to 364 K. Over this range the hydroxylic couplings follow an approximately linear relationship with temperature, having a positive temperature coefficient (which Cirelli *et alia* confirmed by means of complementary quantum mechanical

calculations) and passing through zero at about 280 K. The experimental points of Zeldes and Livingston fall some distance below the linear regression best-fit straight line of Cirelli *et al.*; it is likely that this is a result of hydrogen bonding interactions inherent in the experimental environment used by Zeldes and Livingston. Cirelli *et al.* demonstrate that the addition of ethanol to their solutions in aprotic solvents produces a lowering of the coupling constant of the hydroxylic proton. The experimental method of Cirelli *et al.*, in which the sample consists of 0.05 M aldehyde in an aprotic solvent, effectively removes all hydrogen-bonding and proton exchange interactions between the radical and the solvent, and drastically reduces radical-radical and radical-aldehyde associations by dilution. (That interactions of the latter kind persist to a small extent is shown through a slight dependence of the hydroxylic coupling upon aldehyde concentration which was evident at low temperatures.)

The 2-hydroxyprop-2-yl radical ($(CH_3)_2\dot{C}OH$) was first observed using magnetic resonance techniques by Gibson and co-workers[111], who subjected a 50% H_2O_2/H_2O glass containing isopropanol to ultraviolet irradiation from a mercury arc at a temperature of 77 K. They observed a septet corresponding to the interaction of the unpaired electron with six equivalent methyl protons. The resolution available in their study was not sufficient for the coupling of the hydroxylic proton to be seen. Later liquid phase photolytic investigations by Zeldes and Livingston[117] on acetone and solutions containing acetone revealed a small hydroxylic proton coupling highly sensitive to changes in temperature. They determined the coupling constant to be 1.96 MHz at 26°C, falling through zero at -22.5°C to negative values at lower temperatures, and suggested that this behaviour might meaningfully be attributed to a negative, temperature-independent contribution

from spin density associated with the oxygen atom and a positive, temperature-dependent contribution from spin density associated with the α-carbon atom. More recently this radical has been subjected to a comprehensive ESR study by Lehni[119] in a variety of organic solvents. The characteristic temperature dependences were observed for both methyl and hydroxylic proton couplings. Measurements were not however made at temperatures sufficiently low to drive the coupling of the hydroxylic proton through zero. Using the "rule of thumb" of Krusic and Meakin[120], Lehni obtains a barrier to internal rotation around the C-O bond of at least 3.5 kJ mol^{-1} for the 2-hydroxyprop-2-yl radical. In consideration of the linewidths obtained in his ESR spectra, Lehni notes that when linewidth is plotted against T/η, where η is the viscosity of the solvent, the experimental points fall into two distinct groups. Those obtained in solvents in which some degree of hydrogen-bonding between the radical and the solvent molecule is possible are smaller than those obtained in hydrocarbons by an amount consistent over the whole range of measurement. The qualitative explanation of this phenomenon lies in the formation of hydrogen-bonded structures in associating solvents which influence the Brownian motion of the radicals. Interestingly, Lehni also notes an increase in linewidth at low T/η, attributed to incomplete averaging of anisotropic hyperfine interactions[97].

3.2 Muon Spin Rotation Studies.

3.2.1 The 2-muoxyprop-2-yl Radical Formed in Propan-2-one.

Muon spin rotation and, indeed, more recently Level Crossing Resonance results on muonic radicals formed in propan-2-one have already been published by Hill and others[6,7,121,122,123], but in this study for the first time a full investigation has been made over the whole liquid range of the compound. (An earlier temperature dependence experiment

carried out at PSI[124], referred to by Hill *et al.*[122], yielded results which were not thought to be quantitatively useful due to irregularities in the temperature regulation produced by a faulty cryostat. The following results were obtained with an improved cryostat, and temperatures, where not otherwise specified, may be considered to be accurate to $\pm$0.1 K.)

An equiportion of propan-2-one (supplied by Aldrich) and d6-propan-2-one (supplied by MSD) of the highest grades available was degassed by the standard procedure of repeated freeze-pump-thaw cycles and sealed in a spherical thin-walled glass vessel. Under a transversely applied external magnetic field of 0.2 tesla a set of muon spin rotation spectra were obtained at a variety of temperatures spanning the liquid range of the mixture. **Figure 3.2** shows a selection of the Fourier transformed spectra after the removal of the signal corresponding to muons in diamagnetic environments using a routine based upon the function minimisation package MINUIT[12]. The signals are characteristic of muoxylic radicals[123]; the coupling constants are small, and show a temperature dependence with a positive temperature coefficient. No evidence of splitting corresponding to an isotopomeric difference in the hyperfine coupling constant can be seen. This is unsurprising, as it is well known that isotopic effects on transmission of unpaired spin density attenuate rapidly with displacement of the isotopic substitution from the nucleus at which the measurement is made. This result may be contrasted with the relatively large effects obtained on isotopic substitution at β-positions which are well documented for the ethyl radical[78]. The reduced muon-electron coupling constant obtained in this liquid is found to vary from 3.6 MHz at 180 K up to 9.4 MHz at 319 K, with only a small deviation from linearity in the dependence. The couplings are displayed in full in **Table 3.1.**

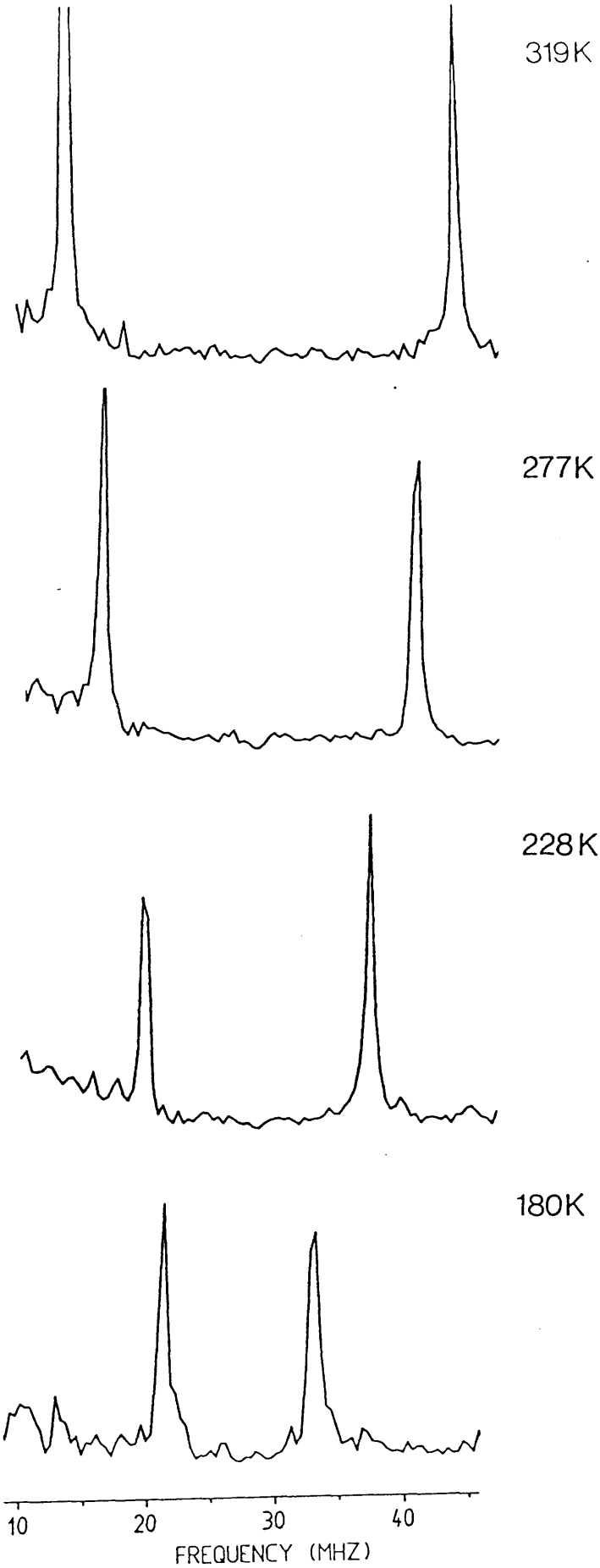

Figure 3.2 Fourier transformed μSR spectra of the 2-muoxyprop-2-yl radical in pure liquid propan-2-one.

Table 3.1 Properties of μSR spectra obtained from a sample consisting of a mixture in proportion 1:1 by volume of propan-2-one with its hexadeuterated isotopomer. Temperatures are in K, transition frequencies and coupling constants in MHz.

T	ν_{12}	ν_{43}	A_μ (A'_μ)
319.0	12.2946	42.1625	29.8679 (9.3827)
300.0	13.6041	40.8703	27.2662 (8.5654)
277.0	15.1290	39.2859	24.1569 (7.5886)
251.0	16.8937	37.3909	20.4972 (6.4390)
228.0	18.4594	35.8995	17.4401 (5.4786)
203.0	20.0172	34.3246	14.3074 (4.4945)
180.0	21.2840	32.8835	11.5995 (3.6439)

Approximately 4×10^7 events were collected per temperature. From the position of ν_D (= 27.3 MHz) the external field was determined to be 0.2013 T.

Figure 3.3 Newman projections of the conformations of the 2-muoxyprop-2-yl radical.

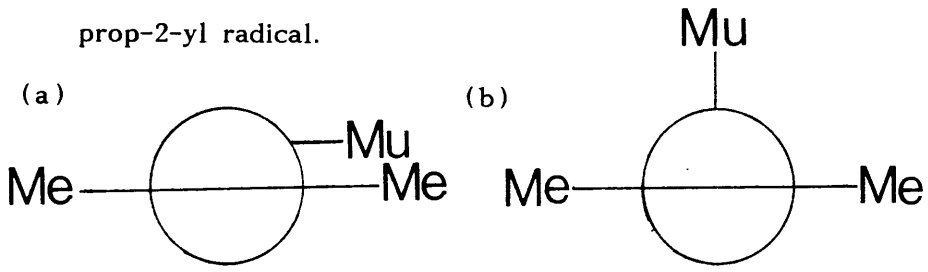

It is commonly assumed that the equilibrium conformation of the 2-muoxyprop-2-yl radical is as shown in **Figure 3.3**(a), having C_s symmetry, a planar radical centre, and the muon lying in the nodal plane of the 2p orbital notionally containing the unpaired electron. The conformation representing the torsional potential maximum around the C-O bond is then supposed to be of C_s symmetry, with the O-Mu bond eclipsing the axis of the 2p orbital, as shown in **Figure 3.3**(b). Within this approximation it is reasonable to assume that the major contribution to the potential barrier to internal rotation is twofold in the torsional angle γ.

Using the statistical theory of rotational averaging, and with a value for the reduced moment of inertia for internal rotation (obtained using the *ab initio* geometry determined in Chapter 5) of $I_R = 1.393 \times 10^{-48}$ kg m^2, a twofold barrier of $V_2 = 3828\,J\,mol^{-1}$ was calculated for this radical in pure acetone, with accompanying hyperfine parameters of A = -117.0 MHz and B = 315.3 MHz. The values obtained for these parameters in this instance are markedly different from those appropriate to the series of isotopically-substituted ethyl radicals, where the angle-independent term A, though significantly still a negative quantity, is much smaller in magnitude. The high temperature limit of the hyperfine coupling constant, given by A + B/2, is 40.65 MHz, still considerably higher than the greatest coupling constant obtained here; hence it is apparent that the torsional barrier is such that free rotational averaging

is not closely approached in the liquid phase for this species. Utilising the torsional eigenvalues obtained from the above calculation, the curve corresponding to the theoretical muon-electron hyperfine coupling constant was determined, extrapolating to temperatures both above and below the extrema of experimental measurement. This curve, illustrated in **Figure 3.4** together with the experimental points, shows a clear minimum at T = 144 K. The value of A'_{μ} at this minimum is 3.2 MHz. This behaviour is qualitatively different from that observed experimentally for the analogous hydrogenic radical, where the coupling constant of the hydroxylic proton can be made to pass through zero at low temperatures.

The explanation of this disparity lies initially in the values of $\langle \cos^2\gamma \rangle_i$, corresponding to the torsional eigenvalues E_i, over which a Boltzmann averaging is performed in order to evaluate the theoretical hyperfine coupling constant at a given temperature. Taking, for example, the hydroxylic proton couplings obtained by Lehni[119] for the 2-hydroxy-prop-2-yl radical in propan-2-ol (which are likely to exhibit the closest resemblance to the μSR results), and subjecting them to a quantum mechanical analysis within the theory of rotational averaging, using a value of 1.231×10^{-47} kg m^2 for the reduced moment of inertia for internal rotation around the C-O bond (larger than that in the muonic radical by a factor of 9), and assuming the equilibrium torsional angle ϑ_0 to be $\pi/2$, the following values for a twofold potential barrier to internal rotation and its associated hyperfine coupling parameters are obtained.

V_2 = 71.4 kJ mol^{-1}

A = -0.041213 MHz

B = 1.3006 MHz

Disregarding for the moment the rather high value calculated for V_2, these results can be subjected to closer scrutiny.

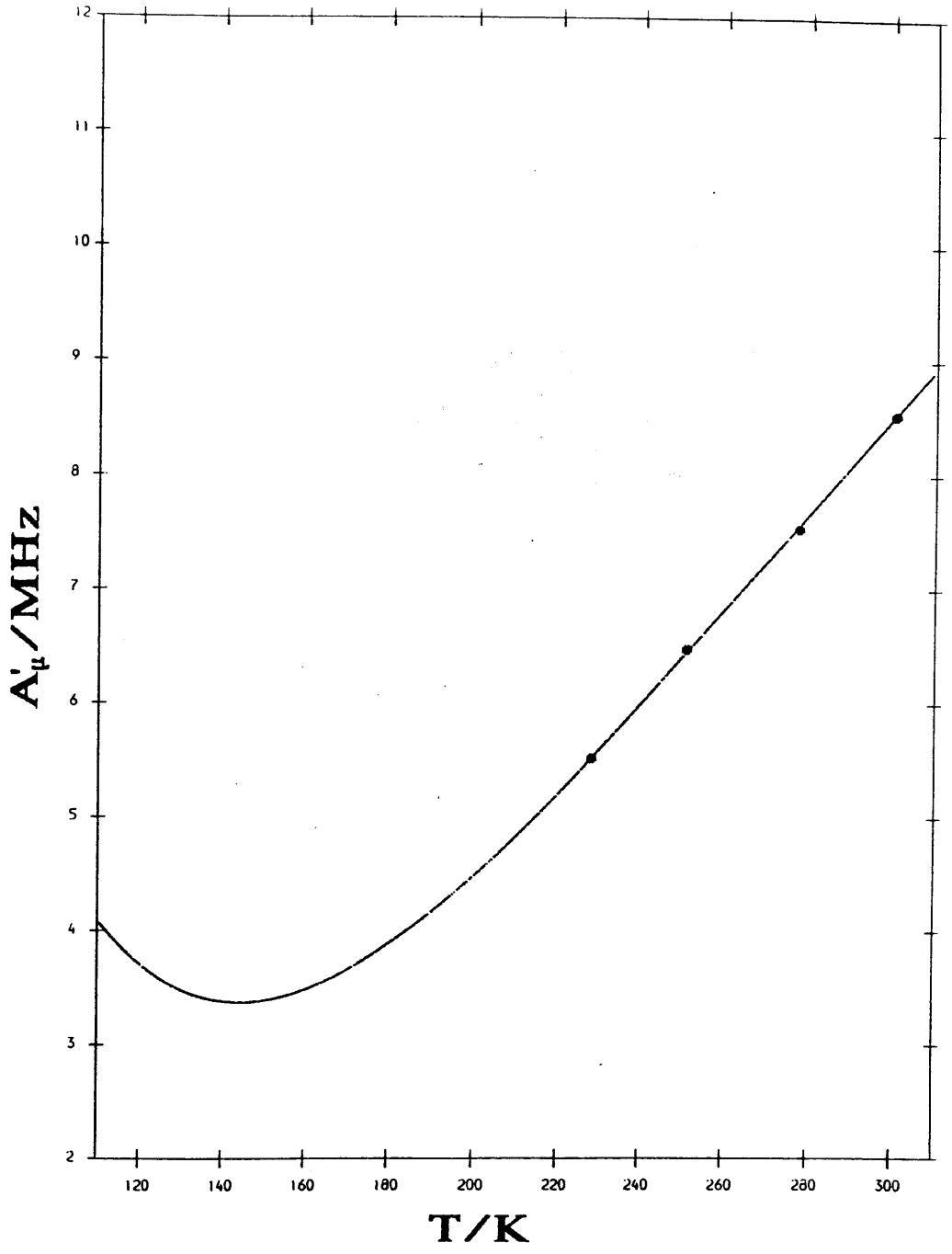

Figure 3.4 Calculated dependence of A'_μ upon T for the 2-muoxyprop-2-yl radical in pure propan-2-one, together with experimental points.

The torsional eigenvalues E_i leading to the above figures are shown in **Table 3.2** below, together with the corresponding values of $\langle \cos^2\gamma \rangle_i$ and the mean hydroxylic proton hyperfine coupling constant $\langle A_H^{OH}(\gamma) \rangle_i$. For all $i > 2$ the coupling constant associated with E_i is positive, and only for $i=1$ is it actually negative. Hence as the temperature is reduced, $A_H^{OH}(T)$ decreases monotonically to a hypothetical limiting value, at absolute zero, of $\langle A_H^{OH}(\gamma) \rangle_1$, or -0.0007 MHz. The temperature dependence of the theoretical hyperfine coupling constant for the hydroxylic proton in the 2-hydroxyprop-2-yl radical is shown in **Figure 3.5.**

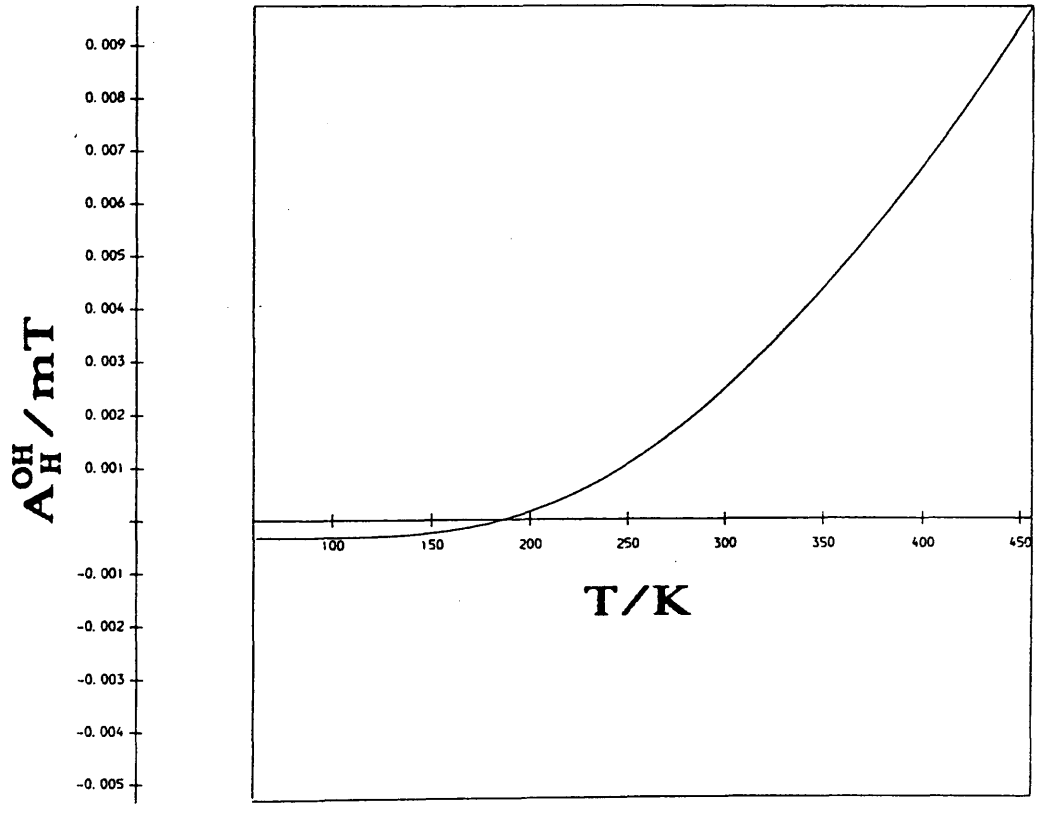

Figure 3.5 Calculated dependence of A_H^{OH} upon T for the 2-hydroxyprop-2-yl radical in isopropanol.

Table 3.2 Torsional eigenvalues E_i (J mol^{-1}) for the 2-hydroxyprop-2-yl radical, together with values of $\langle \cos^2\gamma \rangle_i$ and $\langle A_H^{OH}(\gamma) \rangle_i$ (MHz).

i	E_i	$\langle \cos^2\gamma \rangle_i$	$\langle A_H^{OH}(\gamma) \rangle_i$
1	4343	0.03115	-0.0007
2	4355	0.03171	0.0000
3	12930	0.09582	0.0834
4	13041	0.10049	0.0895
5	21426	0.17018	0.1801
6	21889	0.18678	0.2017
7	30080	0.26311	0.3010
8	31252	0.29866	0.3472
9	39060	0.37701	0.4491
10	41160	0.43220	0.5209
11	48234	0.50525	0.6159
12	51180	0.57570	0.7076
13	57135	0.63933	0.7903
14	60611	0.71333	0.8866
15	65351	0.75520	0.9410
16	67681	0.86021	1.0776
17	70174	0.89097	1.1176
18	77545	0.88597	1.1111
19	78111	0.91494	1.1488
20	81779	0.88062	1.1042
21	81941	0.89136	1.1181

The static potential barrier to internal rotation in the 2-muoxy-prop-2-yl radical as determined by these calculations is smaller by a factor of almost 20 than that in its protonic analogue. This is the reverse of the situation encountered in the substituted ethyl radicals, where the torsional potential minimum occurs at $\vartheta = 0^{o}$ (see section 2.1.5, in which the radicals $CHD_2\dot{C}D_2$ and $CMuD_2\dot{C}D_2$ are compared). The values of E_i, $\langle\cos^2\gamma\rangle_i$, and $\langle A'_{\mu}(\gamma)\rangle_i$ corresponding to the solution of the torsional problem for A, B, and V_2 described above for this radical are listed in **Table 3.3**, and the calculated temperature dependence of the muon-electron hyperfine coupling constant is illustrated in **Figure 3.4**.

From **Figure 3.4** it can be seen that, in the temperature dependence of the β-coupling, the 2-muoxyprop-2-yl radical exhibits properties rather different to its hydrogenic isotopomer. The absolute values are much larger, and there is a minimum at T=144 K, where A'_{μ}=3.2 MHz. The cause of this behaviour lies in the fact that in this case, again, only one torsional state has associated with it a negative coupling constant, but here it is the state for which i=2, whereas in the hydroxylic radical it is the i=1 state. In this case, the i=1 state gives a small positive coupling, and all those with i>2 give positive couplings which are somewhat larger. **Figure 3.6** shows the relative populations of the torsional states at a variety of temperatures.

Figure 3.6(a) represents the populations of the internal rotation states at or near absolute zero. Here all the radicals in the ensemble are in the state of lowest energy, and the net muon-electron coupling is given by $A'_{\mu}(0) = \langle A'_{\mu}(\gamma)\rangle_1 = 10.3$ MHz. **Figure 3.6**(f), which must be regarded as entirely notional, represents the situation at 10^6 K, where the torsional states are almost equally populated. (At such temperatures, of course, no stable molecules would exist.) The intention of this figure is to demonstrate the extent to which it is necessary to raise the

Table 3.3 Torsional eigenvalues E_i ($J\,mol^{-1}$) for the 2-muoxyprop-2-yl radical, together with values of $\langle\cos^2\gamma\rangle_i$ and $\langle A'_\mu(\gamma)\rangle_i$ (MHz).

i	E_i	$\langle\cos^2\gamma\rangle_i$	$\langle A'_\mu(\gamma)\rangle_i$
1	1726.6	0.40372	10.2745
2	3315.0	0.22692	-45.4741
3	5224.3	0.72322	111.0181
4	11495.4	0.48343	35.4076
5	11682.7	0.57965	65.748
6	23564.7	0.51063	43.9853
7	23569.5	0.51433	45.1511
8	40379.3	0.50661	42.7175
9	40379.3	0.50667	42.7348
10	61785.7	0.50415	41.9403
11	61785.7	0.50415	41.9404
12	88439.1	0.50284	41.5291
13	88439.1	0.50284	41.5291
14	119681.2	0.50207	41.2864
15	119681.2	0.50207	41.2864
16	155728.9	0.50158	41.1306
17	155728.9	0.50158	41.1306
18	196594.2	0.50622	42.5938
19	196594.2	0.50622	42.5938
20	242253.0	0.50553	42.3759
21	242253.0	0.50553	42.3759

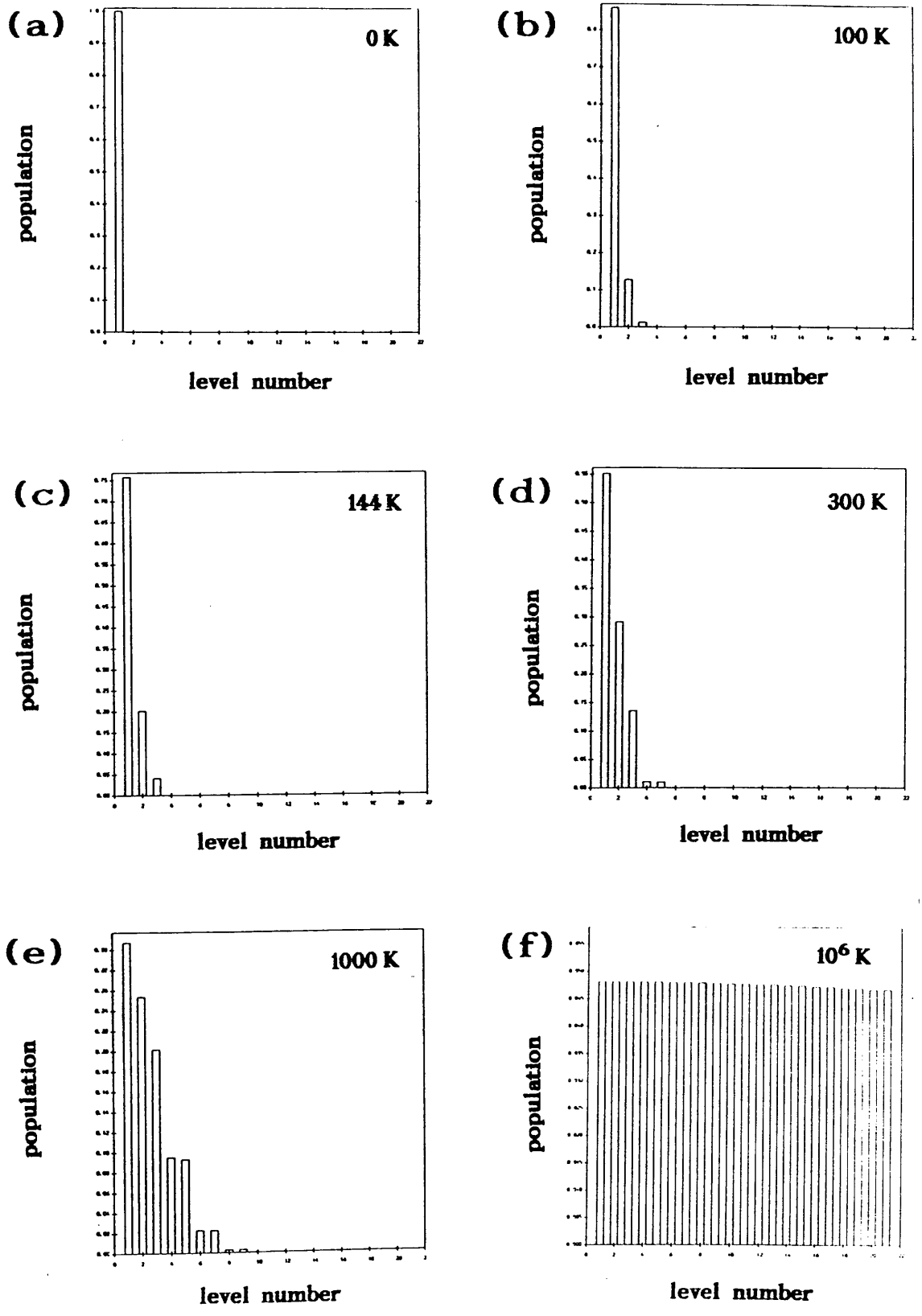

Figure 3.6 Populations of torsional states in $(CH_3)_2\dot{C}OMu$ at six temperatures.

temperature of the system in order to approach the free rotation limit, where $A'_{\mu}(T) = A + B/2$. The intermediate figures show the configuration of the ensemble at temperatures more realistically amenable to experimental investigation. It can be seen that the relative importance of the contribution to the ensemble from the state $i = 2$ is at a maximum at 144 K.

It may also be noticed from the torsional eigenvalues obtained in this calculation that the regime of twofold degeneracy familiar from the theory of free internal rotation, suspended in those levels within or near the static torsional potential well, is restored in the higher levels (at the accuracy of these calculations, in levels above E_7). All these higher levels have similar associated values of $\langle \cos^2\gamma \rangle_i$, and each gives a contribution to A'_{μ} in the vicinity of the latter's high temperature limit. The static twofold potential barrier V_2 and the torsional levels lying within it are pictured in **Figure 3.7**.

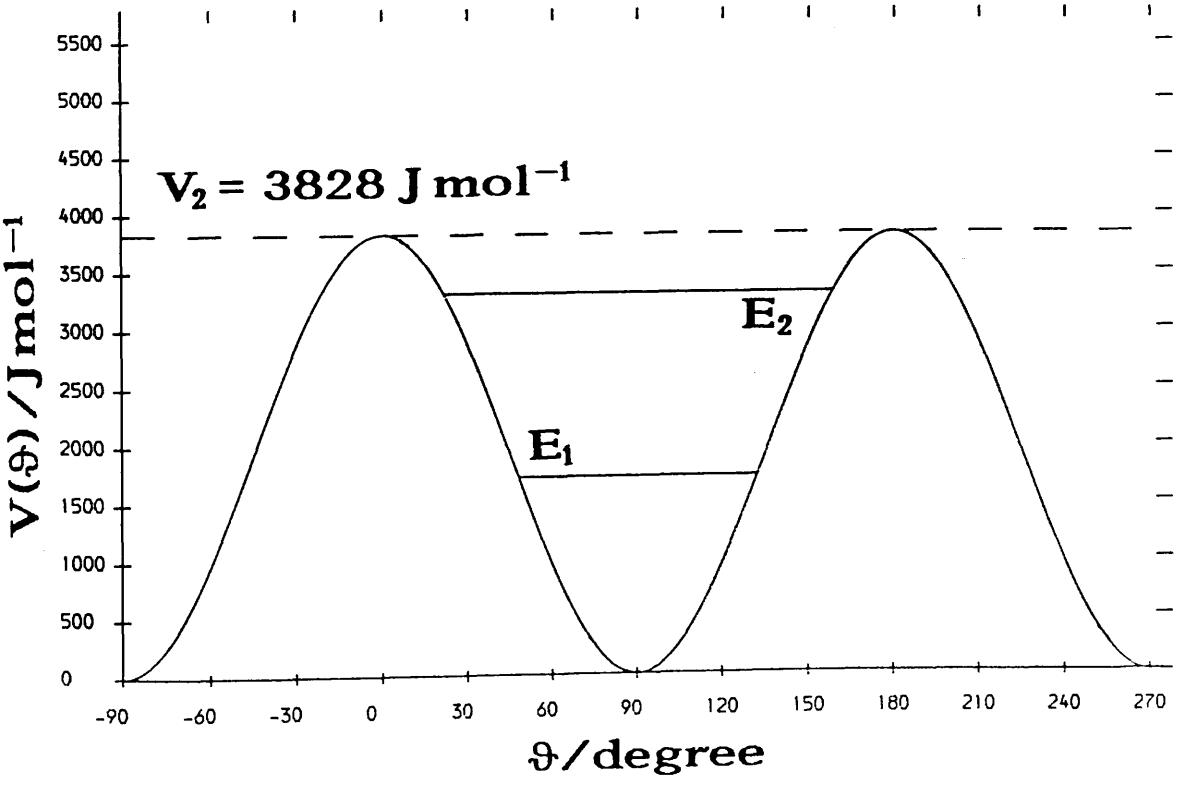

Figure 3.7 Twofold barrier and torsional levels for $(CH_3)_2\dot{C}OMu$.

3.3 The Effect of a Hydrogen-Bonding Solvent on the Dynamical Properties of the 2-muoxyprop-2-yl Radical: μSR Studies on Binary Aqueous Solutions of Propan-2-one.

3.3.1 Radical Environments.

The ESR studies carried out upon α-hydroxyalkyl radicals have, as much by reason of experimental design as of scientific interest, been undertaken in a variety of radical environments. Often, in fact, the nature of the radical environment is not accurately known, for example when the radical is generated by chemical reaction or high energy irradiation. However, as the amount of available data on these radicals increased, it became clear[118,119] that the hyperfine coupling constant of the hydroxylic proton was highly sensitive, not only to variations in temperature, but also to the surroundings in which the radical was generated, to the associations between the radical and its environment.

Radical-radical associations in ESR experiments can, in general, be virtually eliminated by ensuring that the radical concentration remains low, but associations between radicals and solvent molecules cannot so easily be controlled, and it is therefore important that the physical and chemical factors influencing these be understood. Transverse field μSR experiments are typically carried out on pure liquids; hence, barring radiolytical products from the thermalisation of the muon[23], the environment of the muonic radical may be considered entirely to consist of solvent molecules, from which the radical is produced by muonium addition. In the continuous beam μSR experiment, the method of positron counting requires that only one muon be present in the sample at any time; this precludes radical-radical associations. (This is in contrast to the pulsed beam TFμSR experiment, in which 10^3-10^5 are injected into the sample in a single pulse, and consequently there is a small

but non-zero possibility of interactions between muonic species simultaneously present.)

3.3.2 ESR Background.

Lehni[119], in his studies of the 2-hydroxyprop-2-yl radical in a variety of organic solvents, observed not only that the hydroxylic proton coupling showed a strong temperature dependence, but also that the whole curve of hyperfine coupling constant against temperature could be shifted up or down by varying the solvent. The highest couplings were found in n-alkanes and cycloalkanes, where there is very little possibility of interaction between radicals and solvent molecules, and the couplings were found to decrease with both increasing solvent polarity and increasing solvent hydrogen-bonding ability. Close inspection of his data additionally reveals a change in the curvature of the dependence of the coupling constant on temperature as the solvent is varied. Lehni made no attempt at a quantitative theoretical analysis of his ESR data, and these features remain largely unexplained. He did however go some way towards an investigation of the dynamical behaviour of 2-hydroxy-prop-2-yl radicals in solution by examining the linewidths obtained in his ESR spectra, plotting them against T/η, the quotient of temperature and solvent viscosity. A simplification of his findings can be seen in **Figure 3.8.**

Figure 3.8

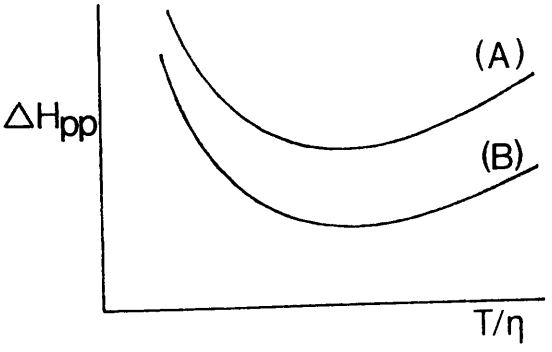

(A) Solvents for which no hydrogen bond formation with the radical is possible.
(B) Solvents for which hydrogen bond formation with the radical is possible.

His results fell into two clear groups, labelled (A) and (B) in this figure. Group (A) consists of solvents such as n-alkanes and cycloalkanes, where hydrogen bonding between the solvent and the radical does not exist; group (B) consists of those in which some degree of hydrogen bonding with the radical is possible, such as alcohols and acetonitrile. Manifestly, the origin of this separation lies in the influence exerted by hydrogen bonding upon the Brownian motion of the 2-hydroxyprop-2-yl radical. A more quantitative explanation is rather difficult.

A linear increase in linewidth with T/η, such as that observed at high T/η, is typically attributed to spin rotation interactions[125]. The contribution of such interactions to the linewidth is approximately proportional to the isotropic angular momentum correlation time, which is given by a modified Stokes-Einstein relation $\tau_J = \frac{I}{8\pi a_o^3 x \eta}$, where I and a_o are respectively the moment of inertia and hydrodynamic radius of the solute molecule, and x is an empirical parameter proportional to the mean square torques acting on the solute molecules[126]. The slower increase in linewidth with T/η for radicals formed in associating solvents may perhaps then be understood in terms of an increase in the effective hydrodynamic radius of the radical through the creation of larger structures by association with solvent molecules.

The linewidth passes through a minimum at roughly the same value of T/η for both group (A) and group (B), and begins to increase again as T/η decreases towards zero. This phenomenon is explained as resulting from the incomplete averaging of anisotropic hyperfine effects[97]. The contribution to the linewidth made by effects of this kind depends in a nonstraightforward way on such factors as nuclear spin state and reorientational correlation time, and for this reason Lehni omits to assess it quantitatively.

One of the most powerfully hydrogen-bonding solvents available to experimenters is of course water, and a study of α-hydroxyalkyl radicals formed in water would no doubt yield much interesting information. Unfortunately, however, no comprehensive study of this kind appears to have been done. (The radical production method used by Lehni is unsuitable for an aqueous environment.) An early result by Zeldes and Livingston[117] in fact suggests an increase in the hydroxylic proton coupling in aqueous solution relative to that in acetone with an admixture of 2% propan-2-ol. Although this observation is used by Hill *et al.*[122] in their derivation of $A_\mu : A_H$, it is based on the comparison of two very small couplings measured at different temperatures with a low degree of accuracy and, especially in the light of the fact that it goes against logical expectation on the basis of data obtained in other hydrogen-bonding solvents, must be regarded a little warily.

3.3.3 μSR Background.

Transverse field μSR spectra obtained at CERN by Hill and co-workers[40,121,122] at room temperature from a series of binary solutions of acetone and water, with the mole fraction of acetone varying from 0.2 to 0.95, and with a reference sample of pure acetone, revealed several interesting features. Firstly, and most surprisingly, there was seen to be a marked drop in the muon-electron coupling constant from the pure acetone value upon the addition of even a small proportion of water (a diminution of 11.4% in the coupling on addition of 5% water). On further addition of water the coupling constant continued to decrease, apparently monotonically (as well as can be judged within the given bounds of experimental error), but much more gradually. The lowest coupling constant measured was 21.7 MHz, at a mole fraction of water of 0.8.

The lowering of the hyperfine coupling constant found in these binary mixtures with water was interpreted by Hill *et al.* in a qualitative fashion as originating in an increase in the number of possible hydrogen-bonding structures available to the 2-muoxyprop-2-yl radical (see **Figure 3.9**). In pure acetone, the only "muonium-bonded" structure available is the radical-acetone complex (i), in which the radical associates with a single solvent molecule. Where water is present there is an increase in the number of possible associated species: in addition to structure (i), which is still of course possible, there is the species (ii) in which the radical is associated with three water molecules, in one case by a muonium bond and in the other two by "conventional" hydrogen bonds. There is also the possibility of the mixed structure (iii), in which the radical is muonium-bonded to one molecule of acetone and hydrogen-bonded to two molecules of water. As Hill *et al.* remark, the conventional hydrogen-bonding interactions are not present when the radical is formed in pure acetone; they are only "switched on" by the presence of water molecules. Evidently they exert a considerable hindering influence upon the librational motions of Mu around the C-O bond.

Figure 3.9.

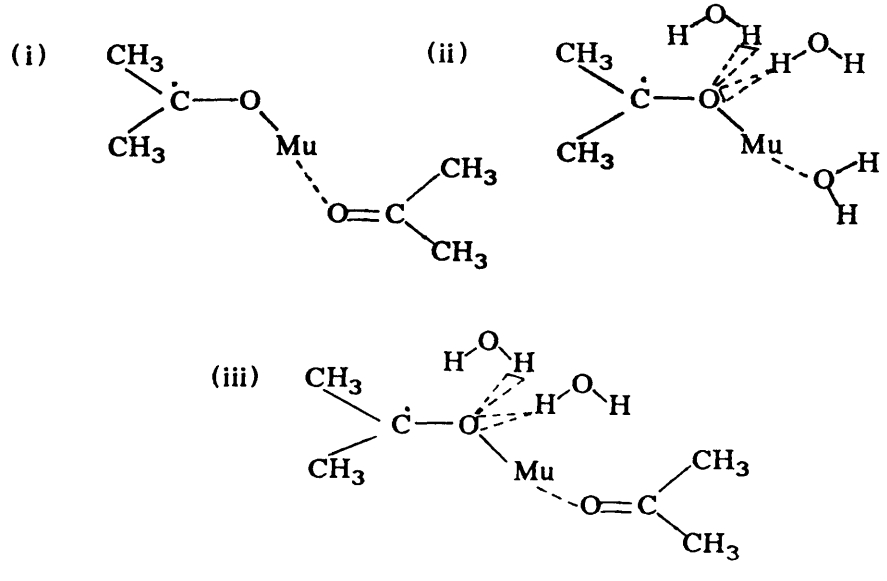

Probably as a result of the presence of the diamagnetic signal, which obscures the spectra of α-muoxyalkyl radicals, especially at low temperatures where the signals begin to coalesce, Hill *et al.* did not attempt a more quantitative study, obtaining values of the muon-electron coupling constant over a full range of temperature and composition. In principle such a study could yield information pertaining to torsional barriers, effective moments of inertia, and hydrodynamic radii.

3.3.4 Radical Formation.

As something of a digression, it should perhaps be pointed out that the process of formation of the 2-muoxyprop-2-yl radical has been the subject of some debate[22,23,121,122]. The formation reaction

$$(CH_3)_2CO + Mu \longrightarrow (CH_3)_2\dot{C}OH \qquad (3.1)$$

was first studied by Percival *et al.*[127], and its rate constant determined to be $k_{Mu} = 8.7 \times 10^7 M^{-1} sec^{-1}$. Since, in a 7M aqueous solution, a field greater than 0.01 tesla depolarises muonium in a time comparable to that required for the direct formation process (3.1) above[121], the radical in high field experiments presumably has its origin in some other mechanism, such as the indirect process described by equations (3.2) and (3.3) below, where e^-_{aq} and μ^+ add separately to the substrate to produce the radical.

$$(CH_3)_2C{=}O + e^-_{aq} \longrightarrow (CH_3)_2\dot{C}{-}O^- \qquad (3.2)$$

$$(CH_3)_2\dot{C}{-}O^- + \mu^+ \longrightarrow (CH_3)_2\dot{C}{-}OMu \qquad (3.3)$$

This two-step mechanism is analogous to that for the radiolytic formation of the protonic analogue in aqueous systems[128].

Cox and Symons[22], in their review of formation processes of muonated radicals, make the observation that in aqueous solutions of acetone several other reactions will play a part. Most directly, water will compete with acetone for the muon, with consequent formation of species such as H_2OMu^+, the muonic hydroxonium ion, which can generate muonium *via* an encounter with a radiolytic electron, thus

suppressing the ionic mechanism of radical production. Also, the hydrogen-bonded species $(CH_3)_2CO\cdots HOH$ will have a reactivity differing from that of "isolated" propan-2-one molecules in two ways. Firstly, the presence of a water molecule in the region of the oxygen atom will sterically block the approach of neutral muonium. Secondly, as the presence of the hydrogen-bonded water molecule decreases the electron density at the carbonyl bond and thus increases the electron affinity of the acetone molecule, the direct formation of the solvated anion in aqueous solution may be said to be favoured over anion formation in pure acetone. Both of these aspects favour the ionic mechanism of radical formation, and the net outcome must therefore be a compromise between these opposing influences. Consideration of line broadening results obtained by Hill *et al.*[122] leads to the conclusion that the dominant phenomenon in aqueous solution is the "damping" of the rate constant for muonium addition, and therefore that hydrogen bonding is the major solvent effect.

Studies by Roduner[23,129] using dimethylbutadiene as a "muonium scavenger" have quantified the relation between "direct" and ionic processes in the formation of the 2-muoxyprop-2-yl radical in propan-2-one and aqueous solutions thereof, and given the first clear idea of the nature of the end of the muon track in organic liquids.

3.3.5 Level Crossing Results.

Most recently, the formation of muonic free radicals in solutions of propan-2-one in hexane, water, and the micelle cetyltrimethylammonium bromide has been studied using the relatively new technique of muon (Avoided) Level Crossing Resonance spectroscopy[124].

The first room temperature observation of the ALC spectrum of pure propan-2-one was made at PSI by Heming and co-workers[6]. An unresolved multiplet corresponding to the six equivalent methyl

protons was seen. By making use of the known muon-electron coupling constant A_μ = 27.0 MHz (averaged from several "room temperature" observations) and the value of the applied field at which the resonance occurred, B_o = 153.8 mT, a figure for the proton coupling of A_H = 55.1 MHz was derived; this is very close to Zeldes and Livingston's[117] result of 54.5 MHz, and indicates that the effect of isotopic substitution of a muon for a proton at the carbonyl oxygen atom upon the spin density at the radical centre is slight.

Subsequent investigations by Venkateswaran *et al.*[124] at TRIUMF showed an upfield shift of 28 mT in the resonance position in a 30% by volume solution of propan-2-one in water relative to that in pure propan-2-one, together with a reduction in signal intensity. Conversely, in a 30% solution by volume of propan-2-one in n-hexane, the signal, of an intensity comparable to that obtained in aqueous solution, was found to have been shifted in position to a field lower by 11.5 mT. Using the TFμSR value obtained by Hill *et alia*[122] for the room temperature muon-electron coupling constant measured in an aqueous propan-2-one solution nominally of the same concentration, they derive a methyl proton coupling constant A_{H_β} = 55.5 MHz, equal within the limits of experimental error to that obtained in pure acetone. The apparent immunity of A_{H_β} to the effects induced by hydrogen bonding implies that interactions in the vicinity of the carbonyl oxygen atom have little effect either on the relative net configuration of the methyl groups and the radical centre or on the long range intramolecular distribution of spin density. No TFμSR result exists for propan-2-one in n-hexane, but Venkateswaran *et al.* derive a value of A_μ = 29.4 MHz from their level crossing experiments. The resonance shifts observed are in accordance with the hydrogen bonding interpretation put forward for the transverse field results.

Venkateswaran *et alia* did not observe any signal corresponding to 2-muoxyprop-2-yl radicals in micellar solutions, even up to fairly high concentrations of propan-2-one. This failure suggests the enhancement of a competitive reaction through isolation of propan-2-one molecules in a micellar phase[130]. The reaction suggested by Venkateswaran *et al.* as that which comes to dominate is the hydrogen atom abstraction (3.4).

$$Mu + (CH_3)_2CO \longrightarrow MuH + CH_3C\dot{O}CH_2 \qquad (3.4)$$

This assertion is supported by the predominance of the abstraction reaction

$$H + (CH_3)_2CO \longrightarrow H_2 + CH_3C\dot{O}CH_2 \qquad (3.5)$$

over the addition reaction

$$H + (CH_3)_2CO \longrightarrow (CH_3)_2\dot{C}OH \qquad (3.6)$$

for hydrogen atoms[131].

3.3.6 A Mixture of Propan-2-one and Water in Volume Ratio 20:1.

Approximately 20ml (15.71g) of high grade propan-2-one (supplied by Aldrich) and approximately 1ml (1.02g) of distilled water were measured into a μSR sample preparation flask. The mixture, in a single liquid phase, was then degassed by the standard procedure and sealed into a glass μSR sample bulb of 35mm diameter. Using the μE4 beamline at PSI a set of muon spin rotation spectra were obtained at eight temperatures spanning the liquid range of the mixture. The transverse field in use was 0.2T. A selection of the frequency domain spectra obtained by Fourier transformation of the raw μSR histograms are shown in **Figure 3.10**. In each case the very strong peak corresponding to muons in diamagnetic environments has been removed, and the two signals characteristic of a radical of the α-muoxyalkyl type can be clearly seen. The radical observed is without doubt the 2-muoxyprop-2-yl radical, previously studied in pure propan-2-one. The qualitative features

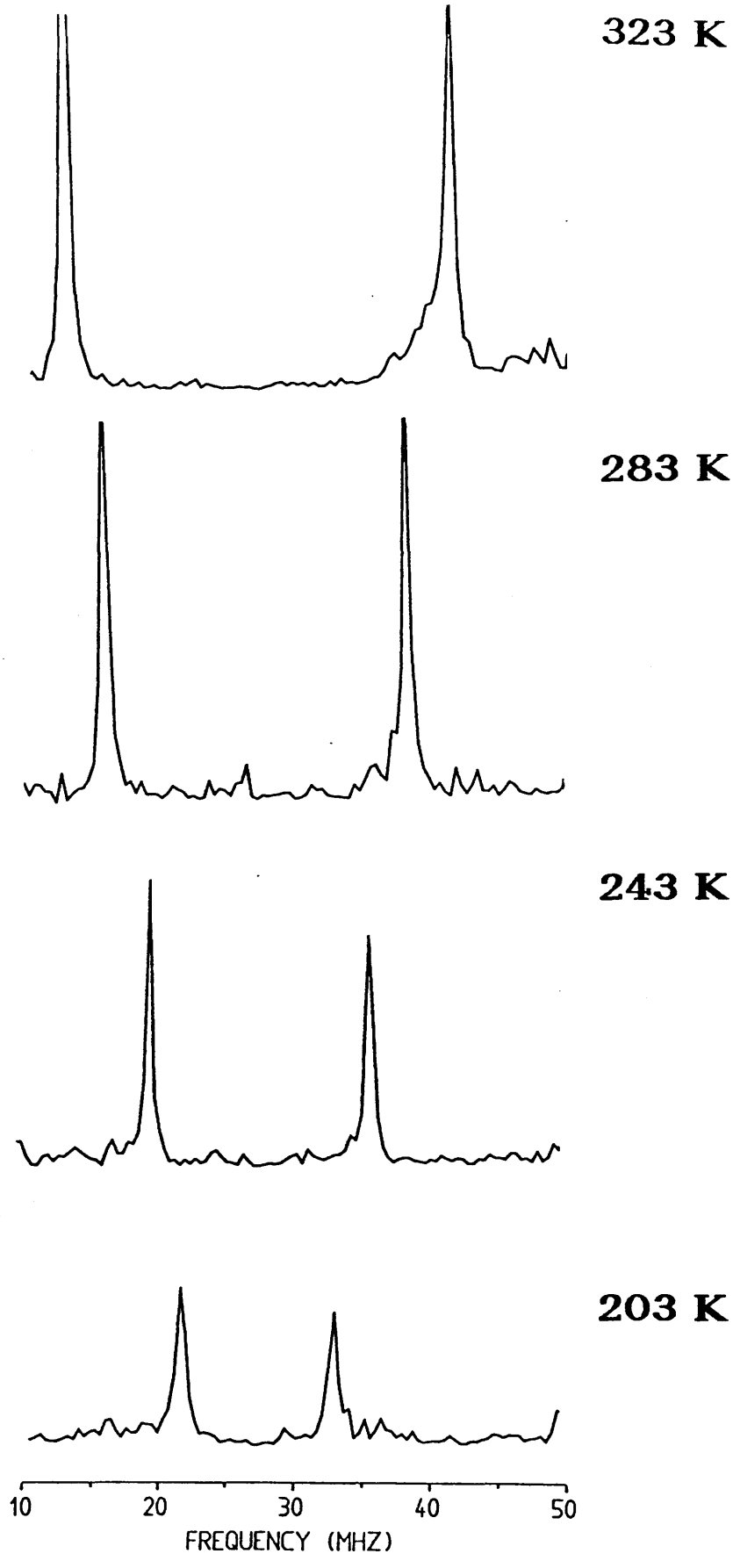

Figure 3.10 Fourier transformed μSR spectra of the 2-muoxyprop-2-yl radical formed in a 20:1 vol/vol binary aqueous solution of propan-2-one.

of the spectra are as before; the coupling constant is small, its temperature dependence positive. However, a more detailed investigation of the results reveals some interesting quantitative differences.

Properties of the spectra are tabulated in **Table 3.4**. A'_μ is found to vary from 2.9 MHz at 183 K to 8.9 MHz at 323 K. At all temperatures it is smaller than in pure propan-2-one. **Figure 3.11** displays graphically the variation of A'_μ with temperature. A distinct upwards curvature is again apparent in the dependence. The amount by which the reduced coupling constant is less than that obtained in pure propan-2-one is virtually temperature-independent, being about 0.7 MHz both at room temperature and at 180 K.

In an attempt to gain some insight into the role played by hydrogen bonding between muonium and the oxygen atoms of water molecules surrounding the radical, a duplicate experiment was performed in which D_2O was substituted for H_2O. Although no net chemical bond is assumed to be present between Mu and H_2O in any of the hydrogen-bonded structures, the physical proximity of the muon to the site of isotopic substitution is sufficiently close that a stronger influence on the dynamical behaviour of the radical might be occasioned than resulted from deuteration of the methyl groups of propan-2-one (see section 3.2.1).

To this end approximately 7.2 ml (5.55 g) of propan-2-one and approximately 0.36 ml (0.42 g) of D_2O were combined in a μSR sample preparation flask to yield a single liquid phase. Any dissolved gas was removed from the mixture by the usual procedure, and the sample was sealed into a glass μSR bulb of 25 mm diameter. Under a transverse magnetic field of 0.2 T the μSR spectrum of the mixture was recorded at room temperature (296 K), yielding a muon-electron hyperfine coupling constant of 23.74 MHz. The reduced coupling constant A'_μ is plotted

Table 3.4 Features of transverse field μSR spectra obtained in a binary solution of propan-2-one and H_2O in volume ratio 20:1. Temperatures are in K, transition frequencies and coupling constants in MHz.

T	ν_{12}	ν_{43}	A_μ
323.0	13.0745	41.2693	28.1948
303.0	14.7066	39.6879	24.9810
283.0	16.1403	38.3516	22.7369
263.0	17.7176	36.7153	18.9977
243.0	19.1447	35.2614	16.1167
223.0	20.5305	33.9127	13.3822
203.0	21.6843	32.7490	11.0647
183.0	22.5535	31.8314	9.2779

All transition frequencies are averaged over four histograms. On average 4×10^7 events were collected per temperature. Temperatures were cryostatically maintained to ± 0.1 K. From $\nu_D = 27.1937$ MHz the external field was determined to be 0.2006 T.

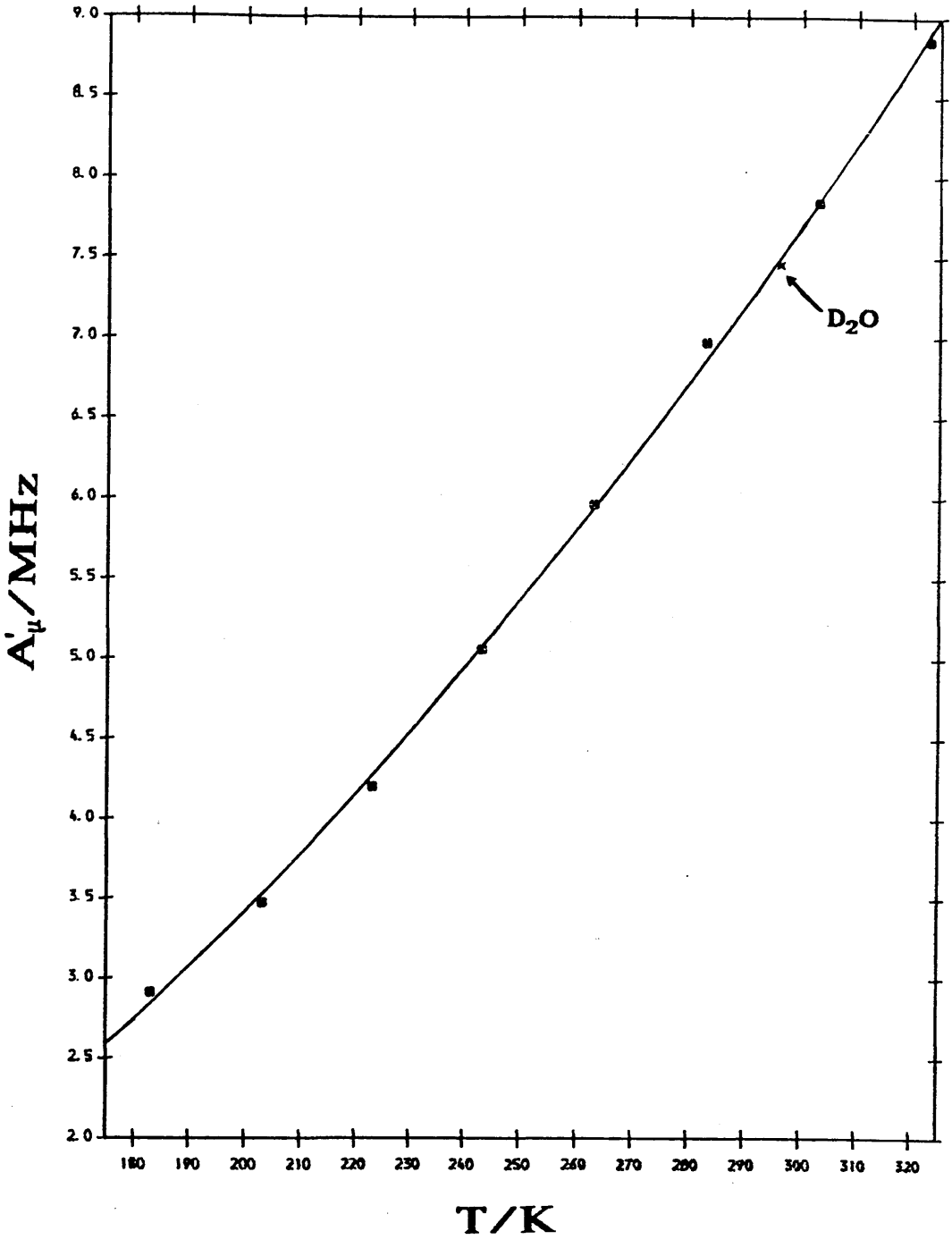

Figure 3.11 A'_μ against T for the 2-muoxyprop-2-yl radical formed in a 20:1 vol/vol binary aqueous solution of propan-2-one.

in **Figure 3.11** along with those obtained from the 20:1 binary solution with H_2O. It can be seen that within the limits of experimental error this point falls exactly onto the temperature dependence curve of the coupling constant obtained with H_2O. The conclusion to be drawn must therefore be that a small change in the mass and vibrational properties of the molecule to which the strongest muonium bonds occur does not significantly affect the overall dynamical behaviour of the muonium-bonded paramagnetic complex.

3.3.7 Barrier to Internal Rotation.

Using the same value for I_R, the reduced moment of inertia for internal rotation, as was employed in the foregoing calculation on the 2-muoxyprop-2-yl radical in propan-2-one (see section 3.2.1), and again considering the equilibrium torsional angle of the radical around the C-O bond, ϑ_o, to be $\pi/2$, the hyperfine coupling data obtained from this μSR experiment were subjected to analysis in order to extract the potential barrier to internal rotation for this radical in its hydrogen-bonded environment, together with the parameters A and B describing respectively those components of the coupling constant independent of and dependent upon the torsional angle γ. The assumption is made as before that only a single twofold term is required for an adequate description of the potential. The results follow.

V_2 = 7037.0 $J mol^{-1}$

A = -76.73 MHz

B = 259.3 MHz

In the aqueous environment the effective barrier is, not surprisingly, considerably larger. Internal rotation around the C-O bond is hindered both by hydrogen bonds between the radical oxygen atom and the hydrogen atoms of surrounding water molecules and by muonium bonds between Mu and the oxygen atoms from the solvation envelope in addition

to those muonium bonds already present in pure propan-2-one. It is surmised that the decrease in hyperfine coupling constants and the increase in the barrier to internal rotation relative to those in pure propan-2-one, rather than being results of a direct influence upon spin density distributions within the radical exerted by hydrogen bonding, arise from purely dynamical effects, through the damping of the muon's librational excursions by means of intermolecular hydrogen-bonding interactions.

It should be noted that there still remains a considerable difference between the coupling constants and barrier to internal rotation found in this mixture and those obtained in studies of the 2-hydroxyprop-2-yl radical[119]. The effect, intramolecular in its nature, of the Mu/H isotopic mass ratio upon the dynamics of the radical is greater by several orders of magnitude than that of external, intermolecular processes such as hydrogen bonding.

3.3.8 Torsional Eigenvalues and Theoretical Temperature-Dependence.

The eigenvalues of the torsional Hamiltonian corresponding to the solution noted above are listed in **Table 3.5**, together with the corresponding values of $\langle\cos^2\gamma\rangle$ and $\langle A'_\mu\rangle$. Again it is noteworthy that only one level, that with i=2, yields a negative coupling constant. That at no temperature does the population of this level influence the Boltzmann distribution sufficiently to render the overall coupling negative can be seen from the theoretical temperature-dependence curve, depicted in **Figure 3.12.** The smallest net hyperfine coupling is obtained at a temperature of 146 K, where A'_μ = 2.54 MHz. At low temperatures A'_μ approaches $\langle A'_\mu\rangle_1$ = 10.2 MHz, while the high temperature limit is A + B/2 = 52.9 MHz. In the range of temperature in which experimental measurements were made the curve virtually parallels that obtained from pure propan-2-one, with an average decrease in the hyperfine coupling constant from the

Table 3.5 Torsional eigenvalues for 2-muoxyprop-2-yl radicals in a 20:1 vol/vol mixture of propan-2-one and H_2O, together with the corresponding expectation values of $\cos^2\gamma$ and A'_μ. The eigenvalues are in J mol^{-1}, the reduced coupling constants in MHz.

i	E_i	$\langle\cos^2\gamma\rangle_i$	$\langle A'_\mu\rangle_i$
1	2908	0.33516	10.1745
2	4016	0.21019	-22.2288
3	7505	0.69785	104.2196
4	13024	0.46964	45.0457
5	13634	0.63414	87.7010
6	25214	0.51693	57.3075
7	25243	0.52927	60.5063
8	42014	0.51206	56.0440
9	42014	0.51240	56.1318
10	63628	0.50763	54.8956
11	63628	0.50763	54.8968
12	90053	0.50523	54.2738
13	90053	0.50523	54.2738
14	121295	0.50382	53.9077
15	121295	0.50382	53.9077
16	157337	0.50291	53.6719
17	157337	0.50291	53.6719
18	198226	0.51143	55.8820
19	198226	0.51143	55.8820
20	243879	0.51016	55.5528
21	243879	0.51016	55.5528

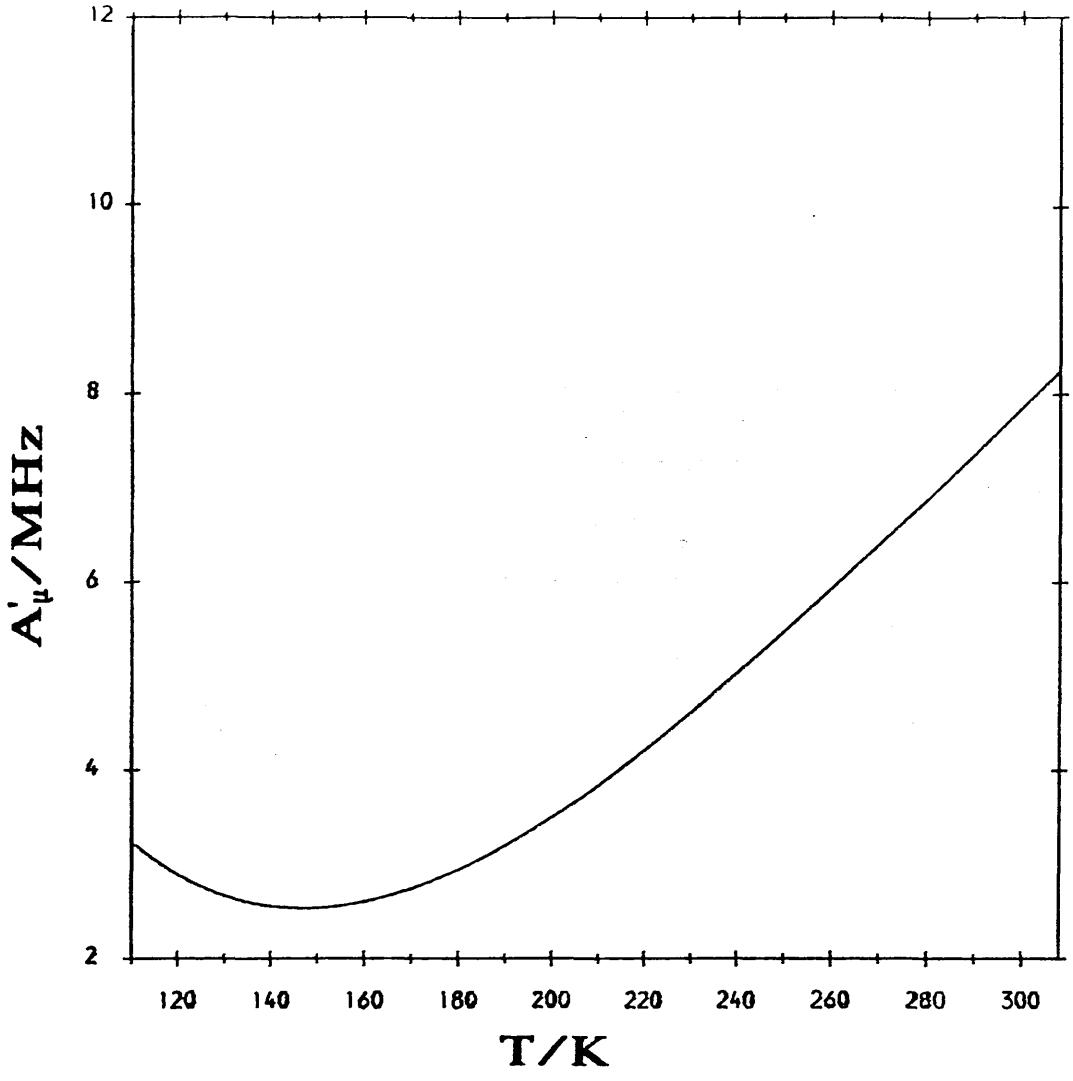

Figure 3.12 Calculated variation of A'_μ with T for the 2-muoxyprop-2-yl radical in a 20:1 binary aqueous solution of propan-2-one.

pure solvent value of 0.7 MHz. The slightly broader minimum obtained in the case of the mixture leads to a greater curvature in the experimental region. The temperature at which the minimum occurs is virtually identical in each case.

3.3.9 Results from Other Mixtures of Propan-2-one and Water.

In order that the composition-dependence of the conformational dynamics of 2-muoxyprop-2-yl radicals formed in binary solutions of propan-2-one and water be better understood it was decided that transverse field μSR experiments should be conducted upon a set of mixtures spanning a range of compositions, in each case obtaining the hyperfine coupling constant at a number of temperatures preferably comprehending the entire liquid range of the mixture. Such experiments were carried out by Mr. D. Buttar of this group at PSI during the December 1988 beam period[132]. The details of preparative method and experimental configuration are materially identical to those previously described. The compositions of the samples studied were (by volume) nominally 100:1, 40:1, and 10:1. In each case the hyperfine coupling constants obtained were small, positive at all the temperatures studied, and showed a temperature dependence with a positive temperature coefficient. The data were subjected to theoretical analysis by the same means and with the same assumptions as before, and the results of this analysis are presented in **Table 3.6**. The key to the table is as follows: A and B are the hyperfine parameters in equation (1.62), V_2 is a twofold static potential barrier to internal rotation, T_{min} and $A'_{\mu_{min}}$ are the co-ordinates of the minimum in the theoretical temperature dependence of the hyperfine coupling constant, $\langle A'_{\mu} \rangle_1$ is the expectation value of the hyperfine coupling corresponding to the lowest torsional eigenvalue (and represents the magnitude at absolute zero of the isotropic hyperfine coupling), and A + B/2 is the limiting value of the

Table 3.6 Properties of 2-muoxyprop-2-yl radicals formed in binary aqueous solutions of propan-2-one in various composition[132]. Compositions are by propan-2-one:water volume ratio, temperatures in K, and hyperfine coupling parameters in MHz. The twofold potential barrier to internal rotation, V_2, is expressed in J mol^{-1}.

Composition	100:1*	40:1	10:1
V_2	4154	5296	7555
A	-127.1	-95.50	-70.44
B	339.0	285.0	246.7
T_{min}	144	146	148
$A'_{\mu min}$	-0.86	2.41	2.57
$\langle A'_\mu \rangle_1$	7.2	10.1	9.87
A + B/2	42.4	47.0	52.9

Values of T_{min}, $A'_{\mu min}$, and $\langle A'_\mu \rangle_1$ are derived from calculations of A, B and V_2 using 5 experimental points. In all cases except that marked with an asterisk no change in the results is obtained by using more points. In case (*) using 7 points, the following results were obtained: V_2 = 4196 J mol^{-1}, A = -125.7 MHz, B = 336.2 MHz, T_{min} = 144 K, $A'_{\mu min}$ = -0.31 MHz.

coupling constant at high temperature. Discussion of these data is deferred until the presentation of the results of one final experiment.

3.3.10 A Mixture of Propan-2-one and Water in Volume Ratio 15:1.

A solution of volume ratio approximately 15:1 of propan-2-one and water was prepared by mixing 30.0 ml of propan-2-one (Aldrich, high purity) with 2.0 ml of distilled water in a flask. Approximately 20 ml of the mixture was then transferred to a μSR sample preparation vessel, where, under vacuum, it was subjected to the degassing procedure previously described in order to remove any dissolved oxygen, and subsequently sealed in a glass μSR sample bulb of 35 mm diameter. Using a transverse field nominally of 0.2 tesla a set of μSR spectra were obtained a several temperatures spanning the liquid range of the solution. (These experiments were performed at PSI, using the μE4 beamline, during the March 1989 beam period.) **Figure 3.13** shows several of the Fourier transformed spectra after the removal of the diamagnetic signal to leave the clear trace of an α-muoxyalkyl radical, in this case, as before, the 2-muoxyprop-2-yl radical, formed by addition of muonium at the oxygen atom of propan-2-one. The features are superficially exactly as before. At all temperatures a single radical is formed, having a small positive muon-electron hyperfine coupling constant with a positive coefficient of temperature. The results are listed in **Table 3.7**, and the temperature dependence of the hyperfine coupling constant is shown graphically in **Figure 3.14**. Again, the coupling constant is smaller at all temperatures than that obtained in pure propan-2-one. However, comparison with the results of the 20:1 propan-2-one/water experiment reveals another, rather interesting, feature: while at temperatures in the vicinity of room temperature the composition dependence of the hyperfine coupling constant would seem to be described by a simple decrease with increasing mole fraction of water, at around 220 K there

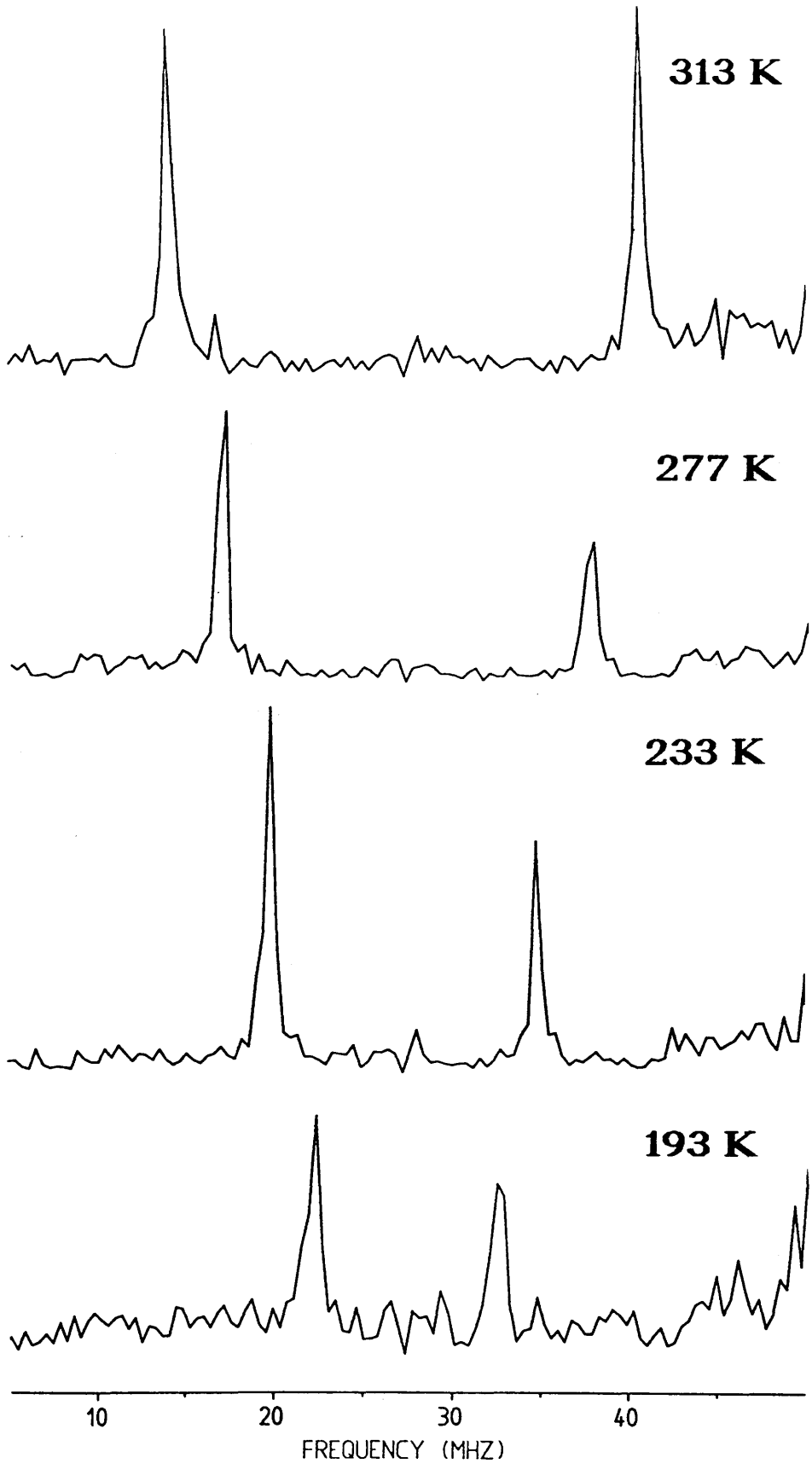

Figure 3.13 Fourier transformed μSR spectra of the 2-muoxyprop-2-yl radical formed in a 15:1 vol/vol binary aqueous solution of propan-2-one.

Table 3.7 Results of transverse field μSR studies on a 15:1 volume/volume binary solution of propan-2-one in water. Temperatures are in K, transition frequencies and hyperfine couplings in MHz.

T	ν_{12}	ν_{43}	A'_{μ}
313.0	14.1261	40.6375	8.3283
291.0	15.8356	38.9002	7.2455
277.0	17.0322	37.7499	6.5082
269.0	17.3567	37.2958	6.2637
250.0	18.7882	35.9383	5.3875
233.0	19.8603	34.8159	4.6981
207.0	21.4122	33.2780	3.7275
193.0	22.1703	32.5268	3.2534

On average 4×10^7 events were collected per temperature. All transition frequencies are averaged over four histograms. Temperatures were cryostatically maintained to ± 0.1 K. From ν_D = 27.37 MHz the external field was calculated to be 0.2015 T.

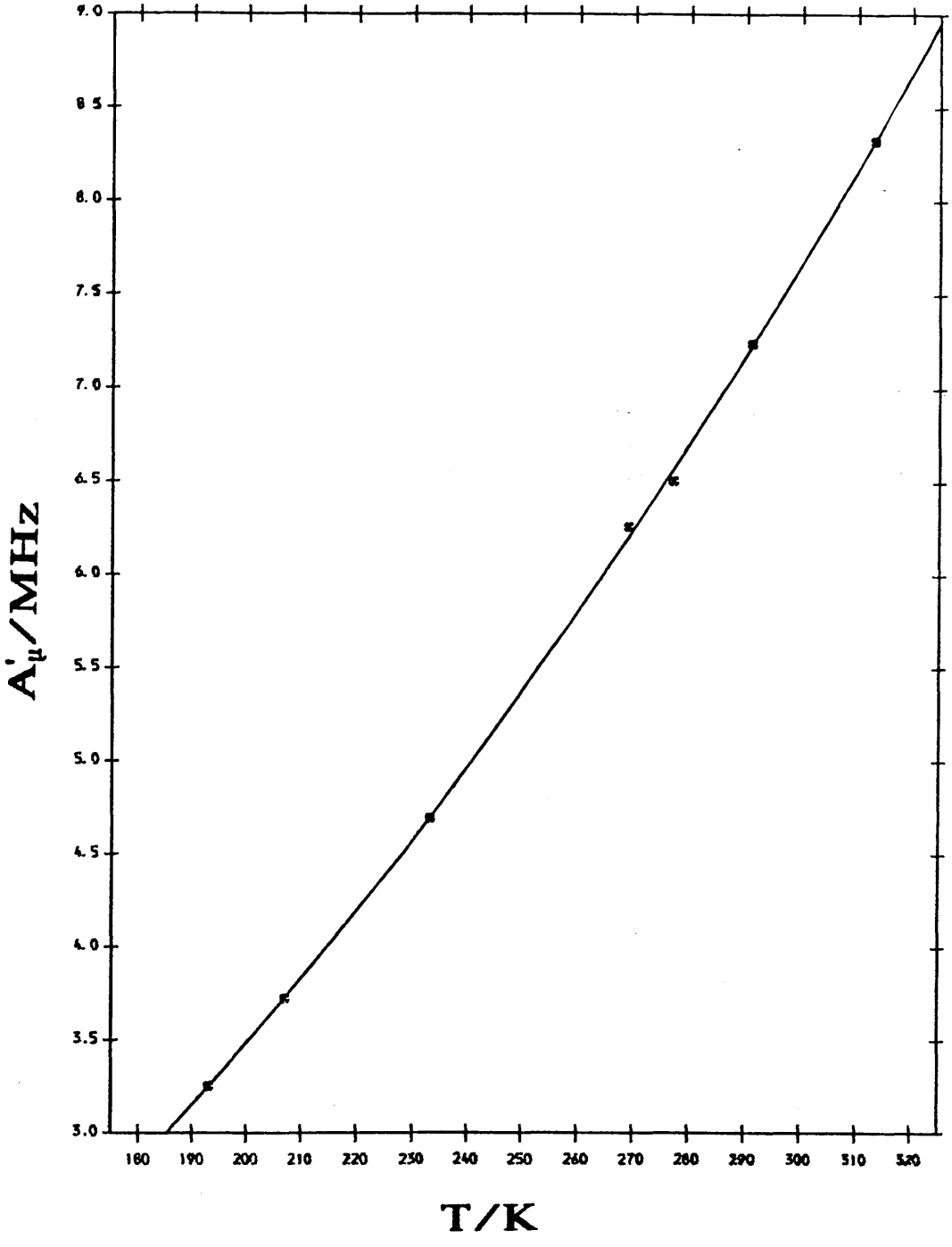

Figure 3.14 A'_{μ} against T for the 2-muoxyprop-2-yl radical in a 15:1 vol/vol binary aqueous solution of propan-2-one.

appears to be a crossing over between the results obtained in the 20:1 solution and those from the 15:1 solution, although both remain well below the pure propan-2-one values. Closer examination of the work of Buttar[132] reveals this behaviour in yet more extreme form in the 10:1 case, where the crossing occurs at a higher temperature (around 235 K).

3.3.11 Barrier to Internal Rotation.

With the usual assumption of a twofold potential barrier to internal rotation around the C-O bond in the 2-muoxyprop-2-yl radical, taking the equilibrium torsional angle ϑ_0 to be $\pi/2$, and again using the same value for I_R as in the previous calculations, the data obtained from this μSR experiment were subjected to the standard theoretical analysis, the results of which are as follows.

V_2 = 8817 J mol^{-1}

A = -69.60 MHz

B = 263.0 MHz

The barrier is larger than in the 20:1 case (although apparently also larger than that obtained from Buttar's data for the 10:1 case — see the following section), clearly indicating the existence of further net hindering of the dynamical behaviour of the radical due to additional water molecules present in the radical's solvation environment.

3.3.12 Discussion.

The values obtained for a twofold static potential barrier to internal rotation in the 2-muoxyprop-2-yl radical formed in pure propan-2-one and five binary aqueous solutions of propan-2-one are shown graphically in **Figure 3.15**. The corresponding composition dependences of the hyperfine coupling parameters A and B are illustrated in **Figure 3.16**. Slight anomalies exist in the behaviour of these quantities which merit further consideration. The general trend expected in the composition dependence of V_2 is

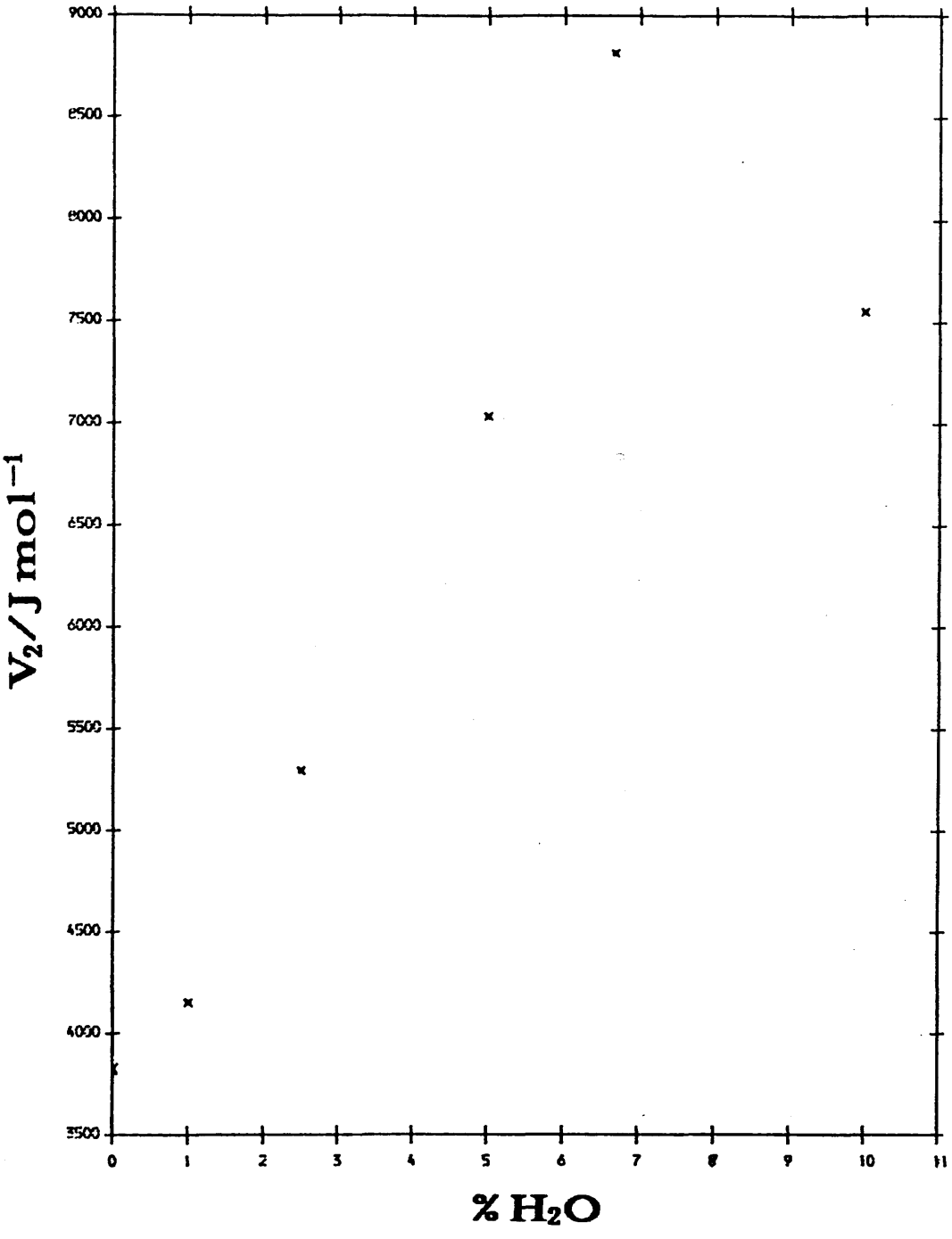

Figure 3.15 Composition-dependence of a twofold torsional barrier in the 2-muoxyprop-2-yl radical formed in binary aqueous solutions of propan-2-one.

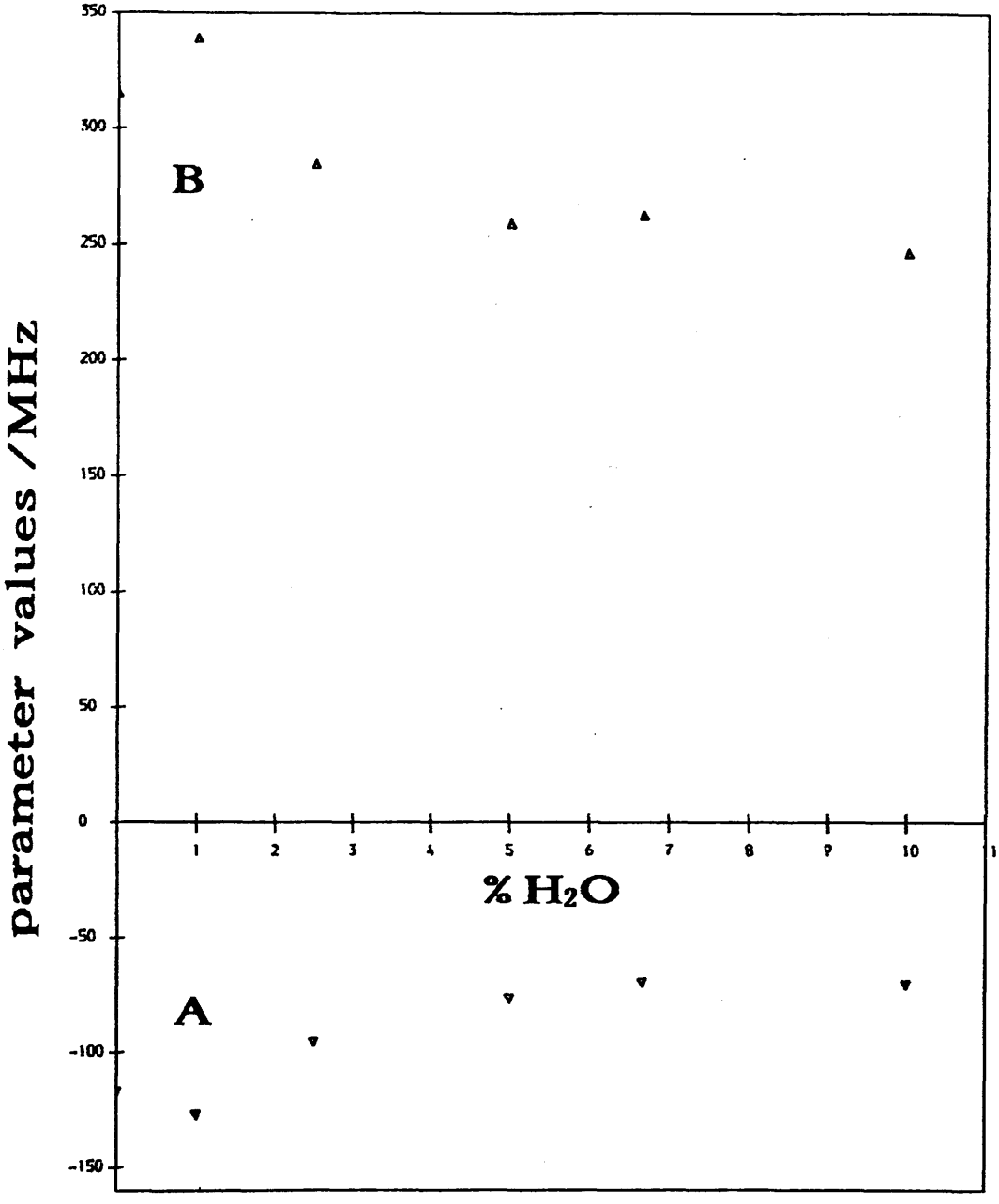

Figure 3.16 Composition-dependence of the hyperfine coupling parameters A and B for the 2-muoxyprop-2-yl radical formed in binary aqueous solutions of propan-2-one.

a steady increase with the amount of water present, as a consequence of the formation of additional hydrogen bonds to the oxygen atom of the radical and muonium bonds to the oxygen atoms of the surrounding water molecules. This behaviour is seen to be followed experimentally up to a water concentration of 1:15, whereupon the calculated barrier decreases from 8817 J mol^{-1} to 7555 J mol^{-1} for a 1:10 concentration. If this effect has a genuine physical (rather than numerical) origin it indicates that a level of complexity as yet unaccounted for exists in the causes of the composition dependence of hydrogen bonding effects in binary mixtures. No evidence of the anomalous nature of this result can be seen in the composition dependences of the hyperfine parameters A and B. Rather in this case it is the 1:100 result which shows a small deviation from the overall behaviour pattern, which is one of mutually complementary decrease in the absolute values of both A and B, tending asymptotically towards a solution in the region of A = -70 MHz, B = 240 MHz. Whether a composition dependence of the "high temperature limit" given by A + B/2 is meaningful, given that at such high temperatures doubtless weak intramolecular effects would become considerably less significant, is dubious, but the behaviour of this quantity parallels that of V_2, varying from 40.63 MHz for pure propan-2-one through 52.92 MHz for the 20:1 mixture to 61.90 MHz for the 15:1 situation, before decreasing again to 52.93 MHz in the 10:1 case.

Figure 3.17 shows the temperature dependence of the linewidths (Δ) of the radical signals for the three cases of pure propan-2-one, propan-2-one/water 20:1, and propan-2-one/water 15:1. This quantity (shown here in arbitrary units) is related to molecular dynamics, and is quite complex in origin. However, insofar as the linewidth is not determined by factors such as field inhomogeneities or temperature variations over the timescale of the experiment, it originates in spin

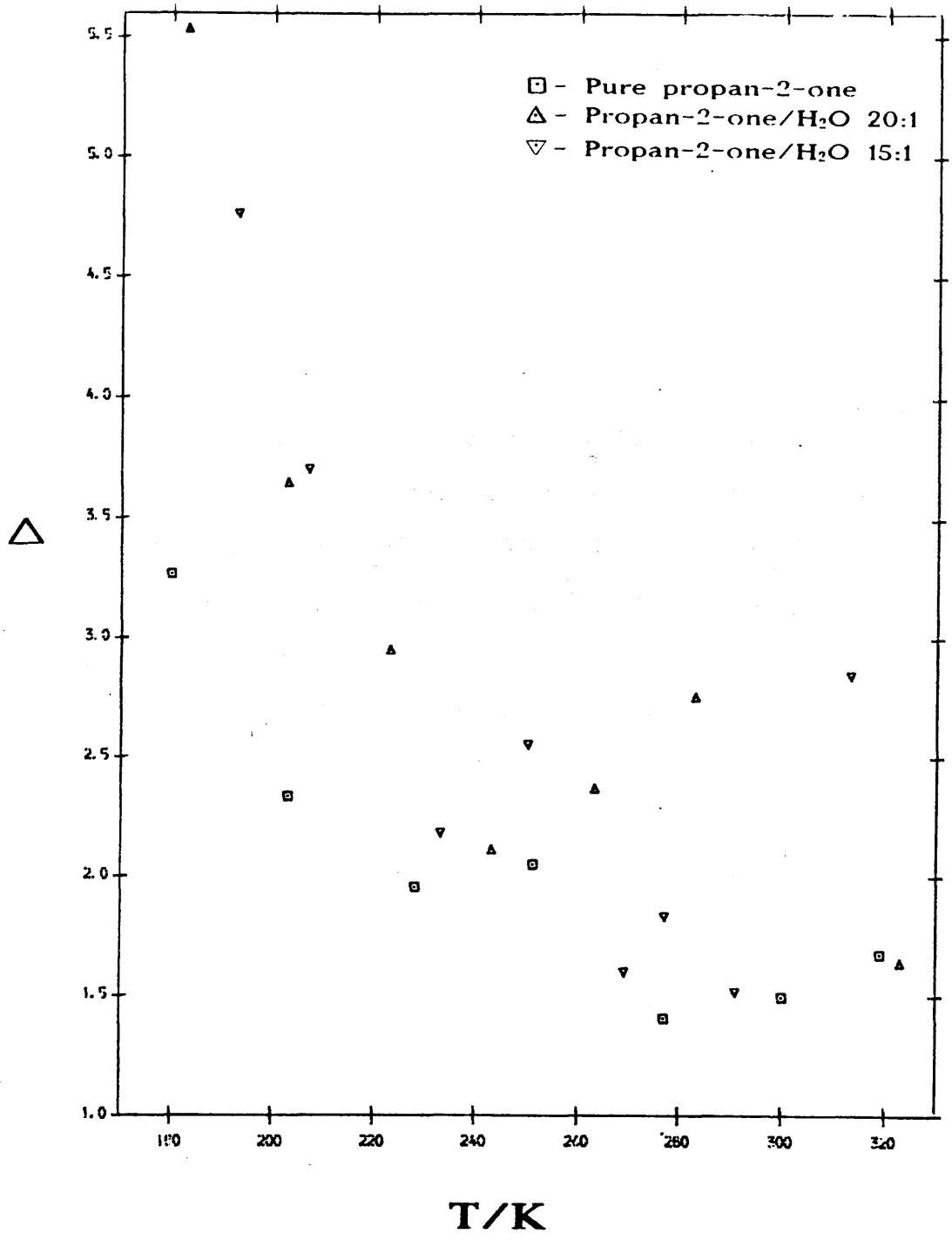

Figure 3.17 Temperature-dependence of linewidth △ (in arbitrary units) for the 2-muoxyprop-2-yl radical formed in propan-2-one and two binary aqueous solutions of propan-2-one.

interactions arising through periodic stochastic modulation of molecular motions. While a large and undetermined random error does exist in the distribution of these experimental points, the prevailing trend in all three data sets is a steep decrease in Δ up to around 240 K, after which point it seems there is a small upturn in the values. This is in keeping with the behaviour described by Lehni for i-propylol radicals and accounted for through a change in the relative importance of hyperfine anisotropy effects and spin-rotation interactions as the temperature is increased. Also noteworthy is the fact that the effect of the presence of H_2O upon the dependence of Δ on T seems to be an upwards shift in the entire curve. This may be understood in a qualitative manner through an increase in the effective hydrodynamic radius of the radical, which affects both the isotropic angular momentum correlation time τ_J (defined in section 3.3.2) in the high temperature region and the reorientational correlation time τ_R (which again incorporates a_o and η in its definition) at lower temperatures, but these effects are too complex for a quantitative analysis to be possible.

CHAPTER 4

Experimental Studies on Other α-Muoxyalkyl Radicals.

4.1 General Introduction.

In addition to the comprehensive study carried out on muonic radicals formed in propan-2-one and various aqueous solutions of propan-2-one, described at length in the previous chapter, investigations were made of various other substrates expected to generate radicals of the α-muoxyalkyl type. The motivations for the experiments were various, ranging from the study of the effect of induction of electronic charge density upon the isotropic hyperfine coupling constant to the study of competitive muonium addition where the parent molecule contains both olefinic and carbonyl functionalities.

4.2 Muonic Radicals formed in 1,1,1-trifluoropropan-2-one.

4.2.1. Introduction

Muons implanted in liquid 1,1,1-trifluoropropan-2-one are expected, by analogy with other carbonyl compounds, to react with the substrate by addition at the carbonyl oxygen atom to form the 2-muoxy-1,1,1-trifluoroprop-2-yl radical (A).

(A)

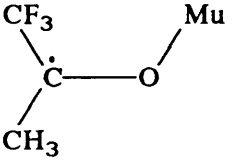

The presence of three electronegative fluorine atoms on one of the methyl groups will occasion a net withdrawal of electronic charge density from the carbon atom at which the radical centre is located. On a simplistic level, it might be expected that this induction of charge density be accompanied by a delocalisation of the unpaired spin density (notionally located in a $2p_z$ orbital at the radical centre) along the C-CF_3 bond onto the carbon atom of the trifluoromethyl group, resulting in a reduction both in the spin density remaining on the radical carbon atom and in that delocalised along the C-O bond onto the O atom.

If this were the case, and the only influence at play, the overall effect would be a diminution in the value of the muon-electron hyperfine coupling constant. However, the isotropic hyperfine coupling constant, as measured by transverse field muon spin rotation spectroscopy on samples in the liquid phase, is effectively a bulk property influenced by intramolecular and intermolecular dynamical effects. The influence of the induction of electronic charge by the three fluorine atoms upon the vibrational and torsional dynamics of the O-Mu group is therefore not so easily predicted.

To date, no electron spin resonance study of the analogous 2-hydroxy-1,1,1-trifluoroprop-2-yl radical has been undertaken, so a comparison between isotopomers of the type familiar from the study of muonic radicals formed in ethene and propan-2-one will not be possible.

4.2.2 Experimental

A sample of approximately 20ml of 97% 1,1,1-trifluoropropan-2-one supplied by Aldrich was degassed using the standard procedure and sealed into a 35mm diameter glass μSR ampoule. Using the μE4 beamline at PSI, and under a transversely applied magnetic field of about 0.2T, muon spin rotation spectra were obtained at eight cryostatically maintained temperatures spanning the liquid range of the compound. The frequency domain spectra obtained by fourier transformation of the original μSR histograms show the presence of just one paramagnetic species, a radical with a small coupling constant. This is the 2-muoxy-1,1,1-trifluoroprop-2-yl radical. As with other α-muoxyalkyl radicals, the very strong signal corresponding to muons in diamagnetic environments falls between the two transition frequencies of the radical, obscuring the spectra. **Figure 4.1** shows a selection of the fourier-transformed spectra from which the diamagnetic signal has been excised. The familiar temperature dependence, with a positive temperature coefficient, can be seen. The

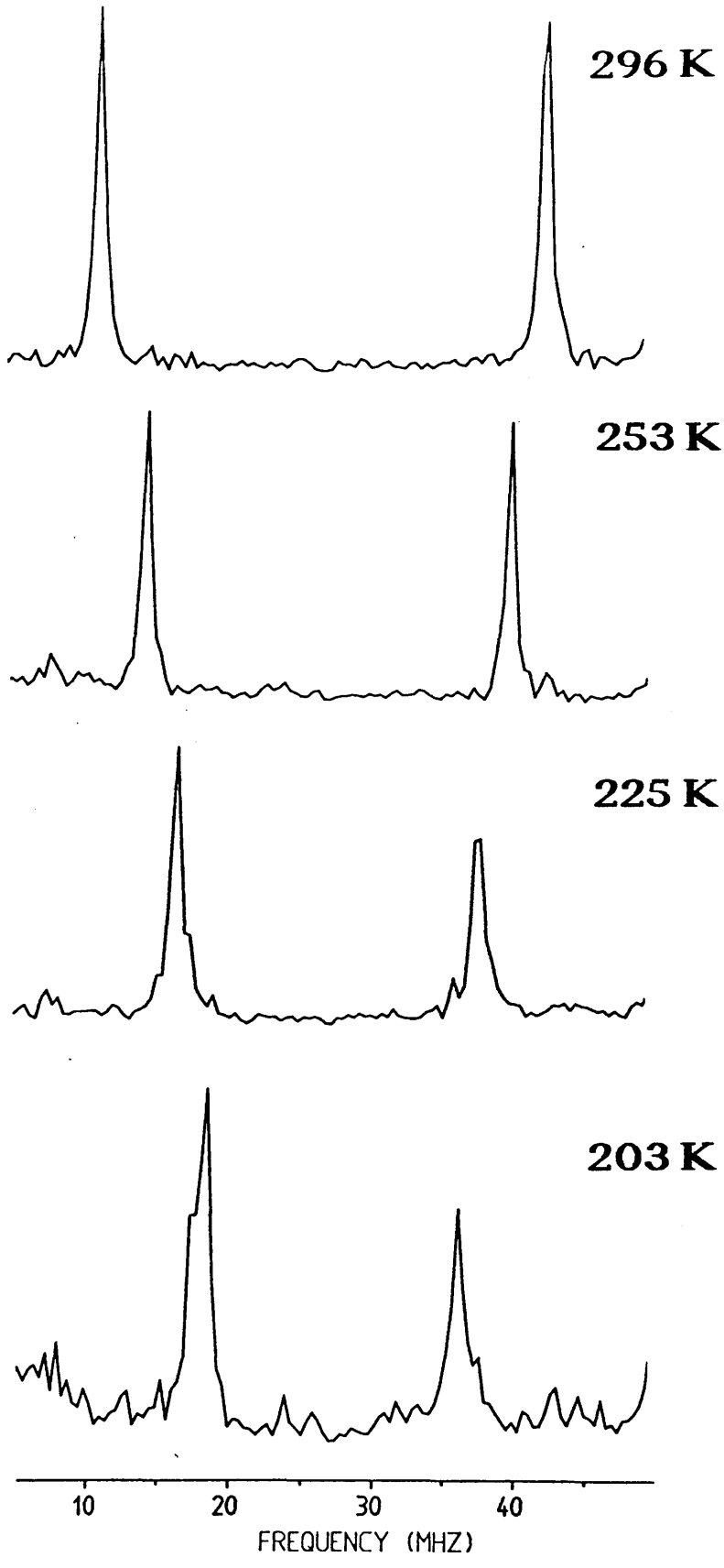

4.1 Fourier transformed μSR spectra of the 2-muoxy-1,1,1-trifluoroprop-2-yl radical formed in pure 1,1,1-trifluoropropan-2-one.

measured hyperfine coupling constants appear in **Table 4.1**. A comparison of the coupling constant of the 2-muoxy-1,1,1-trifluoroprop-2-yl radical at room temperature (see **Figure 4.2**c) with that of the 2-muoxy-prop-2-yl radical in pure propan-2-one (**Figure 4.2**b) or an aqueous solution of propan-2-one (**Figure 4.2**a) reveals a somewhat larger coupling in the case of the fluorine-containing radical (A'_{μ} is greater by approximately 1.2MHz), contrary to predictions made purely on the basis of static inductive effects. A qualitative chemical interpretation of the observed phenomenon is as follows.

4.2.3 Interpretation of the Inductive Effect

Figure 4.3

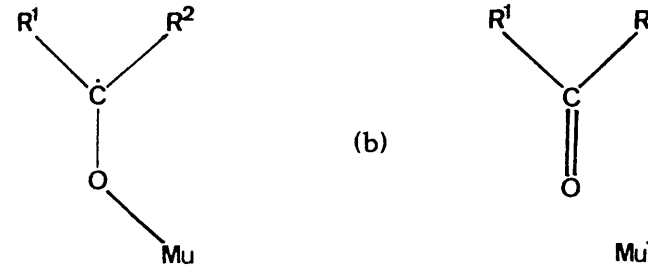

The canonical bond structure conventionally accepted to represent the situation in α-muoxyalkyl radicals (by analogy with their protic isotopomers) is depicted in **Figure 4.3**(a). However, in a manner parallel to that prevailing in bonds to carbon atoms and discussed at some length in Chapter 2, the small mass of Mu as compared to H results in a zero-point vibrational energy which is higher for an O-Mu bond than for an O-H bond. This in turn occasions a greater mean internuclear separation in the case of the muonic radical. It has been noted by Roduner and Reid[133] that the lengthening of a bond can be viewed as one step towards dissociation, and on the basis of such an argument the canonical picture shown in **Figure 4.3**(b) is here put forward as contributing more towards the net radical structure than does the analogous arrangement of bonds and electrons in the α-hydroxyalkyl isotopomer. In the case of the 2-muoxy-1,1,1-trifluoroprop-2-yl radical the highly electron-withdrawing

Table 4.1 Reduced muon-electron coupling constants of 2-muoxy-1,1,1-trifluoroprop-2-yl radicals formed in pure 1,1,1-trifloropropan-2-one. Temperatures are in K, signal frequencies and hyperfine coupling constants in MHz.

T	ν_{12}	ν_{43}	A'_{μ}
296.0	11.6039	42.7265	9.7768
273.0	13.1298	41.1955	8.8165
253.0	14.5232	39.9027	7.9727
233.0	16.0010	38.6531	7.1159
225.0	16.6948	37.8019	6.6306
213.0	17.6102	38.8526	6.0448
203.0	18.1435	35.9773	5.6023
183.0*	19.8540	35.1523	4.8058

On average $4x10^7$ events were collected per temperature. From ν_D= 27.3 MHz the external field is calculated to be 0.201 T. The experimental error on temperature measurement is $\pm$0.1 K. The fitting error on A'_{μ} is $\pm$0.03 MHz.

*At this temperature the signals were weak, and only two histograms were sufficiently good to use in the fourier fit.

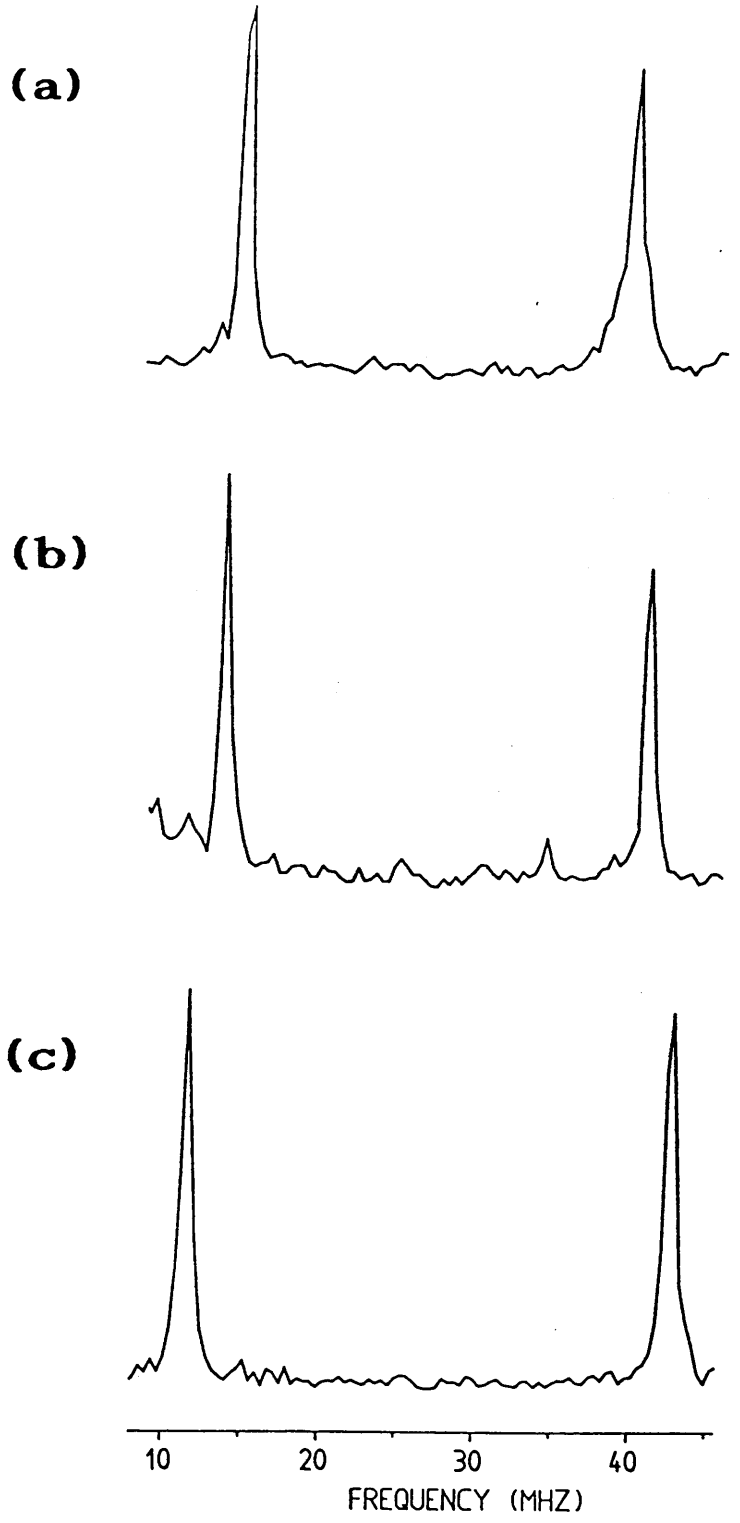

Figure 4.2 Room temperature (≈296 K) spectra of (a) the 2-muoxyprop-2-yl radical formed in a 20:1 vol/vol binary aqueous solution of propan-2-one, (b) the same radical in pure propan-2-one, and (c) the 2-muoxy-1,1,1-trifluoroprop-2-yl radical formed in pure 1,1,1-trifluoropropan-2-one.

nature of the CF_3 group stabilises the C=O double bond and therefore promotes the dissociated structure (b). This allows the net spin density at Mu to be increased in two ways. Firstly, the increased contribution from (b), in which the unpaired spin density is centred upon the muon, leads directly to a higher muon-electron coupling constant. Secondly, the longer O-Mu bond generated through this inductive effect allows greater excursions of the muon from the nodal plane of the $2p_z$ orbital centred upon the carbon atom which contains the unpaired spin density in structure (a) into regions of space where positive overall electronic spin density is encountered by the Mu nucleus.

4.2.4 The Shape of the Temperature Dependence

The values taken by the reduced muon-electron hyperfine coupling constant of the 2-muoxy-1,1,1-trifluoroprop-2-yl radical formed in pure liquid 1,1,1-trifluoropropan-2-one at the various temperatures of experimental measurement are shown graphically in **Figure 4.4**. The solid curve passing through the experimental points is a simple polynomial least-squares fit for illustrative purposes and does not represent any theoretical interpretation. Similarly, the broken curve lying below this is a polynomial least-squares fit to the μSR data obtained in pure propan-2-one. A qualitative difference between the dependences may be seen. In the case of the 2-muoxyprop-2-yl radical the curve shows the slight concavity consistent with the theoretical torsional eigenvalues obtained on the basis of a twofold potential barrier to internal rotation. The shape of the temperature dependence curve for the 2-muoxy-1,1,1-trifluoroprop-2-yl radical is rather more irregular. Clearly the symmetry of the torsional barrier is here reduced, if, indeed, the concept of a simple periodic potential barrier to internal rotation itself retains any validity. Efforts were made to fit the experimental data using a variety of simple and compound periodic potential functions but consideration of these will be deferred until the discussion of the

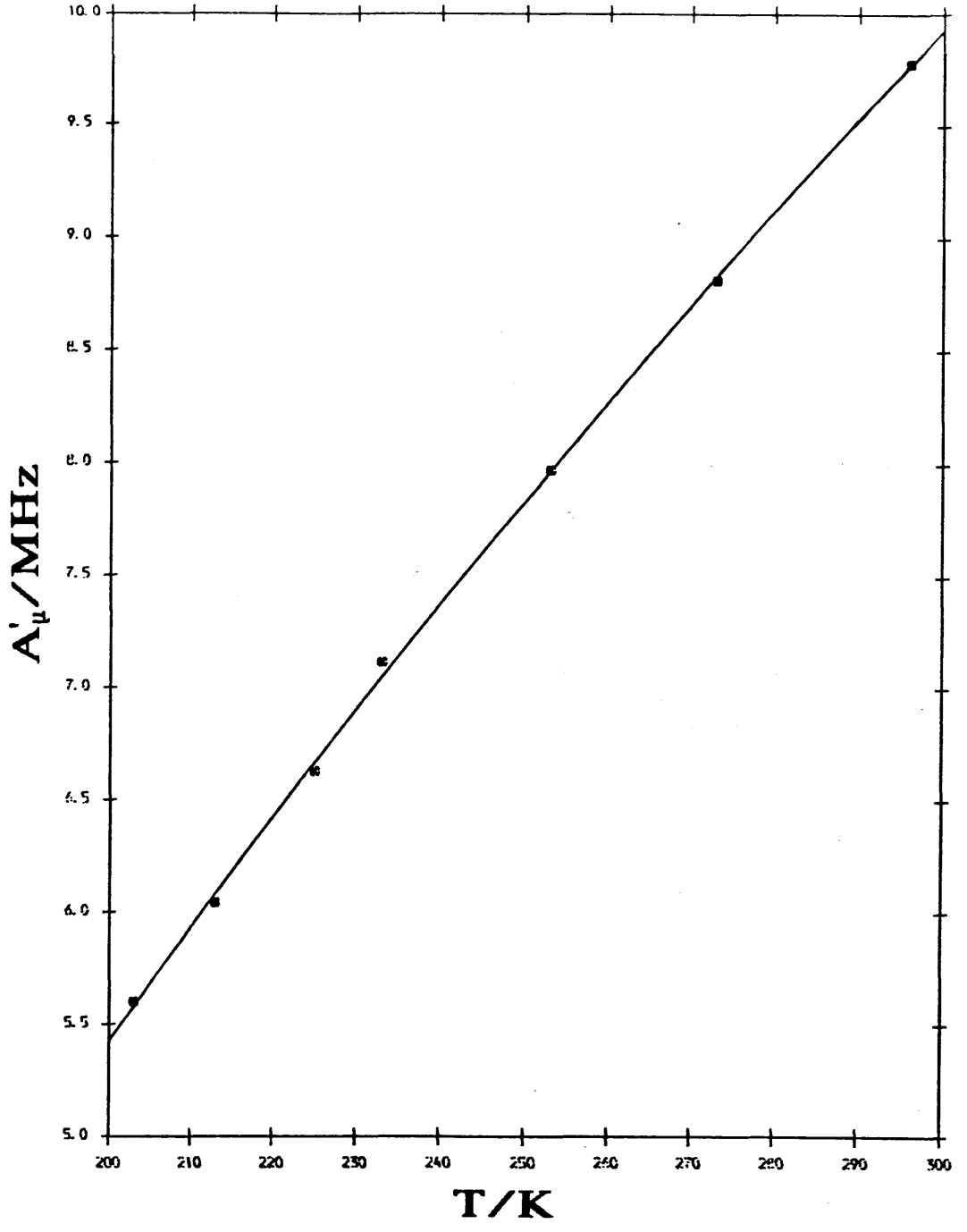

Figure 4.4 A'_μ against T for the 2-muoxy-1,1,1-trifluoroprop-2-yl radical in pure 1,1,1-trifluoropropan-2-one.

origin of the potential barrier in the α-muoxyethyl radical (section 4.3.4).

4.3 Muonic Radicals Formed in Ethanal.

4.3.1 Introduction

When muons are implanted in pure liquid ethanal only one paramagnetic product is anticipated. This is the α-muoxyethyl radical (B), formally generated by addition of an atom of muonium at the oxygen atom of the carbonyl group.

(B) 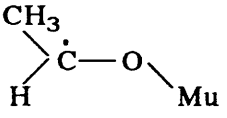

The radical was first observed at CERN in preliminary tests of their μSR apparatus, and has been studied at room temperature by Rhodes and co-workers[123] , forming part of their general catalogue of room temperature studies on muonic radicals formed in carbonyl compounds. They measured its coupling constant to be 23 MHz, which when scaled down by the ratio of the proton and muon angular momenta yields A'_{μ}= 7.2 MHz. The radical is structurally analogous to the hydroxyethyl radical, much studied by ESR spectroscopy[69,113,114] , the most recent and definitive study being by Cirelli et alia[118] . The hydroxylic proton coupling constant (A_H^{OH}) of this radical at room temperature is too small to be resolved, but by interpolation using a linear fit to the data of Cirelli et al. it is estimated to be positive, and in the region of 0.9 MHz. Clearly there is a very large isotope effect at work in this radical, having its origin in the influence of the isotopic mass ratio Mu/H upon intramolecular dynamics, and in particular upon large amplitude internal motions which affect the position of the muon or proton relative to the radical centre. As in the examples previously considered, the main isotope effect is likely to stem from internal rotation around the C-O

bond, for which motion the reduced moment of inertia is nine times smaller in the muonic case than in the protonic.

In the same paper Cirelli et al. cite a value of 2.80 MHz for A_H^{OH} in the 1-hydroxy-1-methylethyl (or 2-hydroxyprop-2-yl) radical, determined under similar experimental conditions. The room temperature muon coupling constants in the corresponding muonic radicals show a difference which is in the same direction and quantitatively almost identical[123]. A tentative explanation for this phenomenon might be sought in arguments pertaining to the relative capacities of an α-proton and an α-methyl group to stabilise unpaired spin density at a carbon radical centre, or, differently put, to release spin density through space or through the C-O bond, either concomitantly with or independently of a release of charge density, but such considerations will be deferred until after the presentation of *ab initio* results in Chapter 5.

In a complementary study using *ab initio* configuration interaction calculations, again in the same paper, Cirelli et al. attempt to obtain a fit to their ESR data using employing hyperfine coupling constants calculated within a model having finite degrees of freedom for internal rotation of the hydroxyl group and inversion at the α-carbon centre. The limited success of these calculations indicates the poor efficiency of the *ab initio* method in reproducing bulk properties dependent on the intramolecular dynamics of a large ensemble of molecules.

4.3.2 Experimental

Approximately 20ml of Aldrich "Gold Label" standard ethanal, degassed by the standard procedure, was sealed into a 35mm diameter glass μSR bulb. Muon spin rotation spectra were obtained at six temperatures ranging from 176K to 288K under a transverse field nominally of 0.2T. **Figure 4.5** shows some of the frequency domain spectra thus obtained. In each case the signal corresponding to muons in diamagnetic environments

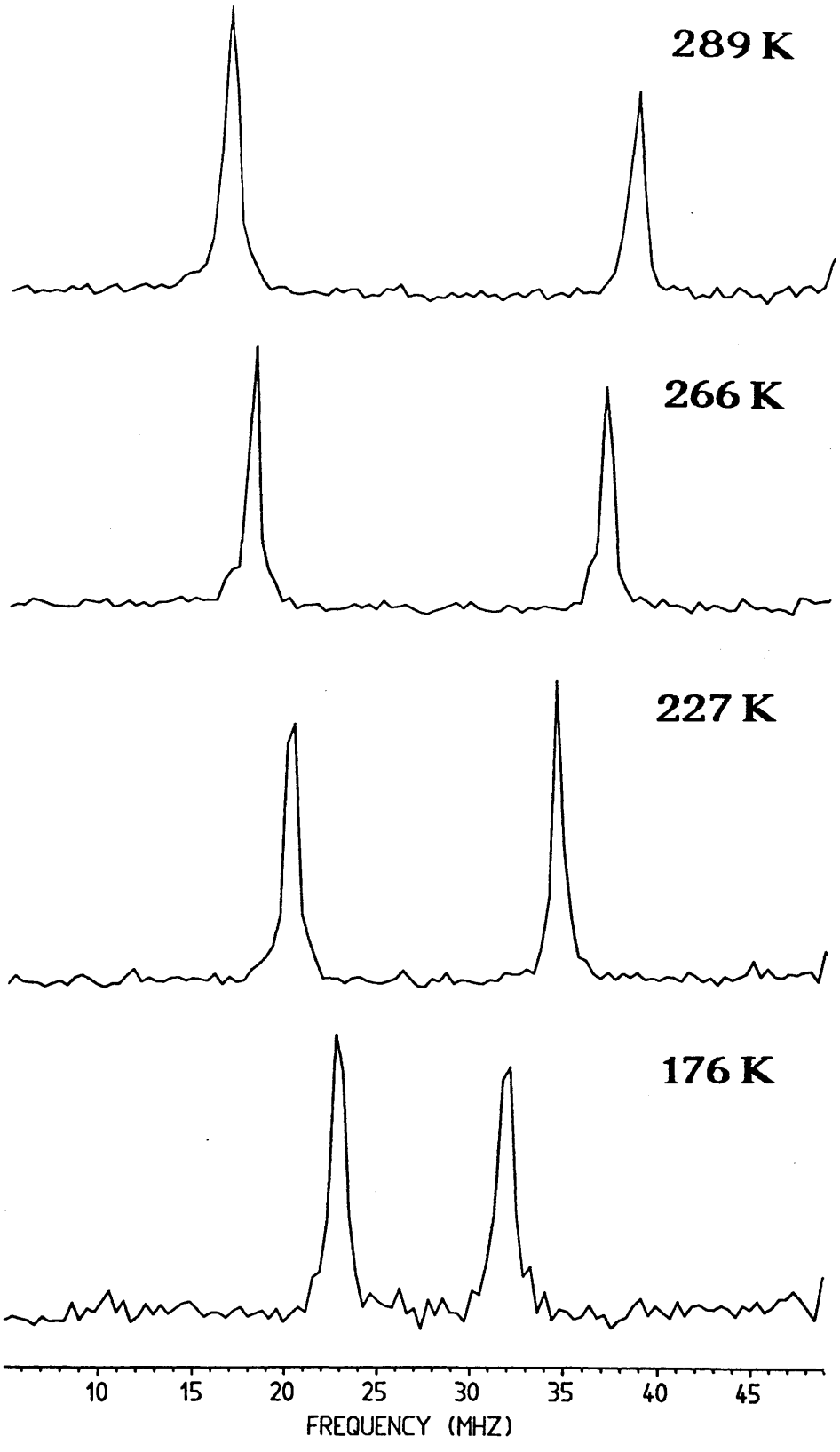

Figure 4.5 Fourier transformed μSR spectra of the muoxyethyl radical formed in pure ethanal.

has been removed, leaving the pair of peaks characteristic of a muonic radical of the α-muoxyalkyl type. This is the muoxyethyl radical, $CH_3\dot{C}HOMu$, the only paramagnetic species detected in this substrate. At all temperatures studied it shows a coupling constant slightly smaller than does the 2-muoxyprop-2-yl radical formed in pure propan-2-one. The values of A'_μ at the temperatures of experimental measurement are collected in **Table 4.2**. The low value of the coupling constant and the positive coefficient of temperature in the temperature-dependence indicate mean radical geometries comparable with those of the 2-muoxyprop-2-yl radical at all temperatures. In other words, from a near-planar conformation of minimum electronic energy, librational excursions of Mu in excited torsional states lead to a net angle of internal rotation different from $\pi/2$ and dependent on temperature.

4.3.3 The Shape of the Temperature Dependence

A plot of A'_μ against T for the muoxyethyl radical formed in pure ethanal is shown in **Figure 4.6**. The solid curve is a polynomial least-squares fit serving only as a visual guide. A slight concavity similar to that observed for the 2-muoxyprop-2-yl radical as formed both in pure propan-2-one and in binary aqueous solutions of propan-2-one is clearly present. However, due to a lessening in the maximum possible symmetry of this radical compared to 2-muoxyprop-2-yl, the potential barrier hindering internal rotation in this radical can patently not be accurately represented by a single term of period π. Terms of period 2π must of necessity enter the reckoning, and may indeed predominate in their effect.

Under the assumption that despite the lowering in symmetry the relation of Heller and McConnell (equation 1.48) still describes the dependence of the hyperfine coupling constant upon the internal rotation coordinate to an acceptable level of accuracy, attempts were made to

Table 4.2 Reduced muon-electron hyperfine coupling constants of α-muoxyethyl radicals formed in pure liquid ethanal. Temperatures are in K, signal frequencies and hyperfine coupling constants in MHz.

T	ν_{12}	ν_{43}	A'_{μ}
288.0	16.5003	38.2124	6.8206
266.0	17.8716	36.7926	5.9438
245.0	19.1127	35.6034	5.1804
227.0	20.1240	34.4447	4.4986
203.0	21.2653	33.2104	3.7524
176.0	22.8175	31.8375	2.8335

At least $5x10^7$ events were collected per temperature. The strength of the external magnetic field, calculated from ν_D= 27.35 MHz, was 0.2018 T. The experimental error on the measured values of T is ±0.1 K. The fitting error on A'_{μ} is ±0.03 MHz.

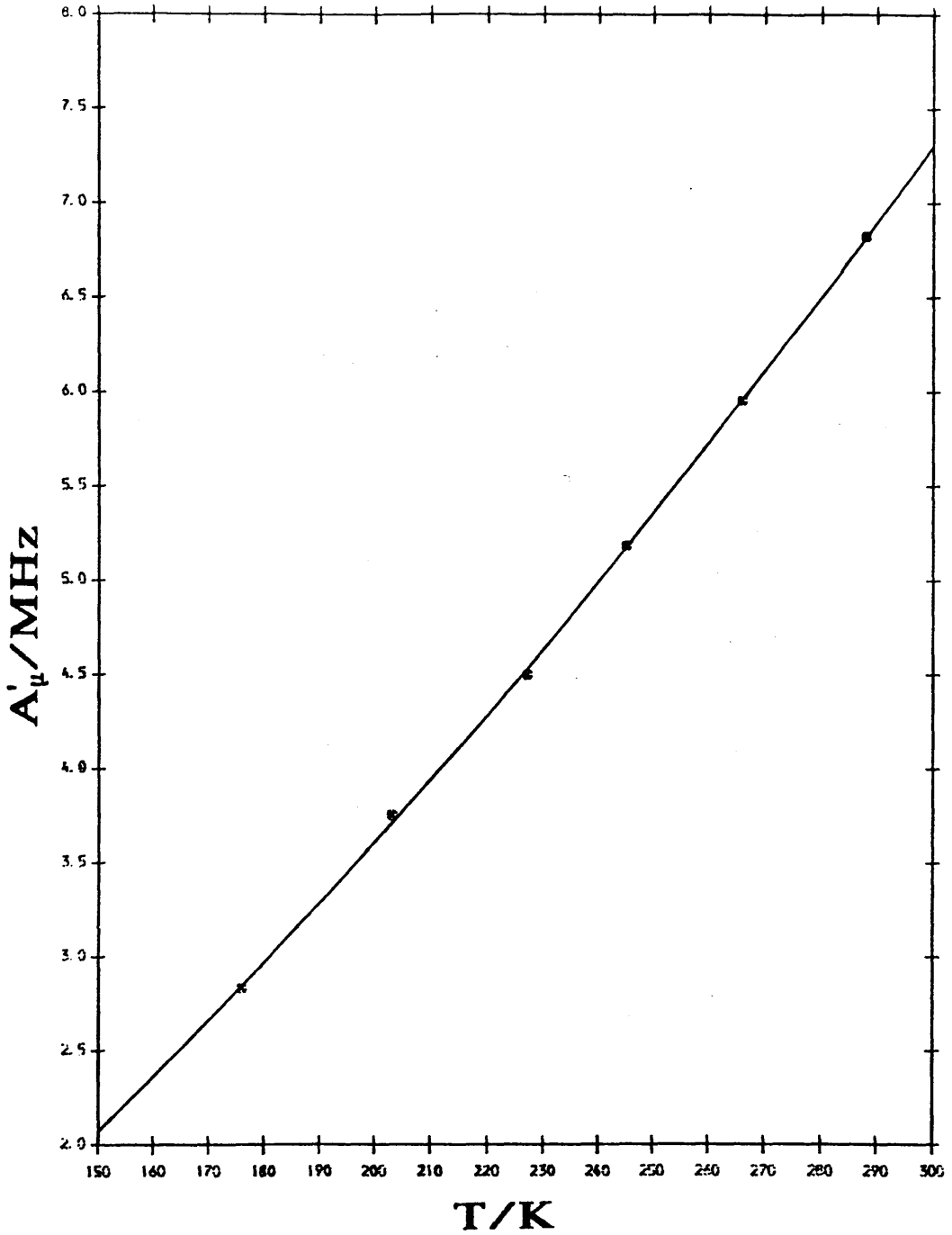

Figure 4.6 A'_{μ} against T for the muoxyethyl radical formed in pure ethanal.

fit the hyperfine coupling data to simple torsional potential functions of period π and 2π, and to a compound function containing terms of both onefold and twofold symmetry in the torsional coordinate. The reduced moment of inertia for internal rotation around the C-O internuclear axis, denoted by I_R, was calculated using a radical geometry derived from an *ab initio* calculation (to be described in Chapter 5), and found to have a value of 1.469×10^{-48} kg m^2. It is a further condition of the model that the torsional potential minimum occurs at a geometry such that $\Theta_0 = \pi/2$ (see **Figure 4.7**). This is the assumption generally made in consideration of species of this type (on the basis of the sign of $\partial A'_\mu/\partial T$ in muonic radicals , or of $\partial A^{OH}_H/\partial T$ in their hydrogenic analogues), and is that used in the case of the 2-muoxy-prop-2-yl radical in Chapter 3. (However, quantum mechanical calculations such as those to be presented in Chapter 5 indicate the optimum SCF geometry of α-hydroxyalkyl radicals in their electronic ground state to be of C_1 symmetry, with a non-planar radical centre, and consequently the barrier calculations that follow must be regarded as accurate only to a first degree of approximation.)

Figure 4.7

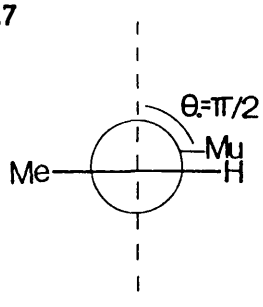

A Newman Projection of the conformation of the muoxyethyl radical corresponding to the minimum in the torsional potential function.

With a potential function consisting of a single variable term onefold in γ, the following results were obtained.

V_1 = 13432 J mol^{-1}

A = -31.1 MHz

B = 108.6 MHz

Using a purely twofold representation of the potential barrier to internal rotation the following solution ensued.

$$V_2 = 2972 \text{ J mol}^{-1}$$

$$A = -117.4 \text{ MHz}$$

$$B = 298.4 \text{ MHz}$$

With the barrier viewed as a combination of V_1 and V_2 terms the solution obtained was as follows.

$$V_1 = 3405 \text{ J mol}^{-1}$$

$$V_2 = 11044 \text{ J mol}^{-1}$$

$$A = -39.9 \text{ MHz}$$

$$B = 153.2 \text{ MHz}$$

4.3.4 The Origin of the Barrier

The barriers to internal rotation in α-hydroxyalkyl radicals and their muonic isotopomers can be conceptually decomposed into two contributions. The first of these originates in the breakdown of π-conjugation as the librational motions of H or Mu bring it out of the nodal plane of the radical π-system, and is essentially twofold in γ. The second contribution, which can be considered to consist of a large positive term onefold in γ, together with a smaller negative twofold term, describes the "steric interference" which occurs when the electronic charge cloud associated (in this case) with Mu interacts with that surrounding the methyl protons. (This is roughly equivalent to a destabilising vicinal bond-orbital interaction.) Of the calculations described above, the one which (by a small margin) achieved the closest fit to the experimental data was that using the compound barrier. The resulting V_1 and V_2 terms indicate that the processes of disintegration and reconstitution of the π-system dominate the barrier to internal rotation. The situation is shown in **Figure 4.8**.

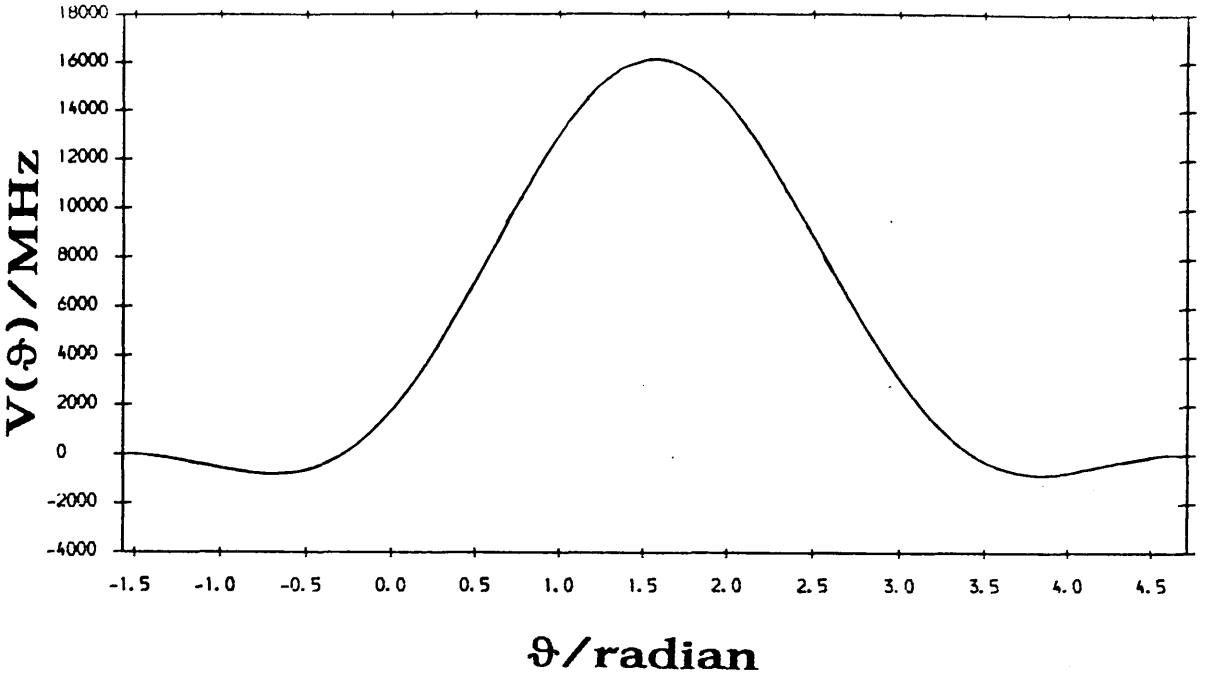

Figure 4.8 Compound torsional barrier in $CH_3\dot{C}HOMu$ consisting of onefold and twofold terms.

If the two-term model of the barrier in the muoxyethyl radical is indeed the most appropriate one, a comparison of the result with the twofold barrier obtained from analysis of the data for the 2-muoxy-prop-2-yl radical in pure propan-2-one lends some further illumination to the balance of processes at work in determining the shape of the torsional potential function. In the 2-muoxyprop-2-yl radical the steric contribution to the barrier, in its simplest form, may be approximated by a twofold term with its minimum at $\vartheta=0$, that is to say, out of phase with the main potential term by $\pi/2$. The effect of this term is to decrease the overall barrier, which remains purely twofold in nature, by raising the energies of the potential minima.

Reconsideration of the data pertaining to the 1,1,1-trifluoro-2-muoxy-prop-2-yl radical gives further credence to this argument. A fit to the experimental points using a purely onefold potential barrier yields the

following results.

$A = -41.43$ MHz

$B = 121.6$ MHz

$V_1 = 7825\ J mol^{-1}$

With a combination potential comprising both V_1 and V_2 terms the resulting converged values of A, B, V_1, and V_2 are as follows:

$A = -54.32$ MHz

$B = 135.3$ MHz

$V_1 = 16146\ J mol^{-1}$

$V_2 = -6267\ J mol^{-1}$.

The balance of V_1 and V_2 terms, together with the fact that V_2 is of negative sign, indicates that in this instance the barrier to internal rotation is dominated by nonbonded "steric" interactions between Mu and the fluorine atoms of the CF_3 group. If this interpretation of the calculated barrier data is correct it is remarkable in the light of the earlier comment that the inductive effect of the CF_3 group seems to stabilise the π-system of the C-O bond.

4.4 Muonic Radicals formed in Hexane-2,5-dione.

4.4.1 Introduction

Hexane-2,5-dione, or acetonylacetone, a γ-diketone, is a liquid at room temperature which freezes at 268 K and boils at 464 K. On implantation of positive muons into a sample of hexane-2,5-dione a single paramagnetic product is anticipated. This is the 2-muoxyhexan-5-on-2-yl radical (C), formed by net addition of an atom of muonium to the oxygen atom of either one of the carbonyl groups in the substrate molecule. This radical is subject to more complex intramolecular dynamics than are

(C)

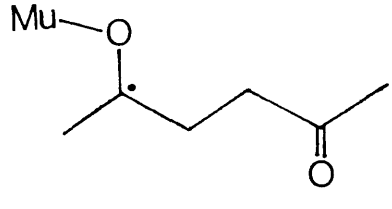

any of those previously studied. Although any electronic inductive effect of the γ-carbonyl group will be very slight, it is possible, by reorientation of the flexible butan-3-on-1-yl moiety, to form structures such as (D), a seven-membered ring containing a symmetrical intramolecular muonium bond. The influence of such processes on the muon-electron hyperfine coupling constant and its variation with temperature remains to be established.

(D)

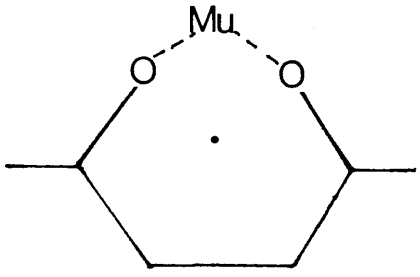

4.4.2 Experimental

Approximately 20ml of hexan-2,5-dione of the highest grade supplied by Aldrich (nominally 97% pure), degassed using the standard procedure, was sealed into a 35mm diameter glass μSR sample bulb. Under an applied field of 0.2T μSR histograms were obtained at five cryostatically controlled temperatures ranging from 270K to 393K. The Fourier power spectra obtained by transformation of these into the frequency domain are shown in **Figure 4.9**. In each case, as usual, the signal corresponding to diamagnetic muons has been subtracted. The remaining pair of peaks present in each spectrum signifies the presence of a single radical species, identified as (C). The coupling constant shows the small absolute value and increase with temperature characteristic of an α-muoxyalkyl radical in which $\vartheta_0 = \pi/2$. The numerical values of the precession frequencies and coupling constant are tabulated in **Table 4.3**. For temperatures over which the liquid ranges of 2,5-hexanedione and propan-2-one overlap, the coupling constants of the radicals formed in the two liquids are nearly identical, that of the 2-muoxyhexan-5-on-2-yl radical being consistently just a little greater. The rationalisation of this effect can proceed along lines of argument similar to those employed in the case

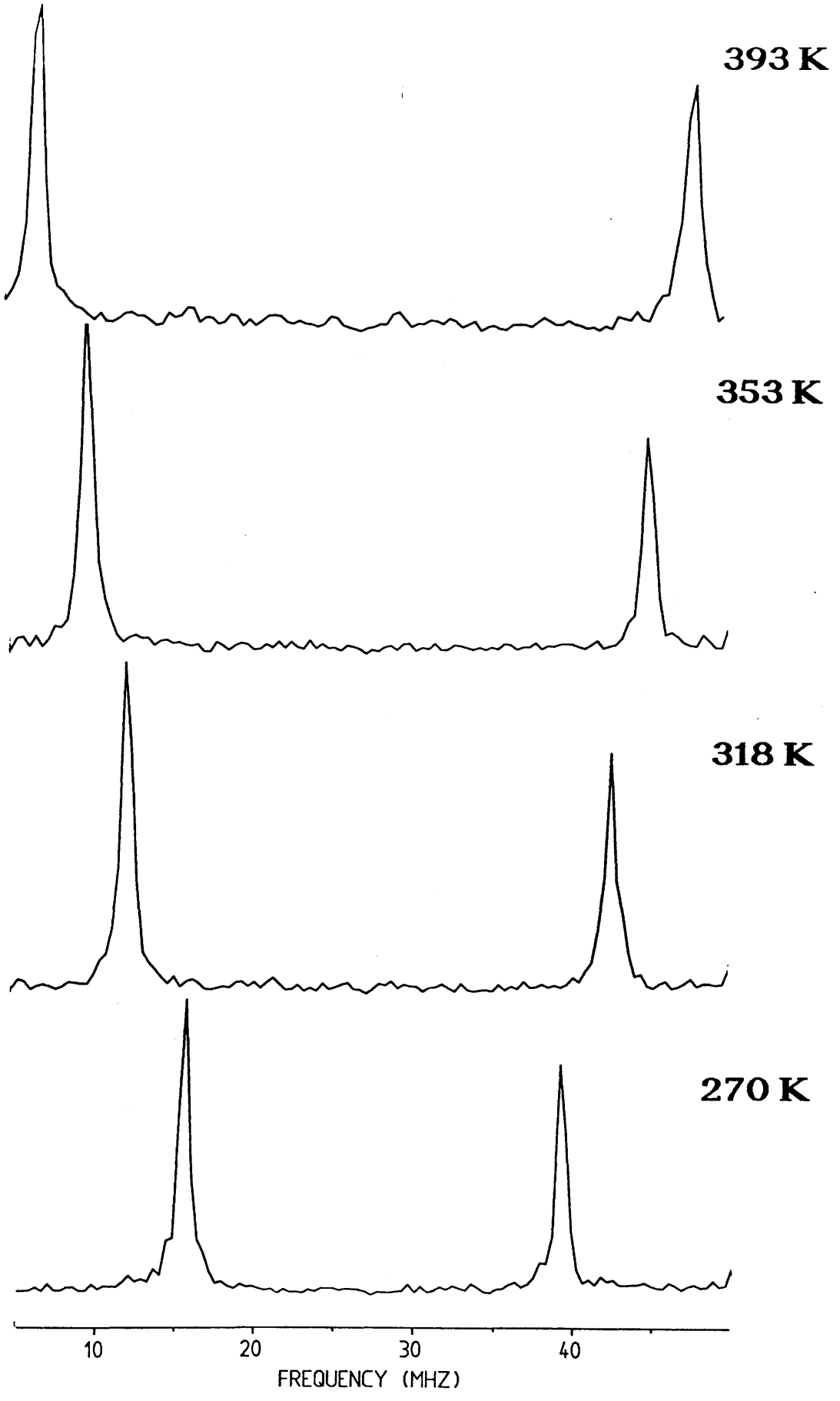

4.9 Fourier transformed μSR spectra for the 2-muoxyhexan-5-on-2-yl radical formed in pure 2,5-hexanedione.

Table 4.3 Transition frequencies and muon-electron hyperfine coupling constants of 2-muoxyhexan-5-on-2-yl radicals formed in pure liquid hexane-2,5-dione. Temperatures are in K, signal frequencies and coupling constants in MHz.

T	ν_{12}	ν_{43}	A'_{μ}
393.0	6.8778	48.0039	12.9193
353.0	9.8182	45.0267	11.0604
318.5	12.2491	42.6190	9.5404
294.0	13.7337	41.0404	8.5781
270.0	15.5569	39.2182	7.4329

Approximately $5x10^7$ events were collected per temperature. From ν_D= 27.36 MHz, the strength of the transverse magnetic field is calculated to be 0.2019 T. The experimental error on the measured T values is $\pm$0.1 K. The fitting error on A'_{μ} is $\pm$0.03 MHz.

of the 2-muoxy-1,1,1-trifluoroprop-2-yl radical. The electron-withdrawing influence of alkyl groups varies in the direction $Pr^i > Et > Me$, and this fact, together with the presence of the carbonyl group in the γ-position relative to the radical C atom, leads to the stabilisation of π-electronic character in the Ċ-O bond, that is to say, of a planar radical centre with a short CO bond and increased spin density on Mu. Clearly, the induction of electronic charge caused by the butan-3-on-1-yl moiety in this instance is considerably less than that occasioned by the trifluoromethyl group in the case of 1,1,1-trifluoropropan-2-one.

4.4.3 The Shape of the Temperature Dependence

In the cases that have gone before it has been the rule to analyse and discuss the temperature dependence of the muon-electron hyperfine coupling constant in terms of the conformational dynamics of the radical concerned, with particular regard to the shape and origins of the barrier to internal rotation around the Ċ-O bond. In some instances it has even been possible to address the problem quantitatively. Here, however, the relatively large size of the molecule leads to a complexity of internal motion which renders detailed analysis difficult. Indeed, the flexibility of the butan-3-on-1-yl moiety leads to difficulties in estimating a reduced moment of inertia for internal rotation. Using (C) as a reference conformation, and with bond lengths and bond angles estimated using values tabulated in the literature for similar compounds[134], I_R is calculated to be in the region of 1.65×10^{-47} kg m^2.

The relationship between A'_μ and temperature for the 2-muoxy-hexan-5-on-2-yl radical in pure 2,5-hexanedione is shown graphically in **Figure 4.10**. No clear nonlinearity in the dependence can be seen from the five experimental points. The best-fit straight line through the data points, indicated on the graph by a solid line, is given by

$$A'_\mu = -4.44 + 0.0440T \qquad (4.1).$$

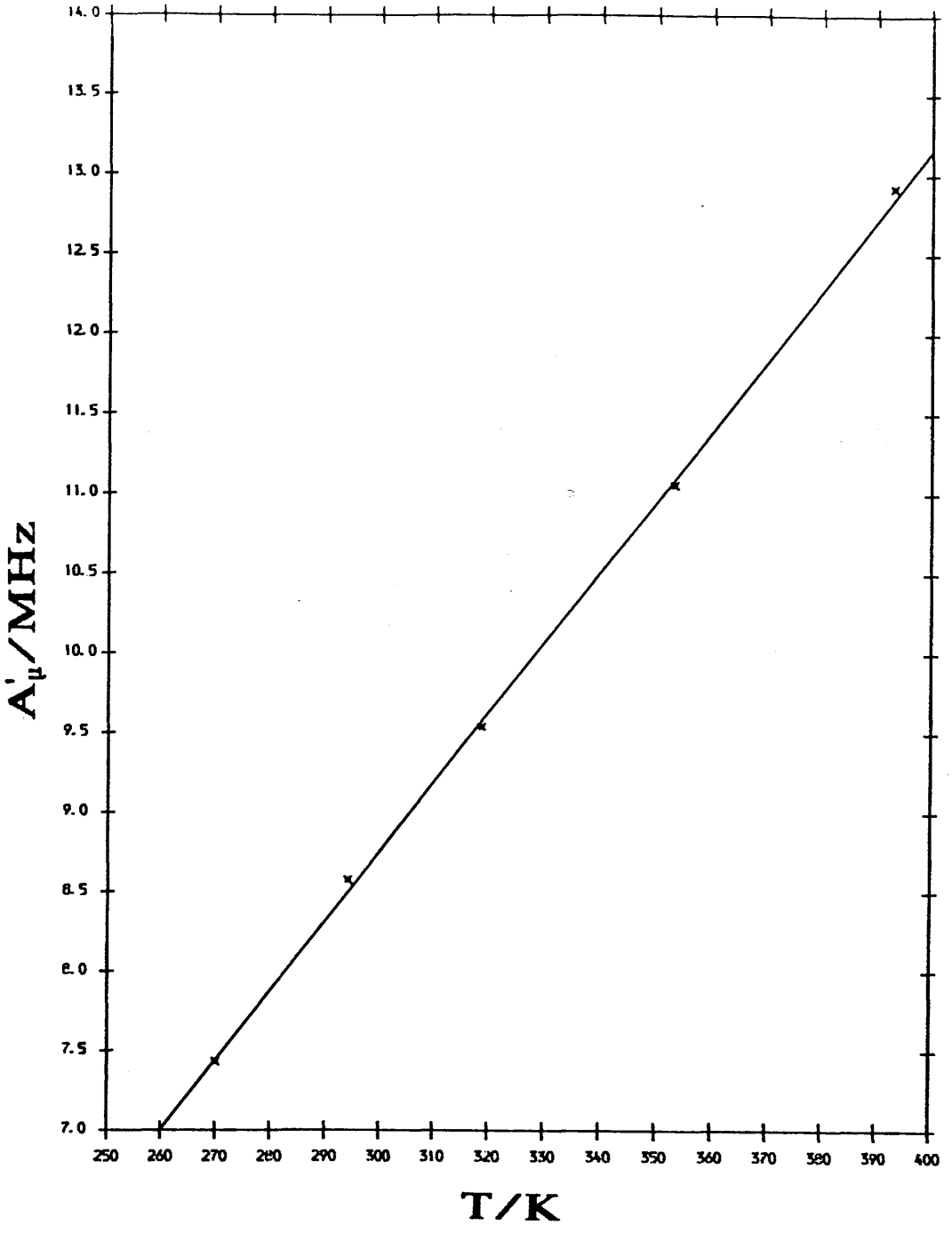

Figure 4.10 A'_{μ} against T for the 2-muoxyhexan-5-on-2-yl radical formed in pure 2,5-hexanedione.

By analogy with the theoretical solutions obtained for the 2-muoxy-prop-2-yl radical it may be said, if such a model is appropriate for this radical also, that in the range of temperature of experimental measurement a local regime of approximate linearity prevails in the curve of the temperature dependence of the hyperfine coupling constant.

Although it is not intended that the results should be interpreted as having quantitative significance, an analysis of the experimental data within the suppositions of the usual model was undertaken, and the resulting optimum values of A, B, V_1, and V_2 thus obtained are presented in **Table 4.4.** (A, B / MHz, V_1, V_2 / J mol^{-1}.)

Table 4.4

model	A	B	V_1	V_2
V_1 only	-32.3	142.5	19796	——
V_2 only	-42.3	193.9	——	9788
V_1 + V_2	-58.5	250.1	96651	-28481

As in the case of 1,1,1-trifluoropropan-2-one, the best fit to the data is obtained using the compound barrier containing both V_1 and V_2 terms, suggesting that the barrier to internal rotation in this radical is largely "steric" in origin.

4.4.4 An Interesting Comparison

It is illuminating to compare the experimental evidence presented above with results obtained from μSR studies on β-diketones such as pentane-2,5-dione[124] . In the latter case no paramagnetic species are seen, whereas in the former the radical signals are as clear and strong as those found in propan-2-one.

A possible explanation for this disparity lies in the phenomenon of keto-enol tautomerism, where an equilibrium exists in the compound between the keto form (i) and the isomeric enol (ii), produced by net transference of an atom of hydrogen from an α-carbon atom to the oxygen atom of the carbonyl group.

(i) 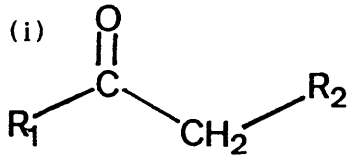 (ii) 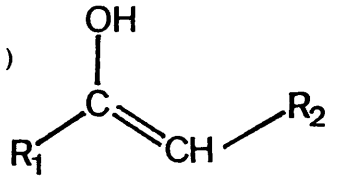

In β-diketones this equilibrium lies considerably further to the right than in monoketones, due to the increased acidity of the α-H. The absence of paramagnetic muon states in β-diketones may originate in the trapping of muons in hydroxonium-like cations of the form (E) over the timescale of the μSR experiment.

(E) 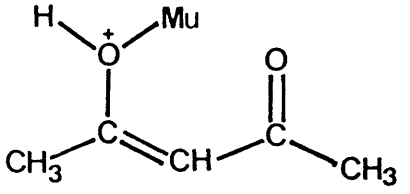

4.5 Muonic Radicals formed in But-2-enal.

4.5.1 Introduction.

But-2-enal, or crotonaldehyde, is an αβ-unsaturated carbonyl compound, and as such presents several possible modes of radical-forming muonium attack. Attachment of Mu at carbon-3 yields an α-carbonyl substituted alkyl radical of the type studied by Strub *et al.*[135] in an examination of their isomerisation kinetics. Attachment at carbon-2 yields a β-carbonyl substituted alkyl radical. These two types of radical differ in their capacity to delocalise the unpaired electron: in the first, the unpaired spin may be spread over both the carbon atom and the oxygen atom of the carbonyl group; in the second, no such mechanism is available. The two categories of radical should be easily distinguishable through the magnitudes of their muon-electron coupling constants, by analogy

with radicals formed in conjugated dienes[80] . A third possible site of muonium attachment is the oxygen atom of the carbonyl group, in which case an αβ-unsaturated muoxyalkyl radical is formed. Such a radical differs somewhat from the α-muoxyalkyl radicals studied in previous sections due, again, to the possibility of conjugative spin delocalisation through the carbon chain. Delocalisation of this kind is expected to lower the value of A_μ. The fourth possibility, that of Mu attachment at the carbonyl carbon atom, is known not to occur to any mensurable extent in aldehydes or ketones, and is not expected to be a major process here. The three respective muonium addition products are shown below.

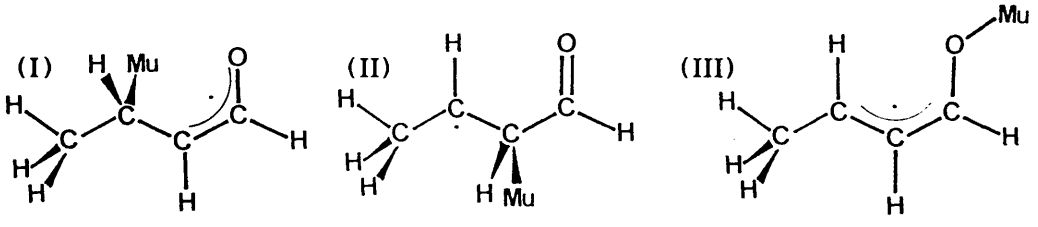

In addition to the conformerism arising through internal rotation around a single bond such as C_2-C_3 (adhering to the numbering system of the parent molecule), akin to that discussed earlier, in radicals of type (I) a second kind of conformational isomerism exists, defined by interchanges between *cisoid* and *transoid* forms through internal rotation around a partial double bond, in this instance C_1-C_2. While on the timescale of the μSR experiment processes of the first type are "fast", and the net μSR signal is therefore an average over all the appropriate torsional states, evidence[135] has shown that Arrhenius barriers to the interconversion of isomers of the second type can be such that exchange is "slow", leading to separate signals from *cisoid* and *transoid* radicals.

4.5.2 Experimental.

The experiments on crotonaldehyde were carried out using the μE4 beamline at PSI. The strength of the transverse field applied was selected

on the basis of clear separation of (temperature-dependent) radical signals from (temperature-independent) artefacts as either 0.2T or 0.3T. The sample of crotonaldehyde used (degassed and sealed by the standard procedure) was "Gold Label" standard, supplied by Aldrich, and almost exclusively of the *trans* isomer (99+%).

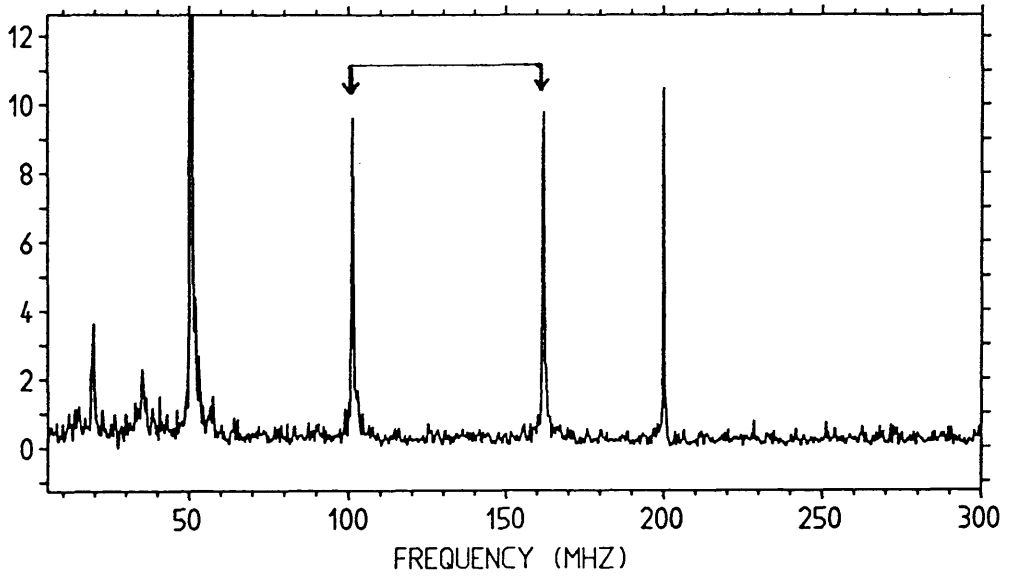

Figure 4.11 Fourier transformed μSR spectrum at room temperature of pure but-2-enal.

Figure 4.11 above shows the Fourier power spectrum, averaged over four histograms, obtained in *trans*-but-2-enal at 353K using a transverse field of 0.2T. The main radical signals are seen at about 100MHz and 162MHz. Unfortunately the signal at 100MHz overlaps the first overtone of the cyclotron frequency, precluding accurate fitting. The peaks at 50MHz and 200MHz are also artefacts of the system. By matching the signal at 162MHz with its theoretical corresponding low frequency signal A_μ for this radical at this temperature is determined to be 263.50MHz. The signals are therefore

assigned to radical (I). No lines at higher frequencies identifiable as belonging to a radical of type (II) can be seen. The very strong signal corresponding to muons in diamagnetic environments, occurring at about 27 MHz, obscures any signals from radicals of type (III). Indeed, it has generally been assumed that in αβ-unsaturated carbonyl compounds muonium addition is almost exclusively to one of the carbon atoms of the C=C double bond. However, excision of the diamagnetic signal by Fourier fitting leaves a pair of weak lines, situated approximately equidistantly from ν_D, one on either side, reminiscent of the transition frequencies characteristic of muoxyalkyl radicals. Fitting of the signals by normal methods is not in this case possible, but the muon-electron coupling constant A_μ is estimated to be roughly 16.1 MHz, less than half of that in acetonylacetone at the same temperature. This is strong evidence for the presence of radical (III). The temperature dependences of the two pairs of signals will be dealt with separately.

4.5.3 Radical (I).

Sections of the frequency domain spectra obtained at the other four temperatures of experimental measurement, each averaged over four histograms, are shown in **Figure 4.12 (a)**. The range of frequencies displayed, 70 MHz to 200 MHz, accommodates both signals corresponding to radical (I) at all temperatures. In each case the measurement was made with a transverse field of 0.3 T.

The coupling constant is fairly large, although smaller than in a primary alkyl radical, and decreases with increasing temperature, ranging from 301.92 MHz at 209 K down to 263.50 MHz at 353 K. These values are tabulated in full in **Table 4.5**. It is supposed that the temperature dependence originates in internal rotation around the single bond C_2-C_3. The potential barrier hindering such internal rotation is sufficiently low that what is manifested in the μSR spectrum is a gradual change with

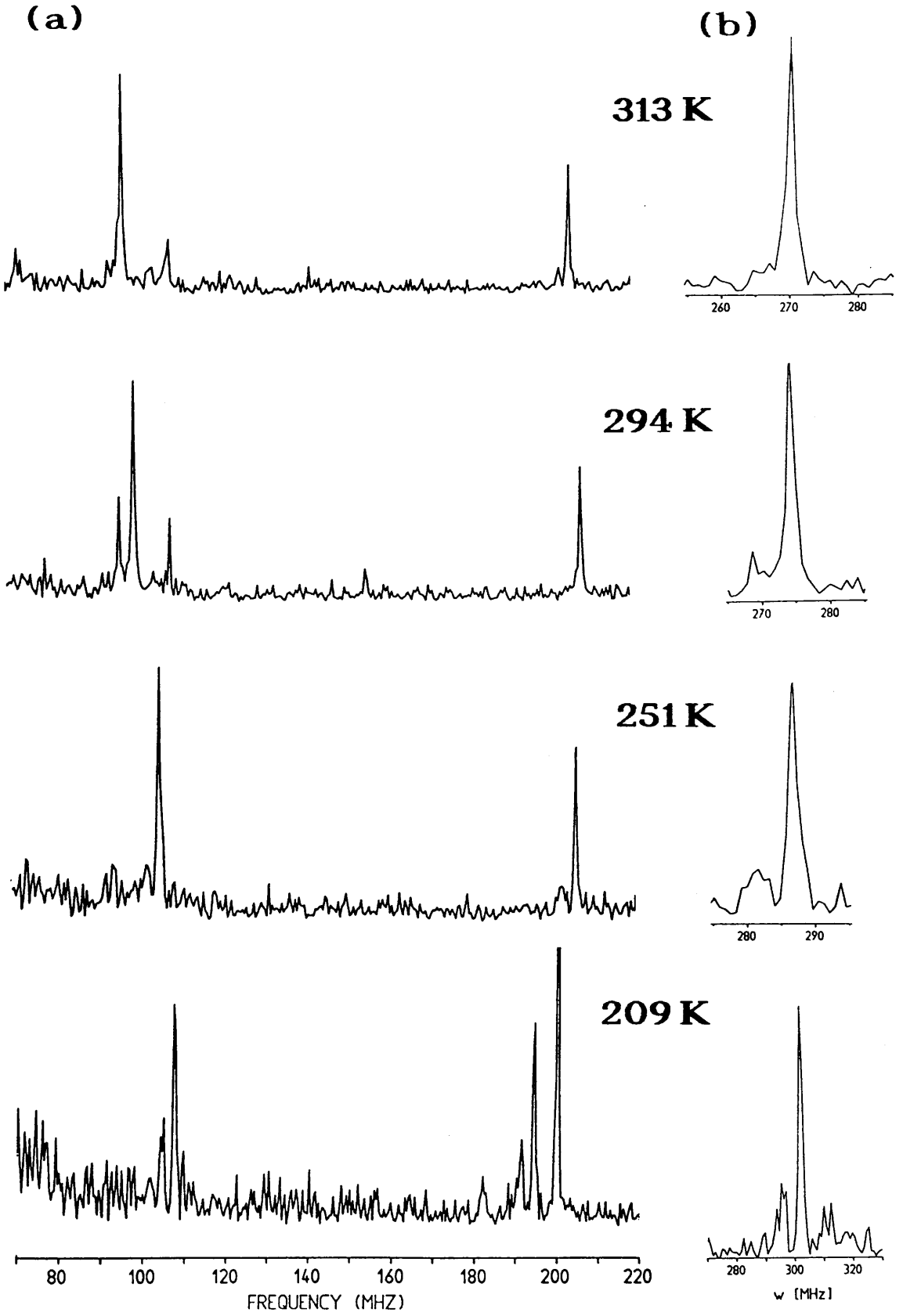

Figure 4.12 Fourier transformed μSR spectra over the range 70-200 MHz (a) and correlation diagrams (b) for but-2-enal showing signals due to radical (I).

Table 4.5 Muon-electron hyperfine coupling constants and transition frequencies for muonic radicals formed in *trans*-but-2-enal. Temperatures are in K, coupling constants and transition frequencies in MHz.

	Radical (I)	Radical (III)		
T	A_μ	ν_{12}	ν_{34}	A_μ
353.0*	263.4981	19.2	35.3	16.1
333.0	266.8094	33.3	47.5	14.2
313.0	270.4371	33.9	47.1	13.2
294.0	274.3228	35.8	45.2	9.4
251.0	286.2071	37.3	44.3	7.0
209.0	301.9201	37.9	44.1	6.2

At least 4×10^7 events were collected per temperature. The experimental error on the measurement of T is $\pm$0.1K, while the fitting error on A_μ for radical (I) is 0.05 MHz.

*This result was obtained with a transverse field of 0.2015 T. For all the others the field was 0.3025 T.

temperature in the population distribution among the torsional states. The conformation of lowest electronic energy is inferred to be that depicted below, with $\vartheta_o(Mu) = \pi/6$.

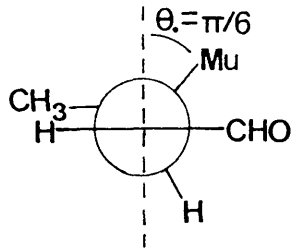

As the temperature increases, so do the populations of torsionally excited states in which the expectation value of the torsional angle approaches its free rotation value of $\pi/4$, and the mean position of the muon draws slightly nearer to the nodal plane of the π-system, extending over C_2, C_1, and O, in which the unpaired electron resides. The net spin density at the muon, and concomitantly the muon-electron hyperfine coupling constant, consequently decrease.

The reduced moment of inertia for internal rotation, I_R, as defined earlier, must be an invariant of the torsional motion. In this case the motion in question is rotation around C_2-C_3. Clearly the radical possesses too many degrees of freedom for I_R to be defined unequivocally and accurately. Also, the Heller-McConnell relation[46] between the hyperfine coupling constant and the angle of internal rotation can no longer be expected to hold due to the loss of twofold symmetry in the π-system with respect to the torsional co-ordinate, this being consequent upon the conjugative delocalisation of the centre of unpaired spin density away from the axis of internal rotation. As a result, quantitative analysis of the hyperfine data in order to determine the barrier to internal rotation around C_2-C_3 must attend the development of a more sophisticated formalism.

In consideration of the conformational isomerism between *cisoid* and *transoid* forms interchanged by internal rotation around the partial

double bond C_1-C_2 it might be expected, given the greater (by analogy with similar radicals[135] and the parent compound) thermodynamic stability of the *transoid* form, either that the spectra show only signals due to *transoid* radicals or that the signal corresponding to the *cisoid* radical be seen only at high temperatures where the activation barrier to *cisoid-transoid* isomerism can be overcome. However, a close inspection of the spectra in **Figure 4.12(a)** reveals that only at the three lowest experimental temperatures is there any suggestion of a second pair of signals, with a coupling constant some 5-10 MHz lower than the dominant pair. Correlation diagrams, produced using a program written by I.D. Reid[136], matching low frequency signals with their high frequency counterparts according to the theory of high transverse field free radical μSR (see Chapter 1), show this phenomenon with greater clarity (**Figure 4.12(b)**). It should be noted that at low temperatures both the correlations and the signals themselves are quite weak; consequently, accurate determination of the hyperfine coupling constant of the second radical is not possible.

Two separate views of the situation underlying the observation described above are conceivable. In the first of these, a regime of fast conformational exchange exists at high temperatures, and the signal observed is the statistical average over both sets of torsional states (about C_2-C_3 and C_1-C_2). In this picture, only at temperatures below about 300 K does conformational exchange become slow on the experimental timescale. This model implies that the activation barrier to *transoid-cisoid* conversion is considerably smaller in this radical than in the radicals of the same type studied by Strub *et al.*[135] In the second model the situation prevailing is one of slow conformational exchange in the *transoid-cisoid* direction, but faster exchange in the reverse direction. In other words, the activation barrier to *cisoid-*

transoid isomerism is small. Only at low temperatures is the lifetime of the *cisoid* conformer sufficiently long that it can be detected. Of these scenarios, the first is perhaps the more likely, but in order that a categorical attribution be made further analysis is indicated.

4.5.4 Radical (III).

A selection of the low frequency parts of the Fourier transform spectra obtained after fitting and excision of the diamagnetic signal is shown in **Figure 4.13**. On either side of ν_D weak signals can be seen. (That these are indeed genuine signals and not simply system noise or the result of poor fitting of ν_D is substantiated by comparison with spectra in which the diamagnetic frequency has been excised but no radical of small coupling is possible. In every such case the diamagnetic signal is removed with complete efficacy to leave a low and regular noise background.) Computer fitting of these signals is not possible due to their low amplitude, but the result of a rough assessment by eye of the signal frequencies and corresponding coupling constants is tabulated in **Table 4.4** along with those of radical (I). The signals suggest the presence of a radical with a small coupling constant, having a temperature dependence with a positive temperature coefficient. These properties are typical of a muoxyalkyl radical, and reinforce the assignment of the signals to radical (III). The spectra therefore represent the first observation of muonium addition to the carbonyl oxygen atom in an αβ-unsaturated carbonyl compound.

More recent studies by D. Buttar of this group[132] upon 3-methyl-but-2-enal show a larger proportion of type (III) radicals to be formed than in crotonaldehyde, and also show a temperature dependence of opposite sign to prevail in the hyperfine coupling constant of the type (I) radical. Both of these phenomena stem from the presence of the extra methyl group. The first can be attributed to steric interference

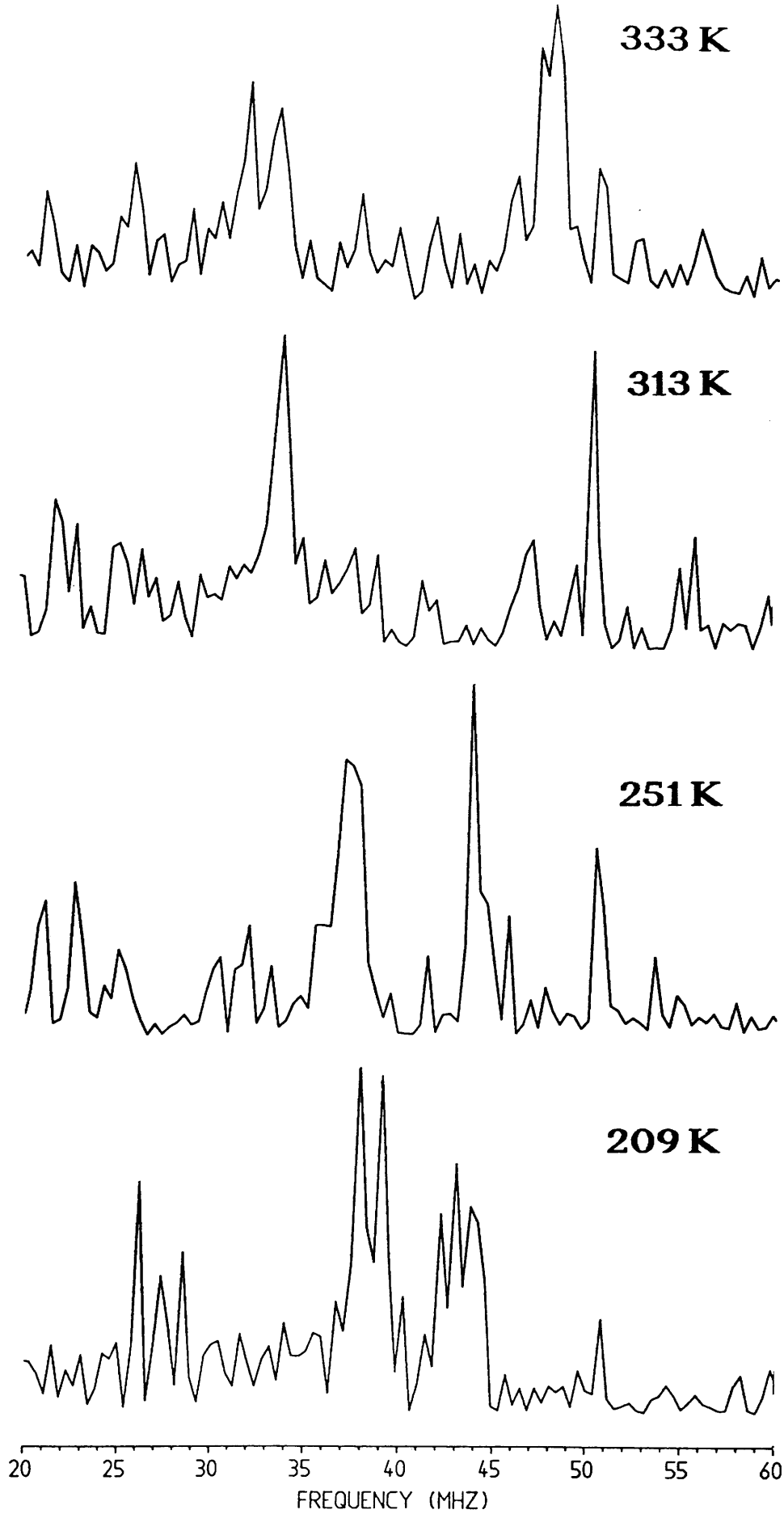

Figure 4.13 Fourier transformed μSR spectra for but-2-enal over the range 0-60 MHz showing the weak signals attributed to radical (III).

to the approach path for muonium addition to the olefinic functionality by the two methyl groups now attached at carbon-3, while the second simply denotes a changed conformational preference.

CHAPTER 5

Ab Initio Calculations on α-Hydroxyalkyl Radicals.

"Given three or four lives I might have accomplished something."

Samuel Beckett.

5.1 General Introduction.

A variety of calculations at the UHF-SCF level are presented which explore some of the conformational properties of α-hydroxyalkyl radicals. These radicals are analogous to the α-muoxyalkyl radicals produced by irradiation of simple carbonyl compounds with positive muons. Of the radicals described here, only 2-hydroxyprop-2-yl and hydroxyethyl have had their muonic analogues subjected to study thus far (see chapters 3 and 4 of this thesis respectively). All calculations were carried out using the CYBER 205 supercomputer at the University of Manchester. The electronic structure packages employed were GAMESS[137], for the optimisation of geometrical parameters, and ATMOL[138], for single-point calculations in which spin projection was carried out (at the UHF-AA level). Geometry optimisations were, unless otherwise stated, performed using the split valence 3-21G basis set of Binkley, Pople, and Hehre[60] (hereinafter referred to as SV-3-21G), while single-point calculations were generally carried out using a "saturated" basis set of nominally triple-zeta accuracy (actually Dunning and McLean's[61,139] [5s3p] contraction of Huzinaga's[101] (10s6p) gaussian primitive basis set), supplemented by polarisation functions consisting of a full d-set on each first row atom and a full p-set on each H atom[140]. The criteria for convergence of the SCF energy cycles and the force minimisation cycles were identical to those defined in Chapter 2.

5.2 Hydroxymethyl Radical.

5.2.1 Introduction.

The history of the study of the hydroxymethyl radical $\dot{C}H_2OH$, a radical isoelectronic with ethyl, by ESR spectroscopy is outlined in

the introductory section of Chapter 3. No corresponding examination of the corresponding muonic radical has to date been undertaken, largely due to the toxicity, volatility and reactivity of pure methanal, which polymerises quite rapidly at temperatures above its freezing point. As the radical is a known intermediate in atmospheric processes relevant to combustion and air pollution[141,142] it has been the subject of several theoretical studies, particularly in connection with the weakly exothermic rearrangement reaction in which it is formed from the methoxy radical $CH_3\dot{O}$.

5.2.2 A Simple Model of Internal Rotation.

Initially a set of calculations were carried out using ATMOL at geometries based upon a very simple model of the hydroxymethyl radical and, in particular, the process of internal rotation therein[145]. A rigid planar structure was devised for the CH_2O part of the molecule using bond lengths obtained from Sutton[134] (this structure is illustrated in **Figure 5.1**). To the O atom of this was attached an H atom, at an internuclear distance of 96pm and a $C\hat{O}H$ bond angle of 109°. Single-point calculations were undertaken at ten values of the torsional angle ϑ equally spaced between 0° and 90°, with Dunning's contracted basis set of [5s4p] for C and O and [3s] for H, but without polarisation functions[102]. The minimum energy was found to occur at $\vartheta = 80°$.

Figure 5.1 Model calculation on $\dot{C}H_2OH$ - geometrical parameters.

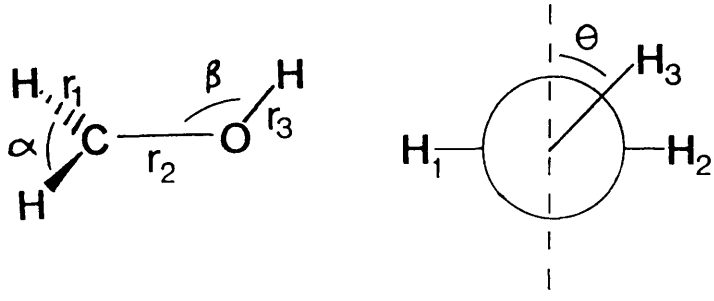

$r_1 = 112pm$; $r_2 = 143pm$; $r_3 = 96pm$; $\alpha = 118°$; $\beta = 109°$.

The total energy corresponding to this conformation was found to be -114.39965 hartree. This is lower by a striking amount (about 0.5 $MJ\,mol^{-1}$) than the energies of the $\vartheta=0^{\circ}$ and $\vartheta=90^{\circ}$ conformations, both of which are in the neighbourhood of -114.2 hartree. While this set of calculations can not be said at any level to represent a real physical process occurring within the radical, they do suggest that "simple" internal rotation around the C-O bond is not a minimum energy path over the potential energy hypersurface, and that the commonly accepted view in which the equilibrium conformation is that in which the hydroxylic proton lies in the nodal plane of the singly-occupied 2p orbital centred on the radical C atom must be called into question. Remarkably, also, at this basis set and geometry the experimental proton hyperfine coupling constants are reproduced with fortuitous accuracy (A_{H_1}= -46.15 MHz, A_{H_2}= -48.96 MHz, A_{H_3}= -1.26 MHz).

5.2.3 Geometry Optimisation - Effect of Basis Set.

The hydroxymethyl radical has sufficiently few geometrical degrees of freedom that full optimisation of all geometrical parameters can be carried out employing a reasonably large extended basis set without incurring prohibitive expense in terms of computational time. Two such calculations are described below.

I. SV-3-21G Basis Set.

The converged geometry yielded by a full optimisation at the SV-3-21G level upon the hydroxymethyl radical is illustrated in **Figure 5.2**. The appropriate numerical values for the converged parameters on exit are given in Key A. The total energy appears below, together with its nuclear and electronic components.

E_{total} = -113.773816 hartree

E_{el} = -148.680674 hartree

E_{nuc} = 34.906858 hartree

The total energy obtained with this basis set is considerably poorer than those generated in the model calculation using the Dunning basis. Clearly, then, the small split-valence set, consisting of a total of 24 contracted functions, must not be expected to represent the electronic structure of the radical to a very high degree of accuracy.

The geometry of the radical at this level of computational accuracy is seen to be of C_1 symmetry, consisting of a roughly planar *transoid* HCOH system ($\angle$HCOH = 177.17°), with the second methylene H displaced from this plane by approximately 35°. This is consistent with calculations by other authors[145]. The C-O bond length has decreased with respect to that in the model calculation (which was based upon the experimental bond length in methanol) by 3.6 pm, indicating a small degree of retention of double bond character in the radical.

II. Triple Zeta Basis Set with Polarisation Functions (TZVP).

The calculation described above was repeated using Dunning's triple zeta basis set supplemented with polarisation functions consisting of a set of d-functions on C and O and a set of p-functions on each H. The final geometry is as depicted in **Figure 5.2**, with numerical values of the converged parameters given by Key B. The total energy corresponding to this geometry, and its nuclear and electronic components, are given below.

E_{total} = -114.459376 hartree

E_{el} = -150.067779 hartree

E_{nuc} = 35.608402 hartree

The large improvement in the total energy over the smaller basis set (0.6856 hartree or 1.8 MJ mol^{-1}) is due, of course, to the inevitable lowering in the electronic energy accompanying an improvement in basis set (in this case, a decrease of 1.4061 hartree). The converged structure using the larger basis set actually has a classical nuclear repulsion

energy which is greater than that of the SV-3-21G geometry by 0.7015 hartree.

Figure 5.2 Optimised Geometry of the Hydroxymethyl Radical.

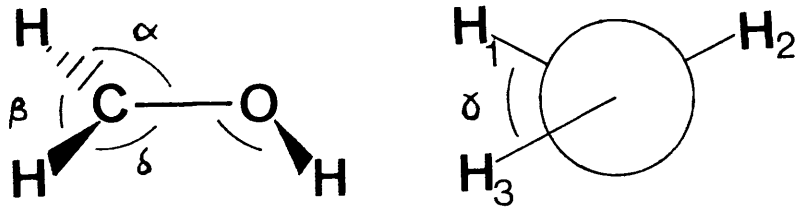

Key A. Converged geometrical parameters at SV-3-21G level.

r_1 = 107.0 pm ; r_2 = 107.5 pm ; r_3 = 96.5 pm ; r_4 = 139.2 pm ;

α = 112.77° ; β = 119.67° ; δ = 119.02° ; ϑ = 112.20° ;

γ = 34.98° .

Key B. Converged geometrical parameters at TZVP level.

r_1 = 107.1 pm ; r_2 = 107.6 pm ; r_3 = 94.0 pm ; r_4 = 135.7 pm ;

α = 113.30° ; β = 119.49° ; δ = 118.11° ; ϑ = 111.10° ;

γ = 34.02° .

In consideration of the geometry it is found that all but one of the internuclear distances between bonded atoms have decreased. While it is the case that the change in total energy in going from a small basis set to a larger one is certainly an improvement (that is to say, the accompanying increase in overlap terms produces a lowering in the variationally-protected SCF energy), the change in bond lengths is not guaranteed in any such way and in general it is found that basis sets smaller than about SV-4-31G tend to yield bond lengths longer than those determined by experimental means, while larger basis sets tend to yield bond lengths shorter than experiment. Notwithstanding,

it is illuminating to compare the two sets of geometrical parameters.

With the Dunning basis the HCOH "*trans*" structure is seen to have approached even closer to planarity, the appropriate torsional angle now taking the value 179.09°. Both C-H bond lengths are typical of methylenic bonds, but it should be noted that the bond lying out of the plane is now distinctly longer than the other. The C-O bond shows yet more double bond character.

Table 5.1 Atomic spin densities and ^1H hyperfine coupling constants for $\dot{C}H_2OH$ at the SV-3-21G and TZVP levels.

	SV-3-21G		TZVP	
atom	s.d.	A_H/MHz	s.d.	A_H/MHz
C	0.41119	——	0.35329	——
O	0.08678	——	0.08244	——
H_1	-0.02889	-41.02	-0.02492	-35.39
H_2	-0.03482	-49.44	-0.03020	-42.88
H_3	-0.00248	-3.52	-0.00282	-4.00

Table 5.1 shows the atom spin densities and ^1H coupling constants associated with the hydroxymethyl radical calculated using the two basis sets. The methylene proton couplings are again surprisingly close to the experimental values[114] considering that even at absolute zero, and disregarding intermolecular effects, the radical is still subject to zero-point vibrational motions about its equilibrium conformation, while at higher temperatures excited vibrational and large amplitude motion

(for example, inversion at the pyramidal radical centre) states will contribute to the mean radical conformation and thus to the hyperfine coupling constants. The extent to which the methylene proton couplings are independent of conformation, together with their sign, indicates that the origin of spin density at these protons is largely through "spin polarisation" processes. The poorer degree of accuracy with which the hydroxylic proton coupling is reproduced is easily explained through the dependence of the experimental coupling constant on the excitation of the torsional mode.

5.3 Hydroxyethyl Radical.

5.3.1 Introduction.

In the case of the hydroxethyl radical $\dot{C}H_3CHOH$ the large number of geometrical degrees of freedom together with the lack of symmetry render a free optimisation at triple zeta level impracticable. However, from the calculations on the hydroxymethyl radical described above it is clear that a large improvement in basis set need not lead to a large change in geometry in a radical consisting only of first row atoms. On the assumption that a structural similarity between these homologous radicals is probable the methodology adopted towards geometry optimisation was as follows. Two starting geometries were chosen, each based upon the converged geometry of $H_2\dot{C}OH$, and in each of which a different methylenic proton was replaced by a stylised methyl group (having C_{3v} symmetry, and "standard" bond lengths[134]). Each geometry was then optimised in a completely unrestricted manner at the SV-3-21G level.

5.3.2 Results.

The converged geometries of the *cisoid* and *transoid* conformers of the hydroxyethyl radical determined from the two calculations described above are shown in **Figure 5.3** (I) and (II) respectively. The

Figure 5.3 Converged geometrical parameters for the α-hydroxyethyl radical using a SV-3-21G basis set.

(I) *Cisoid* conformer.

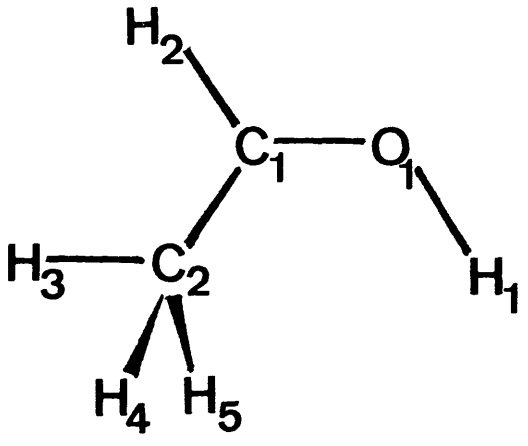

Bond lengths /pm

C_1-O_1 139.8; C_1-C_2 150.5; C_1-H_2 107.2; O_1-H_1 0.966; C_2-H_3 108.2; C_2-H_4 108.7; C_2-H_5 108.9.

Bond angles /°

C_1-O_1-H_1 111.90; O_1-C_1-H_2 110.96; O_1-C_1-C_2 118.78; C_1-C_2-H_3 110.11; C_1-C_2-H_4 111.20; C_1-C_2-H_5 111.40; H_3-C_2-H_4 107.92; H_3-C-H_5 108.30; H_4-C_2-H_5 107.78.

Dihedral angles /°

C_2-C_1-O_1-H_1 -37.84; H_2-C_1-O_1-H_1 177.15; H_3-C_2-C_1-O_1 176.97.

Figure 5.3 (II) *Transoid* conformer.

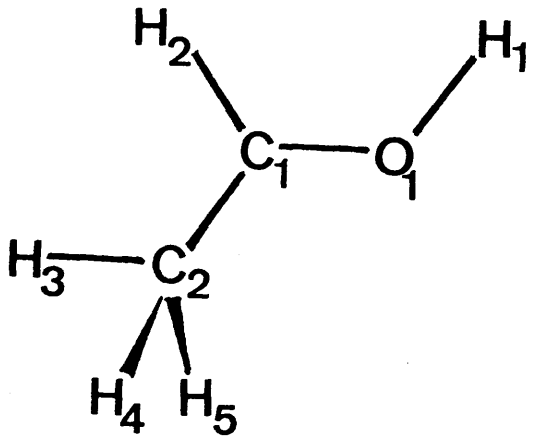

Bond lengths /pm

C_1-O_1 139.9; C_1-C_2 149.8; C_1-H_2 107.8; O_1-H_1 96.5; C_2-H_3 108.3; C_2-H_4 108.8; C_2-H_5 108.3.

Bond angles /°

C_1-O_1-H_1 112.11; O_1-C_1-H_2 117.02; O_1-C_1-C_2 112.83; C_1-C_2-H_3 110.51; C_1-C_2-H_4 111.28; C_1-C_2-H_5 109.57; H_3-C_2-H_4 108.55; H_3-C_2-H_5 109.04; H_4-C_2-H_5 107.78.

Dihedral angles /°

C_2-C_1-O_1-H_1 177.04; H_2-C_1-O_1-H_1 -38.02; H_3-C_2-C_1-O_1 -171.18.

total energy of each conformer, together with the separation of this value into nuclear and electronic contributions, is given in **Table 5.2.**

Table 5.2 UHF-SCF energies (/hartree) calculated at the SV-3-21G level for the *cisoid* and *transoid* conformers of the hydroxyethyl radical.

	cisoid	*transoid*
E_{total}	-152.600248	-152.600321
E_{el}	-226.904533	-227.125094
E_{nuc}	74.304285	74.524773

From these calculations it appears that, due to an improvement in the electronic energy, the *transoid* conformation is favoured over the other by 192 J mol^{-1}. The converged geometrical parameters of this radical are strikingly similar to those of $\dot{C}H_2OH$ determined using the same basis set. The very slightly longer C-O bond found in this species as compared with $\dot{C}H_2OH$ indicates that the presence of the slightly electron-releasing α-methyl group stabilises the unpaired electron on the radical C atom, decreasing contributions to the structure from canonical representations in whch the spin is located on the hydroxylic proton. Little effect on the O-H bond length is evident. Atom spin densities and corresponding coupling constants for both conformers are presented in **Table 5.3.** It can be seen that C_1 carries slightly more spin density in this instance than does $\dot{C}$ in $\dot{C}H_2OH$ (0.45478 as compared with 0.41119).

Table 5.3 Atomic spin densities and ^1H coupling constants for the *cisoid* (I) and *transoid* (II) conformers of $CH_3\dot{C}HOH$ at the SV-3-21G level.

	Conformer (I)		Conformer (II)	
atom	s.d.	A_H/MHz	s.d.	A_H/MHz
C_1	0.45421	——	0.45478	——
C_2	-0.06038	——	-0.07237	——
O_1	0.07496	——	0.07326	——
H_1	-0.00179	-2.54	-0.00184	-2.61
H_2	-0.03222	-45.76	-0.02500	-35.58
H_3	0.00462	6.56	0.00629	8.93
H_4	0.01528	21.70	0.03712	52.71
H_5	0.03719	52.81	0.01399	19.87

5.4 Fluorohydroxymethyl Radical.

5.4.1 Introduction.

Again assuming a structural similarity to exist between the hydroxymethyl radical and its singly fluorinated congener $\dot{C}HFOH$, a radical isoelectronic with $CH_3\dot{C}HOH$, two unrestricted geometry optimisations were carried out on the latter at the UHF-SCF level using a split valence 3-21G basis set. In the first of these, the "out-of-plane" or *cisoid* H was replaced with F; in the second, the "in-plane" or *transoid* H was replaced.

5.4.2 Results.

The converged *cisoid* and *transoid* geometries of $\dot{C}HFOH$ appear in **Figure 5.4** (I) and (II) respectively. The corresponding total, electronic,

Figure 5.4 Optimised UHF-SCF SV-3-21G geometrical parameters for the *cisoid* and *transoid* conformers of $\dot{C}HFOH$.

(I) *Cisoid* conformer.

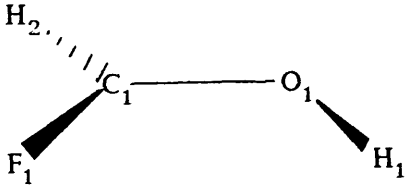

Bond lengths /pm

C_1-O_1 136.6; C_1-F_1 136.9; C-H_2 106.9; O-H_1 96.7.

Bond angles /°

C_1-O_1-H_1 113.29; O_1-C_1-H_2 113.11; O_1-C_1-F_1 114.42; F_1-C_1-H_2 113.92.

Dihedral angles /°

F_1-C_1-O_1-H_1 49.92; H_2-C_1-O_1-H_1 -177.39.

(II) *Transoid* conformer.

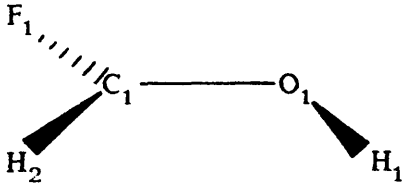

Bond lengths /pm

C_1-O_1 137.2; C_1-F_1 135.5; C_1-H_2 107.6; O_1-H_1 96.4.

Bond angles /°

C_1-O_1-H_1 113.18; O_1-C_1-H_2 118.50; O_1-C_1-F_1 110.67; F_1-C_1-H_2 113.92.

Dihedral angles /°

F_1-C_1-O_1-H_1 174.46; H_2-C_1-O_1-H_1 41.46.

and nuclear energies are given in **Table 5.4.**

Table 5.4 UHF-SCF SV-3-21G energies of the *cisoid* (I) and *transoid* (II) conformers of the fluorohydroxymethyl radical $\dot{C}HFOH$ (/hartree).

	cisoid	*transoid*
E_{total}	-212.104182	-212.096643
E_{el}	-283.593147	-283.764362
E_{nuc}	71.488965	71.667719

In this case it is the *cisoid* conformer, where the substituent is out of the C-O-H plane, that is more stable (by about 20 kJ mol^{-1}), due, in contrast to the previous calculations, to a lowering in the classical internuclear repulsion energy.

Considering the geometrical parameters in greater detail, the C-O bond length is found to be considerably shortened in comparison to those in $\dot{C}H_2OH$ and $CH_3\dot{C}HOH$. There is an accompanying small increase in the O-H internuclear distance. This indicates that the effect of the electron-withdrawing F substituent is to increase the contribution to the overall structure from the doubly-bonded canonical form in which the excess spin is located on the hydroxylic proton. Further evidence for the validity of this conceptual approach is given by the calculated atomic spin densities, tabulated in **Table 5.5.**

Table 5.5 SV-3-21G UHF-SCF atomic spin densities for the *cisoid* (I) and *transoid* (II) conformers of the fluorohydroxymethyl radical $\dot{C}$HFOH.

	conformer	
atom	(I)	(II)
C	0.57463	0.55281
O	0.05274	0.08858
F	0.11250	0.09508
H_1	0.00104	-0.00521
H_2	-0.00959	-0.00124

In the lower energy conformer (I) the residual spin density on the hydroxylic proton has positive sign (in contrast to the previous cases) and corresponds to a coupling constant of around 1.5 MHz. The spin density at the methylenic proton, while still negative, is considerably smaller in absolute value. However, the net spin density at $\dot{C}$ is increased in this radical from its value in the two previously studied, while that at O is decreased, which suggests an enhancement by the presence of F of the spin polarisation mechanism in the C-O-H system.

Although the unpaired spin density on $\dot{C}$ is increased by the presence of the α-F atom the effect on the gross Mulliken atomic population[146,147,148] is, not unexpectedly, in the opposite direction. The slightly smaller Mulliken population associated with $\dot{C}$ in $CH_3\dot{C}HOH$ (5.88205) as compared with that in $\dot{C}H_2OH$ (6.09995) is due not to an electron-withdrawing influence from the α-Me group (the sum of the Mulliken populations of the atoms in this group is 9.00087), but rather to the fact that in this instance $\dot{C}$ withdraws electronic charge density from

only one α-H instead of two (as in the case of $\dot{C}H_2OH$).

The SOMO (or, to be more precise, since it is the UHF approximation which is in use, the highest energy occupied MO of α-spin) energies of CH_2OH, $CH_3\dot{C}HOH$, and $\dot{C}HFOH$, are (in hartree) -0.340610, -0.322601, and -0.374635 respectively, indicating that substitution of H by F has a stabilising effect on the orbital containing the unpaired electron, while substitution by Me has the opposite effect. This MO is found to consist mainly of p_z functions centred on $\dot{C}$, in accordance with the traditional picture of the location of the unpaired electron in free radicals, with contributions from the p_z functions on O in all three radicals, on F in $\dot{C}HFOH$, and with small additional contributions from hydrogenic s-functions.

5.5 Difluorohydroxymethyl Radical.

A full geometry optimisation at the UHF-SCF level using the SV-3-21G basis set was also carried out on the doubly F-substituted hydroxymethyl radical, $\dot{C}F_2OH$, to yield the energies shown below and the converged geometrical parameters displayed in **Figure 5.5.**

E_{total} = -310.437157 hartree

E_{el} = -434.736870 hartree

E_{nuc} = 124.299713 hartree

The C-O bond shows a further decrease in length, and the O-H bond a corresponding small increase. The other trends are also followed: an increase in the spin density at $\dot{C}$ (to 0.80619) is accompanied by a decrease in Mulliken population at $\dot{C}$ (to 4.93104) and an increase in that at O (from 8.70270 to 8.71681). The energy of the highest α-MO has decreased to -0.418408 hartree, and the MO shows an increased contribution from the O atom.

Figure 5.5 Converged geometrical parameters for $\dot{C}F_2OH$ obtained from an *ab initio* optimisation at the UHF-SCF SV-3-21G level.

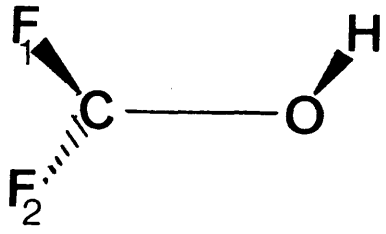

Bond lengths/pm

C-O 135.1; C-F_1 135.2; C-F_2 133.4; O-H 96.6.

Bond angles/°

C-O-H 113.90; O-C-F_1 113.77; O-C-F_2 111.04; F_1-C-F_2 110.72.

Dihedral angles/°

F_1-C-O-H 44.91; F_2-C-O-H 170.62.

5.6 2-Hydroxyprop-2-yl Radical.

Ab initio calculations were carried out at the SV-3-21G level using the UHF-SCF approximation upon three conformations of the 2-hydroxy-prop-2-yl (or 1-hydroxy-1-methylethyl or isopropylol) radical $(CH_3)_2\dot{C}OH$, a radical isoelectronic both with $\dot{C}F_2OH$ (see Section 5.5) and with the much-studied t-butyl radical $(CH_3)_3\dot{C}$ [149,150], in order to examine variations in energy and changes in the distribution of electronic charge and spin density during the internal rotation process.

Initially, a calculation was carried out in which all 27 independent geometrical parameters were freely optimised. The resulting geometry, Conformer (I), can be seen in **Figure 5.6**. The corresponding energies are

E_{total} = -191.427011 hartree

E_{el} = -316.729798 hartree

E_{nuc} = 125.302787 hartree

Figure 5.6 Converged geometrical parameters extracted from an unrestricted optimisation upon the 2-hydroxyprop-2-yl radical at the UHF-SCF SV-3-21G level.

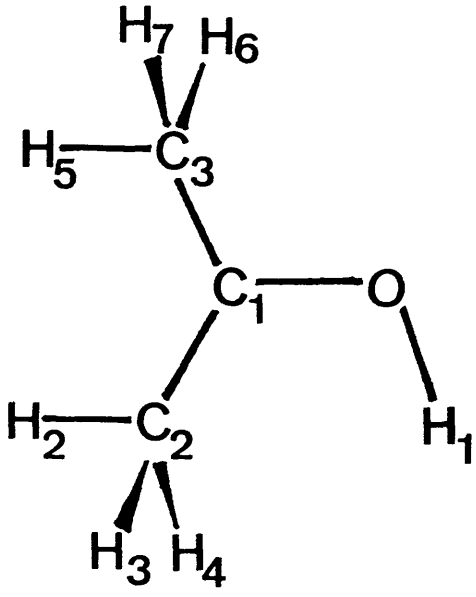

Bond lengths /pm

C_1-O_1 140.5; C_1-C_2 150.9; C_1-C_3 150.1; O_1-H_1 96.5; C_2-H_2 108.2; C_2-H_3 108.9; C_2-H_4 108.6; C_3-H_5 108.3; C_3-H_6 108.2; C_3-H_7 108.9.

Bond angles /°

C_1-O_1-H_1 111.95; O_1-C_1-C_2 116.75; O_1-C_1-C_3 111.01; C_2-C_1-C_3 119.43; C_1-C_2-H_2 110.31; C_1-C_2-H_3 110.89; C_1-C_2-H_4 111.36; H_2-C_2-H_3 108.35; H_2-C_2-H_4 107.97; H_3-C_2-H_4 107.85; C_1-C_3-H_5 110.63; C_1-C_3-H_6 109.76; C_1-C_3-H_7 110.82; H_5-C_3-H_6 109.15; H_5-C_3-H_7 108.50; H_6-C_3-H_7 107.91.

Dihedral angles /°

H_1-O_1-C_1-C_2 39.00; H_1-O_1-C_1-C_3 -179.46; O_1-C_1-C_2-H_2 -172.44; O_1-C_1-C_2-H_3 67.52; O_1-C_1-C_2-H_4 -52.57; O_1-C_1-C_3-H_5 167.26; O_1-C_1-C_3-H_6 46.74; O_1-C_1-C_3-H_7 -72.34; C_2-C_1-C_3-H_5 -52.37; C_2-C_1-C_3-H_6 -172.89; C_2-C_1-C_3-H_7 68.02; C_3-C_1-C_2-H_2 49.38; C_3-C_1-C_2-H_3 -70.66; C_3-C_1-C_2-H_4 169.24.

The total energy is better by 9.26 millihartree ($\approx 24\,kJ\,mol^{-1}$) than that obtained by Lien and Hopkinson[151] using the SV-3-21G basis set within an RHF calculation, but poorer than that obtained by the same authors using 6-31G*/RHF by a margin of 61.85 millihartree ($\approx 160\,kJ\,mol^{-1}$).

A second calculation was undertaken upon the torsional barrier geometry, of C_s symmetry, where the O-H bond eclipses the axis of the p_z orbital containing the unpaired electron. Convergence was achieved to yield energies of

E_{total} = -191.423665 hartree

E_{el} = -316.308262 hartree

E_{nuc} = 124.884597 hartree

and a set of geometrical parameters (designated Conformer (II)) depicted in **Figure 5.7**. The energy difference between conformations is calculated to be 8785 $J\,mol^{-1}$, considerably smaller than V_2 for this radical as determined from Lehni's ESR data[119] (see Section 3.2.1), but comparable in scale with barriers obtained from μSR data on the 2-muoxyprop-2-yl radical, especially in binary aqueous solutions of propan-2-one (see Sections 3.2, 3.3). In common with the ethyl radical (Chapter 2) the geometry of minimum energy is determined by a local minimum in the electronic energy (the classical internuclear repulsion energy is higher than in the barrier geometry) while the torsional barrier geometry represents a local minimum in the internuclear repulsion energy. This phenomenon of an approximate mirror image relationship between the nuclear and electronic energy surfaces is one commonly encountered in *ab initio* quantum chemical calculations[152]. In going from Conformer (I) to Conformer (II) the spin density on $\dot{C}$ decreases slightly, from 0.49880 to 0.48188, but this is accompanied by a much larger decrease in the spin density on O, which drops by a factor of ≈16 to 0.00405. This is a consequence of a change in the shape of the highest α-MO, which

Figure 5.7 Converged geometry at the UHF-SCF SV-3-21G level of the torsional barrier conformation (symmetry C_s) of the 2-hydroxyprop-2-yl radical.

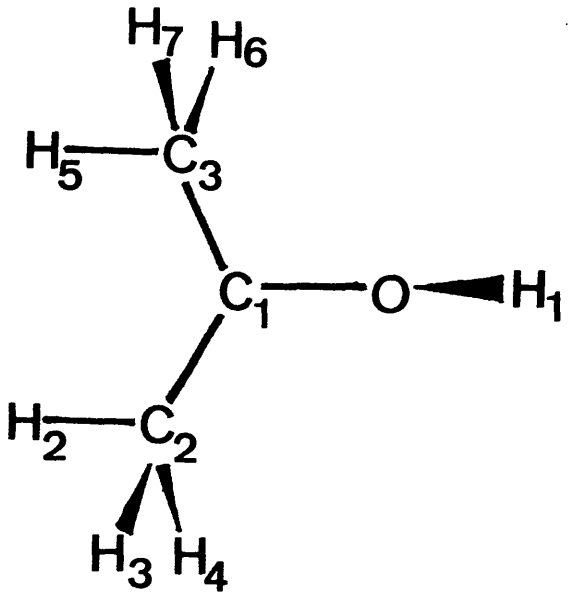

Bond lengths /pm

C_1-O_1 141.5; C_1-C_2 150.4; C_1-C_3 150.4; O_1-H_1 96.7; C_2-H_2 108.3; C_2-H_3 108.4; C_2-H_4 108.9; C_3-H_5 108.3; C_3-H_6 108.9; C_3-H_7 108.4.

Bond angles /°

C_1-O_1-H_1 111.69; O_1-C_1-C_2 114.07; O_1-C_1-C_3 114.07; C_2-C_1-C_3 119.84; C_1-C_2-H_2 110.87; C_1-C_2-H_3 110.50; C_1-C_2-H_4 110.40; H_2-C_2-H_3 108.89; H_2-C_2-H_4 108.47; H_3-C_2-H_4 107.62; C_1-C_3-H_5 110.87; C_1-C_3-H_6 110.40; C_1-C_3-H_7 110.50; H_5-C_3-H_6 108.47; H_5-C_3-H_7 108.89; H_6-C_3-H_7 107.62.

Dihedral angles /°

H_1-O_1-C_1-C_2 -108.60; H_1-O_1-C_1-C_3 108.60; O_1-C_1-C_2-H_2 171.72; O_1-C_1-C_2-H_3 50.89; O_1-C_1-C_2-H_4 -68.05; O_1-C_1-C_3-H_5 -171.72; O_1-C_1-C_3-H_6 68.05; O_1-C_1-C_3-H_7 -50.89; C_2-C_1-C_3-H_5 47.81; C_2-C_1-C_3-H_6 -72.43; C_2-C_1-C_3-H_7 168.64; C_3-C_1-C_2-H_2 -47.81; C_3-C_1-C_2-H_3 -168.64; C_3-C_1-C_2-H_4 72.43.

loses all of the p_z character on $\dot{C}$ and O which allowed transmission of spin density to the O nucleus, and takes on a character dominated by p_x orbitals centred on $\dot{C}$.

The third and final calculation performed upon this radical was an optimisation again constrained to C_s symmetry, in which all three carbon atoms, plus the O atom and the hydroxylic H, were forced into coplanarity. This resembles the traditional view of the equilibrium geometries of α-hydroxyalkyl radicals, where the unpaired electron is held in a $2p_z$ orbital on a carbon atom in a trigonal planar environment. The results of this calculation are rather striking. Convergence was finally achieved at a geometry in which the O-H internuclear distance was 300.6 pm or, in other words, at which dissociation into a molecule of propan-2-one and an H atom had effectively taken place. (The geometry yielded by this calculation for the $(CH_3)_2CO$ moiety is in fact identical to that obtained for propan-2-one using the same basis set and geometrical convergence criteria.) In the converged state the spin density on the carbon atom which was formerly the "radical centre" was found to have decreased to -0.00160, while that on the formerly hydroxylic H had increased to 0.39309. The total energy found to correspond to this state was -191.379433 hartree.

Tracing the origins of this dissociation within the calculation it is found that at the starting geometry, where the O-H internuclear distance was chosen to be 96 pm, the force on this internal co-ordinate is -0.209 hartree/bohr, a factor of 13 greater than that on any other bond stretching co-ordinate. The highest MO of α-spin, consisting to a large extent of s-functions centred on the hydroxylic H atom, has an energy of -0.036182 hartree, greater by 0.274 hartree ($\approx$0.7 MJ mol^{-1}) than that of Conformer (I).

As the above calculation was performed within the point group C_s, the statement cannot confidently be made that the planar conformation of this radical is unstable without recourse to further computation in which the methyl groups are allowed freedom of rotation. Also, at the SCF level used here any influence exerted on the internal rotation process by excited electronic configurations goes undetected; in order to establish such influence the employment of configuration interaction is indicated. However, the result does suggest that complex effects are at work in determining the electronic structure of even the simplest of radicals, and therefore that it is dangerous to make inferences by resorting to standard formal conceptions.

5.7 Methoxymethyl Radical.

The methoxymethyl radical, $\dot{C}H_2OCH_3$, is an isomer of the hydroxyethyl radical, $\dot{C}H_3CHOH$. A set of *ab initio* calculations were carried out at the UHF-SCF level using a split-valence 3-21G basis set which parallel those studies made of the 2-hydroxyprop-2-yl radical (Section 5.6). As the radical does not fall into the category of α-hydroxyalkyl radicals with which this chapter nominally deals, the treatment will be kept short.

In Conformer (I) all geometrical parameters were freely optimised, while in Conformer (II) the radical was constrained, within the C_s point group, to a geometry in which the O-C_{Me} bond eclipses the $2p_z$ orbital on $\dot{C}$, and in Conformer (III), again within C_s, to one in which all the atoms except for two of the methyl H lie in a plane. Selected attributes of these three conformers appear in **Table 5.6**.

Table 5.6 Attributes calculated for conformers of the methoxymethyl radical at the UHF-SCF SV-3-21G level. (Energies are in hartree, bond lengths in pm.)

		conformer		
		(I)	(II)	(III)
energies	E_{total}	-152.587657	-152.582943	-152.586309
	E_{el}	-229.052039	-228.688427	-229.102372
	E_{nuc}	76.464382	76.105484	76.516063
spin densities	$\dot{C}$	0.40933	0.36151	0.33960
	O	0.08779	0.07421	0.10249
	C_{Me}	-0.00141	0.08103	-0.00666
gross atom populations (Mulliken)	$\dot{C}$	6.07748	6.06761	6.09994
	O	8.64801	8.64641	8.64557
	C_{Me}	6.25402	6.25275	6.25369
bond lengths	$\dot{C}$-O	138.4	138.9	138.2
	O-C_{Me}	143.9	144.7	143.6

The energy of the lowest energy conformer (I) is higher than that of the isomeric hydroxyethyl radical by $\approx 33\,kJ\,mol^{-1}$ due to an increase in the internuclear repulsion term for which the associated decrease in E_{el} does not adequately compensate. This is in keeping with the well known trend in homologous sets of radicals containing first row atoms in which secondary radicals are found to be more stable than

primary. In contrast with the 2-hydroxyprop-2-yl radical, the planar conformation (III) seems quite stable, differing in energy from Conformer (I) by only 3.5 kJ mol^{-1}. The $\dot{C}$-O and O-C_{Me} bond lengths are actually shorter than in (I). The highest α-MO consists almost exclusively of p_z functions on $\dot{C}$, O, and C_{Me}, with small contributions of opposite sign from the two out-of-plane methyl protons, and has an energy of -0.316147 hartree. Evidently, then, the stability of the planar form of this radical compared to 2-hydroxyprop-2-yl can be attributed to the ability of the β-methyl group to take on π-symmetry.

5.8 Single-Point Calculations.

Single-point SCF calculations were carried out on the five hydroxyalkyl and fluorohydroxyalkyl radicals described above using basis sets of TZVP standard. The values of E_{total} thus obtained are displayed in **Table 5.7**, together with the improvement in energy engendered by the basis set change in each case.

Table 5.7

radical	E_{total}/hartree	ΔE_{total}/hartree
$H_2\dot{C}OH$	-114.459376	0.685560
$CH_3\dot{C}HOH$	-153.512326	0.912005
$(CH_3)_2\dot{C}OH$	-192.565649	1.138638
$\dot{C}HFOH$	-213.356795	1.252613
$\dot{C}F_2OH$	-312.257592	1.820435

In the case of $\dot{C}H_2OH$, the geometry at which the calculation was carried out was in fact the optimum TZVP geometry. The other single-

point calculations were carried out at geometries optimised using a split-valence 3-21G basis set. The wavefunctions obtained in these calculations were subsequently spin-projected using the UHF-AA technique[63], and the proton hyperfine coupling constants calculated from the resulting spin density difference matrices. As noted by Feller and Davidson[104], projected wavefunctions tend to lead to absolute values for hyperfine coupling constants which are smaller than those determined experimentally, and those calculated here for α-hydroxyalkyl radicals are a case in point. The ^1H coupling constants obtained for $(CH_3)_2\dot{C}OH$ are given below as an example. (Methyl couplings are averaged over all three protons.)

$$A_H^{OH} = 0.127 \text{ MHz}$$

$$A_H^{Me}(\text{cis}) = 9.25 \text{ MHz}$$

$$A_H^{Me}(\text{trans}) = 9.42 \text{ MHz}$$

For each hydroxyalkyl and fluorohydroxyalkyl radical the charge density and spin density were calculated over a grid of points determining a plane section through the nuclear framework, and plotted graphically in the form of three-dimensional contour maps (**Figure 5.8**). The plane chosen in each case was the C-O-H plane, the better to illustrate the effect of changing α-substituents upon the distribution of the unpaired spin density.

Figure 5.8 Sections through the charge density (i) and spin density (ii) distributions in the hydroxymethyl (a), hydroxyethyl (b), 2-hydroxy-prop-2-yl (c), fluorohydroxymethyl (d), and difluorohydroxymethyl (e) radicals.

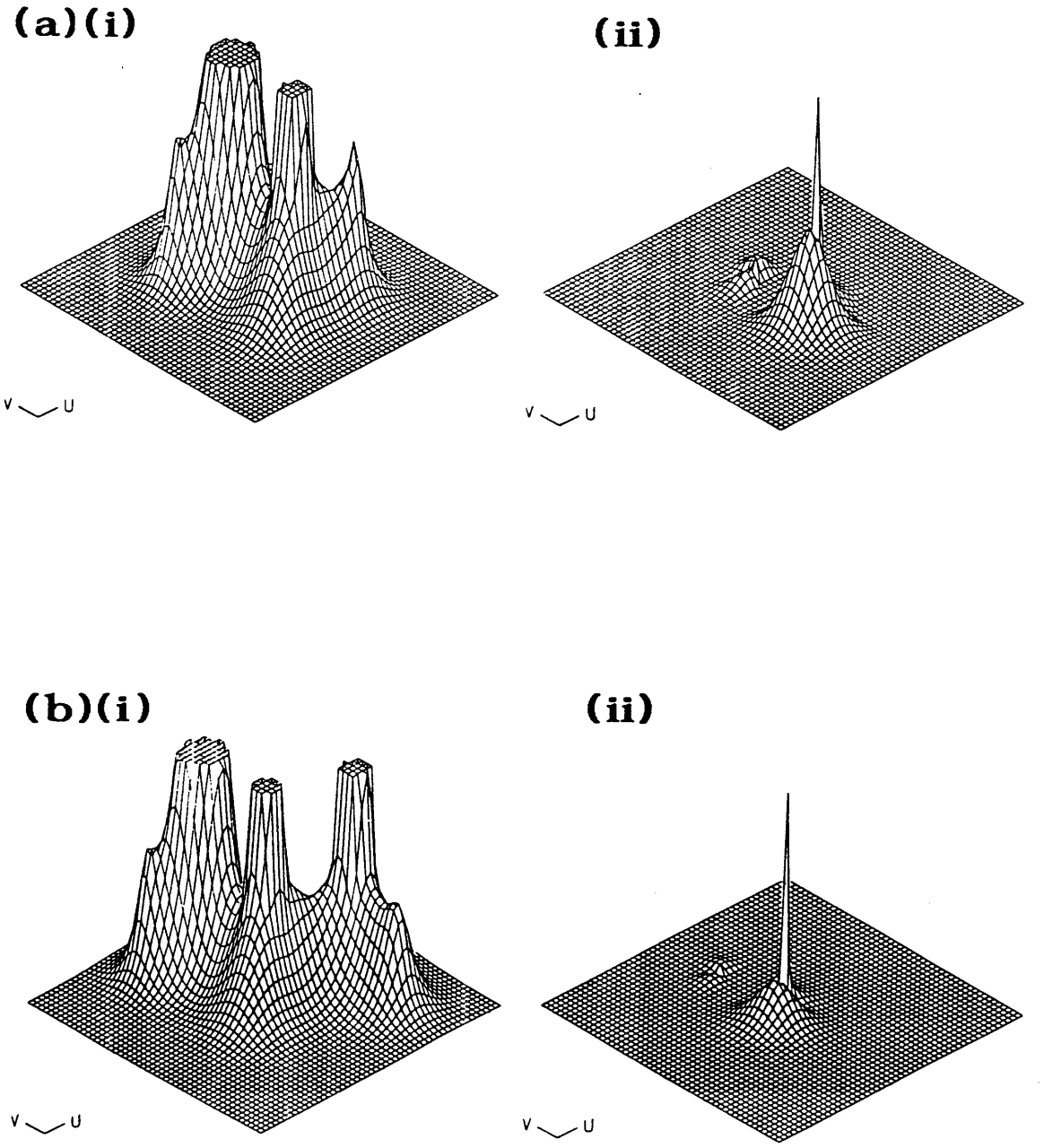

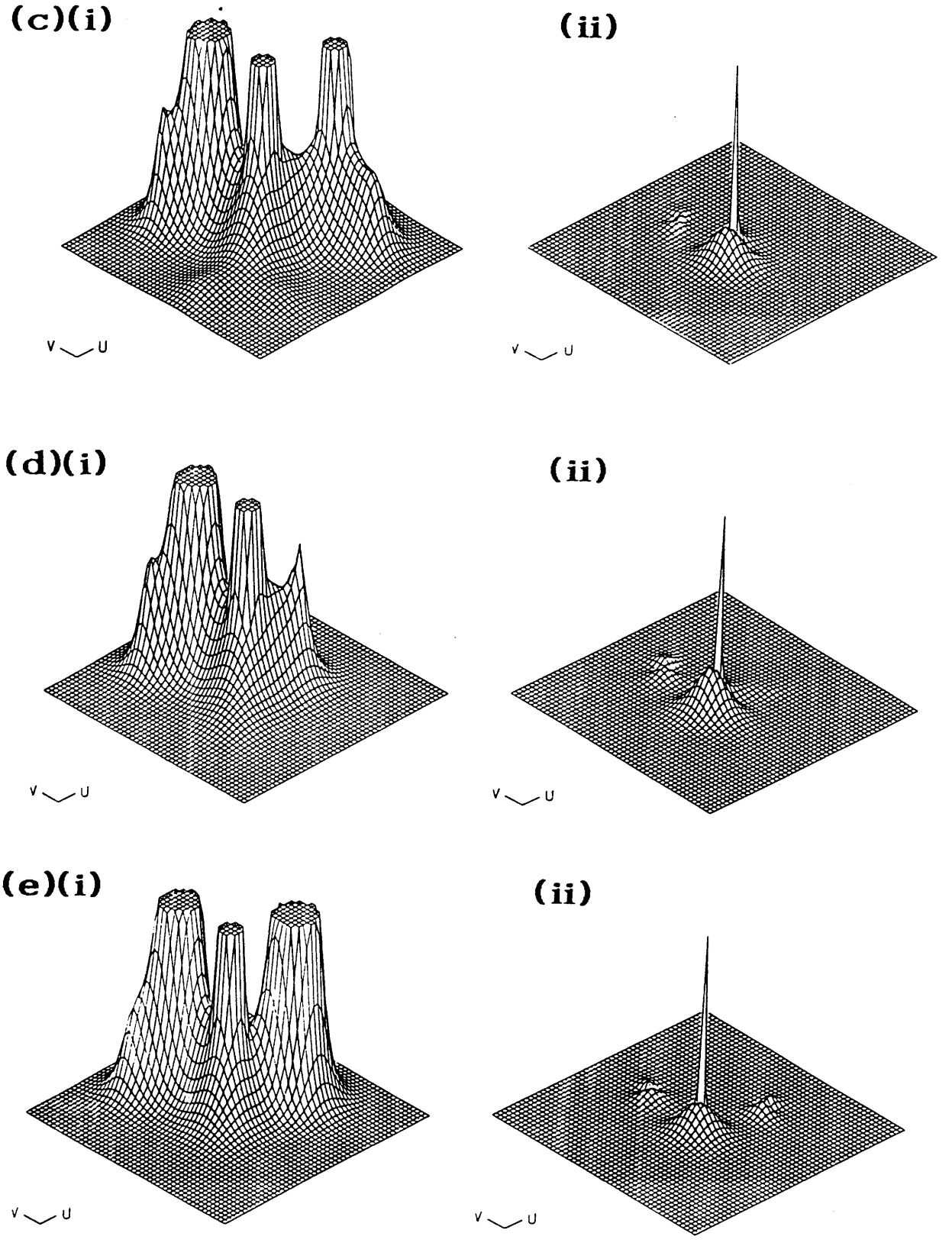
(c)(i)
(ii)
(d)(i)
(ii)
(e)(i)
(ii)

APPENDIX

Further μSR Work.

A.1 Introduction.

Other μSR studies were carried out at PSI which are less easily fitted into the body of this thesis. In addition to further work on radicals formed in unsaturated liquids, some preliminary experiments were performed on Mu created in disordered inorganic solids of catalytic importance. Brief accounts of experiments of both types are given here without detailed analysis.

A.2 Butadiene.

The catalogue of μSR data on organic free radicals which appeared in 1982[80] included results at room temperature for nine dienes comprising butadiene and associated conjugated dienes produced by single, double, or triple methyl-substitution of butadiene. A further study of these compounds was published in 1983[34] in which the stereoselectivity of muonic radical formation was discussed in the context of the Evans-Polanyi relation[153,154]. However, to date, no detailed investigation of the dependence of the measured properties upon temperature has appeared in the literature.

In butadiene the muonium atom has two possible positions of attack, as illustrated below.

(I)  (II) 

* - muonium attack
• - radical centre

These two distinct types of radical can be distinguished by the magnitudes of their coupling constants. Radical (I) is of the allyl type, which tend to show coupilng constants in the range $50 \leq A'_{\mu} \leq 65$ MHz, usually decreasing with temperature, while radical (II) is a primary alkyl radical, expected to have a coupling constant $A'_{\mu} \geq 100$ MHz. In the case of type (I) radicals distinguishable *exo* and *endo* products are possible.

Approximately 20ml of buta-1,3-diene of the highest standard supplied by Aldrich was degassed using the standard procedure and sealed into

a 35 mm diameter glass μSR bulb. With an applied transverse field of 0.2 T μSR spectra were obtained at seven temperatures within the compound's liquid range. A selection of these are shown in **Figure A.1.** At low temperatures two pairs of signals can be seen, corresponding to two distinct radicals. The first of these, which has a lower coupling constant (60-65 MHz) which decreases with increasing temperature, is assigned to the allylic radical (I), while the second, having a higher coupling constant (110-120 MHz) which again shows a decrease with increasing temperature, is assigned to the alkyl radical (II). The yield of (I) is clearly much greater. At higher temperatures (273 K, 293 K) only radical (I) is seen. The numerical values of A'_{μ} for these two radicals at the temperatures of measurement are collected in **Table A.1.**

For terminal methyl groups in allylic species proton coupling constants are in the region $33.6 \leq A_H \leq 42$ MHz and represent free internal rotation about the C-C bond. In the case of radical (I), A'_{μ} for the CH_2Mu group is seen to be about 50% greater than this in magnitude and to decrease with increasing temperature towards the free internal rotation value. ϑ_0(Mu) is thus inferred to be 0°. The planar *trans* form of butadiene is thermodynamically favoured and predominates at room temperature[155-158]. Retention of this configuration during Mu addition leatd to *exo* character in the CH_2Mu substituent. (It is possible, however, that in this relatively sterically unhindered compound configurational scrambling may lead to the observed signal being averaged over *endo* and *exo* isomers.) The direction of the temperature dependence of A'_{μ} for radical (II) again indicates the existence of a hindered internal rotation process between the groups $\dot{C}H_2$ and $CHMuCHCH_2$ for which ϑ_0(Mu) is most probably again 0°. Analysis of the temperature dependences of A'_{μ} within the theory of rotational averaging conceptually yields the barriers for these internal rotation processes, although the large size and low symmetry

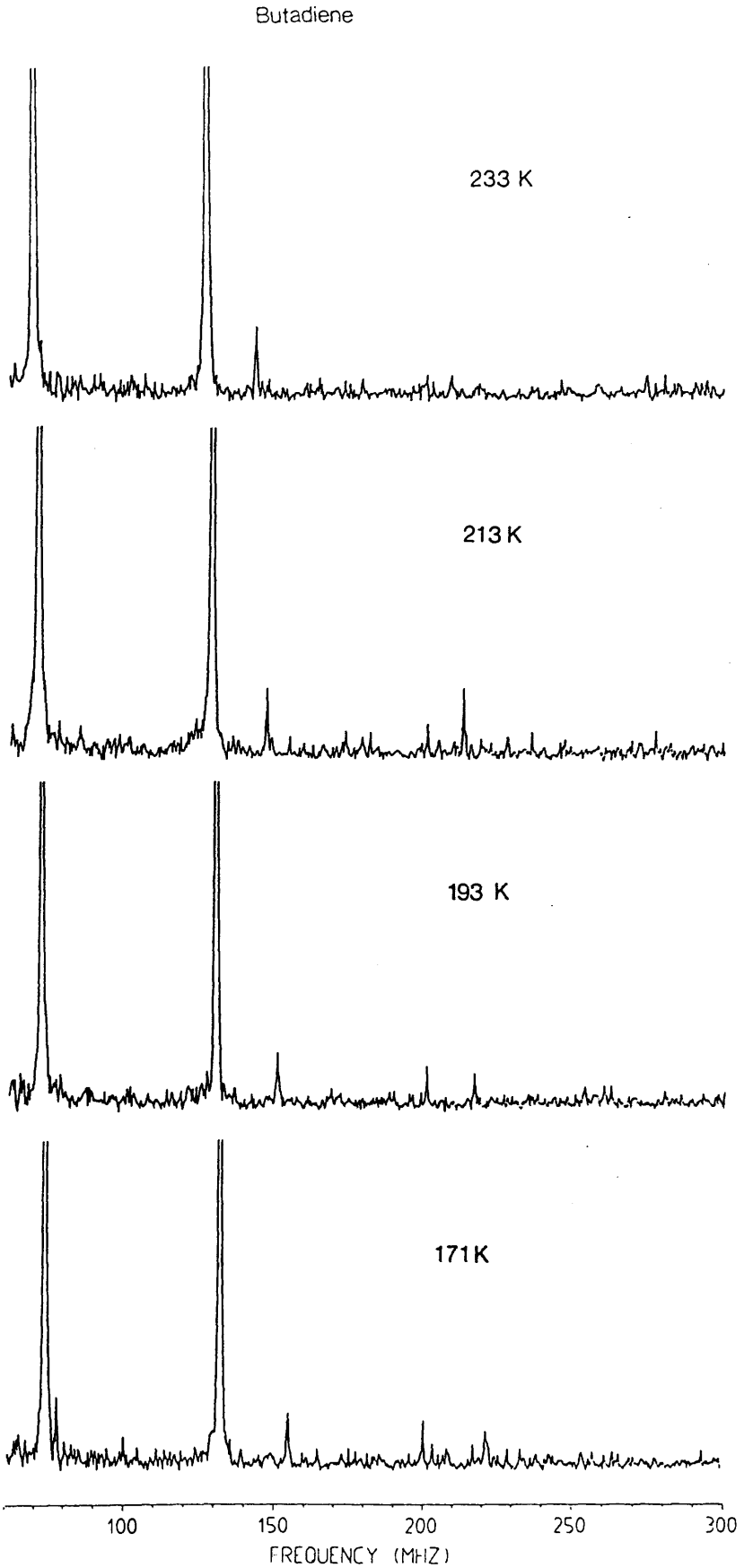

Figure A.1 Fourier transformed μSR spectra obtained in pure buta-1,3-diene.

Table A.1 Coupling constants (A'_μ in MHz) of muonic radicals formed in buta-1,3-diene. Temperatures are in K. Radical nomenclature is as in the text.

T	A'_μ	
	Radical (I)	Radical (II)
171	64.6833	118.0141
193	63.2987	115.1551
213	62.2883	112.6331
233	61.3206	110.2740
253	60.4859	108.1525
273	59.7333	——
293	59.0632	——

of these radicals mitigate against the success of this procedure. Similarly the variation with temperature of the polarisations corresponding to the radical signals (not tabulated) should be a key to the understanding of the kinetics of the radical formation reactions.

A.3 Toluene-d8.

Since the first reports of muonic cyclohexadienyl radicals $C_6H_6Mu^{\bullet}$ formed by μ^+ irradiation of liquid benzene[16,33], studies of the formation and reactions of muonic radicals in aromatic compounds have been widespread[1], ranging from kinetic studies of the reactions of muonic cyclohexadienyl radicals with oxidants[28], through investigations of "capto-dative" approaches to substituent interactions[159], to detailed examinations of isotope and substituent effects on position (*ortho*, *meta*, *para*) and rate of Mu addition[35] . Complementary semiempirical calculations have been undertaken[160] and the effect of Mu-substitution upon the methylenic coupling assessed. Recently, muon level crossing resonance (LCR or ALC) tachniques have been used to measure the ^{13}C coupling constants of muonic cyclohexadienyl radicals generated in ^{13}C-enriched benzene[161]. These coupling constants, valuable towards the understanding of the distribution of spin density across a conjugated system, are inaccessible by ESR due to the reactivity of cyclohexadienyl radicals.

Presented here without analysis are the μSR data collected using the μE4 beamline at PSI from a 20ml sample of perdeuterotoluene of high isotopic purity (Aldrich , 99.6%D), degassed and sealed by the usual method, under an applied transverse field of 0.3T at 293K. The spectrum in Fourier space, illustrated in **Figure A.2**, clearly shows the three pairs of signals corresponding to *ortho*-, *meta*-, and *para*-addition. The smaller peaks to the left of each of the two groups may correspond to *ipso*-addition, or merely to the presence of a small protium

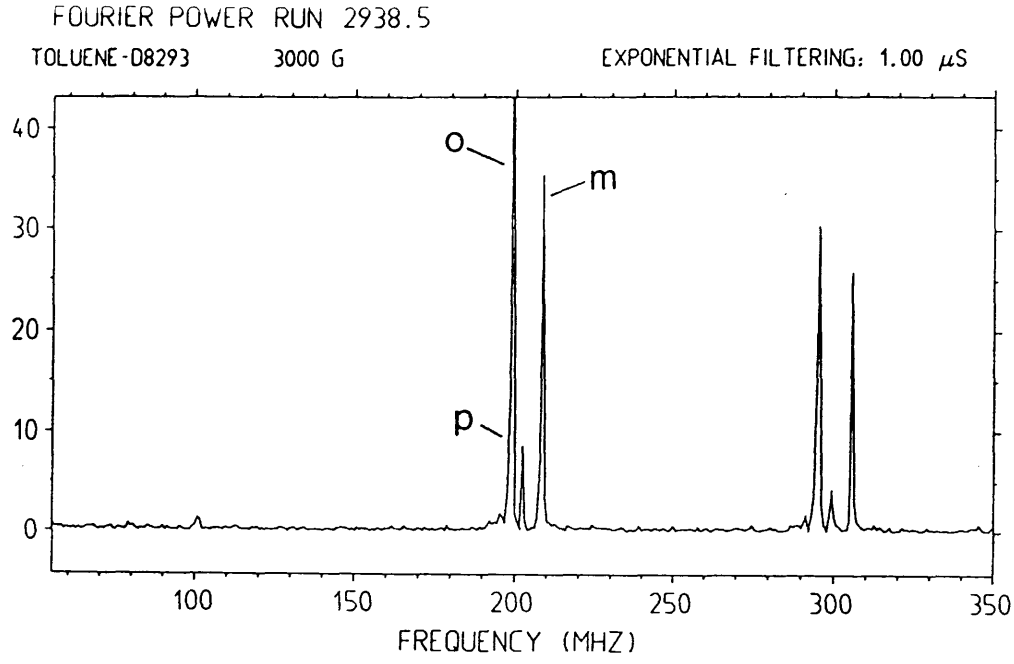

Figure A.2 Fourier transformed μSR spectrum obtained in pure perdeuterotoluene at room temperature.

impurity in the deuterated sample. The signal frequencies, their associated polarisations, and the corresponding reduced coupling constants are tabulated in **Table A.2**. Results from Roduner *et al.*[35] are presented in the last three columns for comparison and illustration of the isotope shift.

A.4 EUROPT-1.

EUROPT-1 is a platinum catalyst supported on silica. Here, the situation is somewhat different from that appertaining in the foregoing experiments. The medium is a disordered granular solid rather than a liquid, and the object of the experiment, rather than the detection of muonic radicals, is the determination of whether muonium itself forms in this substrate, and if so to assess the nature of its immediate environment — whether it is simply "free" (that is to say, effectively *in vacuo*) or bonded in some way either to the metal or the support. In this respect, muonium is essentially acting as a hydrogen atom, allowing measurements to

Table A.2 Transition frequencies (MHz), fractional polarisations and reduced coupling constants (MHz) for muonic radicals formed in per-deuterotoluene, with literature coupling constants for related compounds tabulated for comparison.

Position of Addition		Parent Molecule		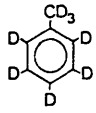			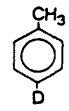
		ν	P	A'_μ	A'_μ	A'_μ	A'_μ
ortho	ν_{12}	199.01	0.0747	155.20	153.8	154.9	154.0
	ν_{43}	295.04	0.0674				
meta	ν_{12}	208.43	0.0613	161.46	160.0	160.5	160.3
	ν_{43}	305.53	0.0489				
para	ν_{12}	202.53	0.0849	157.59	155.9	155.8	157.2
	ν_{43}	299.14	0.0679				

be made which would not be possible using any other technique.

Studies at TRIUMF, Canada, using a target of Cabosil (a catalytic material consisting of high grade SiO_2) indicated formation of Mu in the extragranular voids[162]. Such enquiries led to work on the formation and dynamics of radicals of radicals in the adsorbed state by μSR[164], yielding information on reorientational correlation times and activation energies.

The results here presented, again without analysis, are somewhat preliminary in nature, but give some flavour of this new branch of muon research. The transverse field method was again used, with the standard counting technique. The sample was EUROPT-1 (Johnson-Matthey, 6.3%Pt w/w, surface area 185 $m^2 g^{-1}$ [165,166]), sealed into a glass μSR bulb. A run at low field (approximately 1 mT) showed a signal characteristic of muonium at about 19 MHz with some suggestion of splitting. This is illustrated in **Figure A.3**. In order to resolve the two signals clearly, a second run was carried out at a field of 18 mT, yielding the frequency domain spectrum shown in **Figure A.4**. The measured muonium hyperfine frequency was $\Delta = 29.81$ MHz, corresponding to $\omega_0 = 4425.2$ MHz, resembling the value for Mu in H_2O (= 4423 MHz), but strikingly different from the *in vacuo* figure (= 4463 MHz). indicating that some degree of interaction exists between Mu and some component of the catalytic system. (These initial considerations suggest the interaction to be with the oxygen atoms of the silica support.)

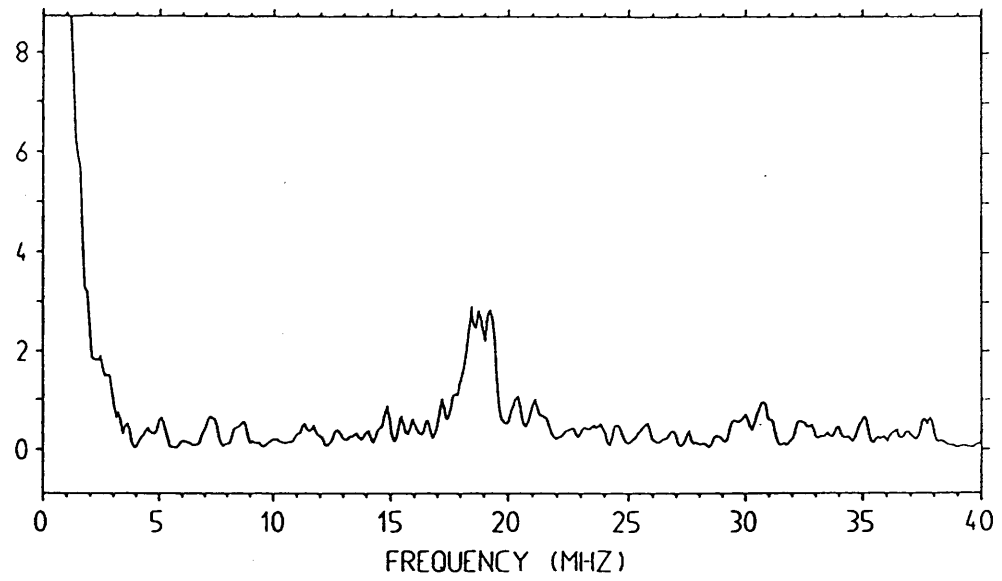

Figure A.3 Fourier transformed μSR spectrum at room temperature of the catalyst EUROPT-1, under an applied field of 1 mT.

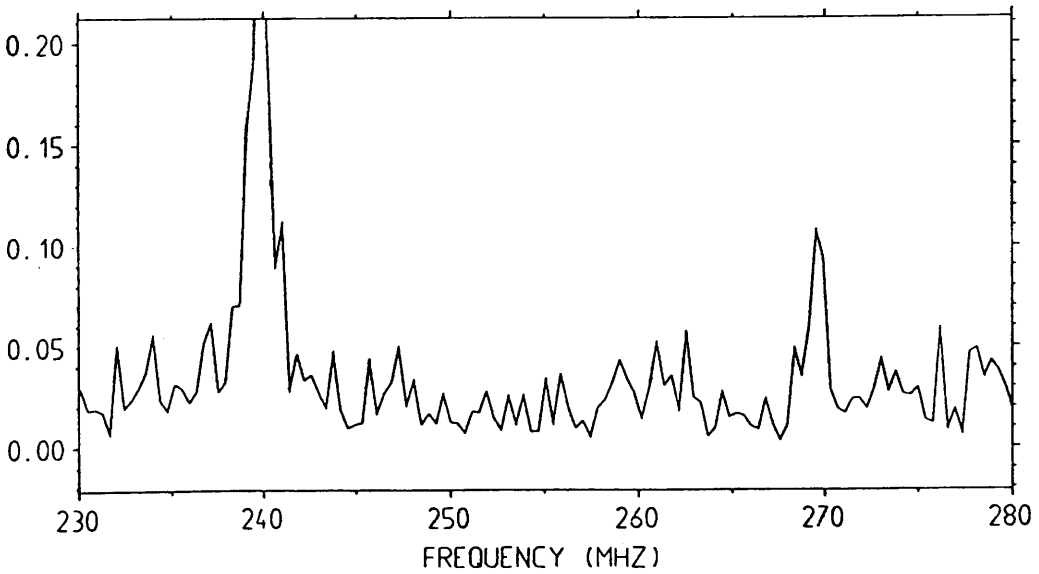

Figure A.4 Fourier transformed μSR spectrum at room temperature of the catalyst EUROPT-1, under an applied field of 18 mT.

Envoi

"My propositions serve as elucidations in the following way: anyone who understands me eventually recognises them as nonsensical, when he has used them — as steps — to climb up beyond them. (He must, so to speak, throw away the ladder after he has climbed up it.)"

Ludwig Wittgenstein

References.

1. E. Roduner, *The Positive Muon as a Probe in Free Radical Chemistry*, Springer, Heidelberg, 1988.
2. E. R. Cohen, B. N. Taylor, *J. Phys. Chem. Ref. Data*, **2**, (1973), 663.
3. M. Goldhaber, L. Grozdins, A. W. Sunyar, *Phys. Rev.*, **106**, (1957), 826.
4. A. Schenck, *Muon Spin Rotation Spectroscopy: Principles and Applications in Solid State Physics*, Adam Hilger, Bristol, 1985.
5. A. Abragam, *C. R. Acad. Sci. Paris*, c299 Série II, no. **3**, (1984), 95.
6. M. Heming, E. Roduner, B. D. Patterson, W. Odermatt, J. Schneider, H. Baumeler, H. Keller, I. M. Savić, *Chem. Phys. Letters*, **128**, (1986), 100.
7. K. Venkateswaran, R. F. Kiefl, M. V. Barnabas, J. M. Stadlbauer, B. W. Ng, Z. Wu, D. C. Walker, *Chem. Phys. Letters*, **145**, (1988), 289.
8. T. G. Eck, L. L. Foldy, H. Wieder, *Phys. Rev. Letters*, **10**, (1963), 239.
9. D. T. Edmonds, *Phys. Rept.*, **29C**, (1977), 233.
10. V. W. Hughes, C. S. Wu, (eds.), *Muon Physics*, volumes 1-3, Academic Press, New York, 1975.
11. P. W. Percival, *Radiochim. Acta*, (1979), 345ff.
12. F. James, M. Roos, *Comp. Phys. Comm.*, **10**, (1975), 343.
13. D. C. Walker, *Muon and Muonium Chemistry*, Cambridge University Press, 1983.
14. J. Chappert, R. I. Grynszpan, *Muons and Pions in Materials Research*, North-Holland, Amsterdam, 1984.
15. J. H. Brewer, D. G. Fleming, P. W. Percival, in Marshall (ed.), *Fourier, Hadamard, and Hilbert Transforms in Chemistry*, Plenum Press, New York, 1982.
16. E. Roduner, H. Fischer, *Chem. Phys.*, **54**, (1981), 261.
17. B. C. Webster, *Ann. Rept. C. Royal Soc. Chem.*, (1984), 3.
18. J. I. Friedman, V. L. Telegdi, *Phys. Rev.*, **106**, (1957), 1290.
19. P. F. Meier, in *Exotic Atoms '79*, Plenum Press, New York, p. 331.

20. J. H. Brewer, K. M. Crowe, F. N. Gygax, A. Schenck, in Ref. 10, volume 3, pp. 3-139.

21. C. J. Rhodes, M. C. R. Symons, *J. Chem. Soc. Chem. Commun.*, (1988), 3.

22. S. F. J. Cox, M. C. R. Symons, *Radiat. Phys. Chem.*, **27**, (1986), 53.

23. E. Roduner, *Radiat. Phys. Chem.*, **28**, (1986), 75.

24. R. M. Mobley, *J. Chem. Phys.*, **44**, (1966), 4354.

25. C. Bucci, G. Guidi, G. M. de'Munari, M. Manfredi, P. Podini, R. Tedeschi, P. R. Grippa, A. Vecli, *Chem. Phys. Letters*, **57**, (1978), 41.

26. E. Roduner, P. W. Percival, D. G. Fleming, J. Hochmann, H. Fischer, *Chem. Phys. Letters*, **57**, (1978), 37.

27. S. F. J. Cox, *J. Physics C: Solid State Physics*, **20**, (1987), 3187.

28. E. Roduner, *Prog. Reaction Kinetics*, **14**, (1986), 1.

29. A. Schenck, in Warren (ed.), *Nuclear and Particle Physics at Intermediate Energies*, Plenum Press, New York, 1975, p. 159.

30. P. W. Percival, H. Fischer, *Chem. Phys.*, **16**, (1976), 89.

31. E. Roduner, H. Fischer, *Chem. Phys. Letters*, **65**, (1979), 582.

32. L. D. Landau, E. M. Lifshitz, *Quantum Mechanics*, Pergamon Press, Oxford, 1965.

33. E. Roduner, Doctoral Thesis, Zürich, 1979.

34. E. Roduner, B. C. Webster, *J. Chem. Soc. Faraday Trans. 1*, **79**, (1983), 1939.

35. E. Roduner, G. A. Brinkman, P. W. F. Louwrier, *Chem. Phys.*, **73**, (1982), 117.

36. P. W. Percival, E. Roduner, H. Fischer, *Chem. Phys.*, **32**, (1978), 353.

37. Y. Ito, B. W. Ng, Y. Jean, D. C. Walker, *Can. J. Chem.*, **58**, (1980), 2395.

38. P. W. Percival, *Hyperfine Interactions*, **8**, (1981), 315.

39. P. W. Percival, J. C. Brodovitch, K. E. Newman, *Chem. Phys. Letters*, **91**, (1982), 1.

40. S. F. J. Cox, A. Hill, R. de Renzi, *J. Chem. Soc. Faraday Trans. 1*, **78**, (1982), 2975.

41. K. Venkateswaran, M. V. Barnabas, Z. Wu, J. M. Stadlbauer, B. W. Ng, D. C. Walker, *Chem. Phys.*, **137**, (1989), 239.

42. G. Breit, I. I. Rabi, *Phys. Rev.*, **38**, (1931), 2082.

43. M. Born, J. R. Oppenheimer, *Ann. Phys.*, **84**, (1927), 457.

44. S. Califano, *Vibrational States*, Wiley-Interscience, London, 1976.

45. E. B. Wilson, Jr., J. C. Decius, P. C. Cross, *Molecular Vibrations*, McGraw-Hill, New York, 1955.

46. C. Heller, H. M. McConnell, *J. Chem. Phys.*, **32**, (1960), 1535.

47. R. W. Fessenden, *J. Chim. Phys.*, **61**, (1964), 1570.

48. P. J. Krusic, P. Meakin, J. P. Jesson, *J. Phys. Chem.*, **75**, (1971), 3438.

49. J. K. Kochi, *Advances in Free Radical Chemistry*, **5**, (1975), 189.

50. P. D. Sullivan, E. M. Menger, *Adv. Magn. Reson.*, **9**, (1977), 1.

51. D. G. Lister, J. N. MacDonald, N. L. Owen, *Internal Rotation and Inversion - An Introduction to Large Amplitude Motions in Molecules*, Academic Press, London, 1978.

52. W. H. Flygare, *Molecular Structure and Dynamics*, Prentice-Hall, Englewood Cliffs, NJ, 1978.

53. H. Primas, *Chemistry, Quantum Mechanics, and Reductionism*, Springer, Berlin, 1983.

54. R. G. Wooley, (ed.), *Quantum Dynamics of Molecules*, Plenum Press, New York, 1980.

55. D. McKenna, B. C. Webster, *J. Chem. Soc. Faraday Trans. 2*, **80**, (1984), 589.

56. E. U. Condon, E. Shortley, *The Theory of Atomic Spectra*, Cambridge University Press, 1935.

57. C. Møller, M. S. Plesset, *Phys. Rev.*, **46**, (1934), 618.

58. J. Cizek, *J. Chem. Phys.*, **45**, (1966), 4256.

59. E. M. Evleth, H. Z. Cao, E. Kassab, A. Sevin, *Chem. Phys. Letters*, **109**, (1984), 45.

60. J. S. Binkley, J. A. Pople, W. J. Hehre, *J. Amer. Chem. Soc.*, **102**, (1980), 939.

61. T. H. Dunning, *J. Chem. Phys.*, **55**, (1971), 716.

62. A. T. Amos, G. G. Hall, *Proc. Roy. Soc. A*, **263**, (1961), 483.

63. A. T. Amos, L. C. Snyder, *J. Chem. Phys.*, **41**, (1964), 1773.

64. P. H. Phillips, J. C. Schug, *J. Chem. Phys.*, **61**, (1974), 1031.

65. J. E. Harriman, *J. Chem. Phys.*, **40**, (1964), 2827.

66. C. E. Dykstra, *Ab Initio Calculation of the Structures and Properties of Molecules*, Elsevier, Amsterdam, 1988.

67. R. McWeeny, *Methods of Molecular Quantum Mechanics*, 2ed., Academic Press, London, 1989.

68. S.-I. Mizushima, *Structure of Molecules and Internal Rotation*, Academic Press, New York, 1954.

69. B. Smaller, M. S. Matheson, *J. Chem. Phys.*, **28**, (1958), 1169.

70. R. W. Fessenden, R. H. Schuler, *J. Chem. Phys.*, **39**, (1963), 2147.

71. J. K. Kochi, P. J. Krusic, *J. Amer. Chem. Soc.*, **91**, (1969), 3940.

72. C. A. McDowell, P. Raghunathan, K. Shimohoshi, *J. Chem. Phys.*, **58**, (1973), 114.

73. J. Pacansky, M. Dupuis, *J. Chem. Phys.*, **68**, (1978), 4276.

74. D. M. Chipman, *J. Chem. Phys.*, **71**, (1979), 761.

75. J. Pacansky, H. Coufal, *J. Chem. Phys.*, **72**, (1980), 5285.

76. D. C. McKean, J. E. Boggs, L. Schäfer, *J. Mol. Struct.*, **116**, (1984), 313.

77. D. McKenna, Doctoral Thesis, Glasgow, 1983.

78. M. J. Ramos, D. McKenna, B. C. Webster, E. Roduner, *J. Chem. Soc. Faraday Trans. 1*, **80**, (1984), 255.

79. A. M. Brodskii, *Sov. Phys. JETP*, **17**, (1963), 1085.

80. E. Roduner, W. Strub, J. Hochmann, P. Burkhard, P. W. Percival, H. Fischer, M. J. Ramos, B. C. Webster, *Chem. Phys.*, **67**, (1982), 275.

81. M. J. Ramos, Doctoral Thesis, Glasgow, 1983.

82. M. J. Ramos, D. McKenna, B. C. Webster, E. Roduner, *J. Chem. Soc. Faraday Trans. 1*, **80**, (1984), 267.

83. B. C. Webster, M. J. Ramos, E. Roduner, *Proc. 5th Symp. on Radiation Chem.*, Akadémiai Kiadó, Budapest, 1982.

84. J. A. Nelder, R. Mead, *Computer J.*, **7**, (1965), 308.

85. S. F. J. Cox, T. A. Claxton, M. C. R. Symons, *Radiat. Phys. Chem.*, **28**, (1986), 107.

86. T. A. Claxton, A. M. Graham, *J. Chem. Soc. Faraday Trans. 2*, **83**, (1987), 2307.

87. T. A. Claxton, A. M. Graham, *J. Chem. Soc. Chem. Commun.*, (1987), 1167.

88. D. Buttar, Thesis, Glasgow, 1988.

89. L. S. Bartell, *J. Amer. Chem. Soc.*, **83**, (1961), 3567.

90. J. Pacansky, M. Dupuis, *J. Amer. Chem. Soc.*, **104**, (1982), 415.

91. T. A. Claxton, A. M. Graham, M. C. R. Symons, *Chem. Phys. Letters*, **138**, (1987), 610.

92. S. F. J. Cox, personal communication.

93. R. S. Mulliken, C. A. Rieke, W. G. Brown, *J. Amer. Chem. Soc.*, **63**, (1941), 41.

94. J. W. Baker, W. S. Nathan, *J. Chem. Soc.*, (1935), 1844.

95. V. J. Shiner, E. Campaigne (co-chairmen), *Tetrahedron*, **5**, (1959), 107-274.

96. F. W. King, *Chemical Reviews*, **76**, (1976), 157.

97. A. Carrington, A. D. McLachlan, *Introduction to Magnetic Resonance with Applications to Chemistry and Chemical Physics*, Chapman and Hall, London, 1979.

98. D. E. Sunko, I. Szele, W. J. Hehre, *J. Amer. Chem. Soc.*, **99**, (1977), 5000.

99. D. J. DeFrees, W. J. Hehre, D. E. Sunko, *J. Amer. Chem. Soc.*, **101**, (1979), 2323.

100. M. Wolfsberg, L. Helmholz, *J. Chem. Phys.*, **20**, (1952), 837.

101. S. Huzinaga, *J. Chem. Phys.*, **42**, (1965), 1293.

102. T. H. Dunning, *J. Chem. Phys.*, **55**, (1971), 3958.

103. D. M. Chipman, *J. Chem. Phys.*, **78**, (1983), 4785.

104. D. Feller, E. R. Davidson, *Theor. Chim. Acta*, **68**, (1985), 57.

105. R. A. Poirier, R. Daudel, I. G. Csizmadia, *Int. J. Quantum Chem.*, **18**, (1980), 727.

106. E. Magnusson, *Australian J. Chem.*, **39**, (1986), 747.

107. A. C. Hopkinson, M. H. Lien, *Int. J. Quantum Chem.*, **13**, (1978), 349.

108. T. K. Brunck, F. Weinhold, *J. Amer. Chem. Soc.*, **101**, (1979), 1700.

109. A. Gavezzotti, L. S. Bartell, *J. Amer. Chem. Soc.*, **101**, (1979), 5142.

110. K. Venkateswaran, S. F. J. Cox, *Chem. Phys. Letters*, in press.

111. J. F. Gibson, D. J. E. Ingram, M. C. R. Symons, M. G. Townsend, *Trans. Faraday Soc.*, **53**, (1957), 914.

112. M. Fujimoto, D. J. E. Ingram, *Trans. Faraday Soc.*, **54**, (1958), 1304.

113. W. T. Dixon, R. O. C. Norman, *J. Chem. Soc.*, (1963), 3119.

114. H. Zeldes, R. Livingston, *J. Chem. Phys.*, **30**, (1959), 40.

115. R. Livingston, H. Zeldes, *J. Chem. Phys.*, **44**, (1966), 1245.

116. H. Fischer, *Z. Naturforsch.*, **20a**, (1965), 488.

117. H. Zeldes, R. Livingston, *J. Chem. Phys.*, **45**, (1966), 1245.

118. G. Cirelli, T.-K. Ha, R. Meyer, Hs. H. Günthard, *Chem. Phys.*, **72**, (1982), 15.

119. M. Lehni, Doctoral Thesis, Zürich, 1983.

120. P. J. Krusic, P. Meakin, *J. Amer. Chem. Soc.*, **98**, (1976), 228.

121. A. Hill, S. F. J. Cox, R. de Renzi, C. Bucci, A. Vecli, M. C. R. Symons, *Hyperfine Interactions*, **17-19**, (1984), 815.

122. A. Hill, M. C. R. Symons, S. F. J. Cox, R. de Renzi, C. A. Scott, C. Bucci, A. Vecli, *J. Chem. Soc. Faraday Trans. 1*, **81**, (1985), 433.

123. S. F. J. Cox, D. A. Geeson, C. J. Rhodes, E. Roduner, C. A. Scott, M. C. R. Symons, *Hyperfine Interactions*, **32**, (1986), 763.

124. E. Roduner, personal communication.

125. J. E. Wertz, J. R. Bolton, *Electron Spin Resonance, Elementary Theory and Practical Application*, McGraw-Hill, New York, 1972.

126. H. Paul, *Chem. Phys. Letters*, **32**, (1975), 472.

127. P. W. Percival, E. Roduner, H. Fischer, *Advances in Chemistry Series*, **175**, (1979), 335.

128. E. J. Hart, in *Actions Chimiques et Biologiques des Radiations*, Ed. Masson et Cie., Paris, 1966.

129. E. Roduner, *Faraday Discuss. Chem. Soc.*, **78**, (1984), 340.

130. K. Venkateswaran, M. V. Barnabas, Z. Wu, J. M. Stadlbauer, B. W. Ng, D. C. Walker, *Chem. Phys. Letters*, **143**, (1988), 313.

131. R. A. Witter, P. Neta, *J. Org. Chem.*, **38**, (1973), 484.

132. D. Buttar, personal communication.

133. E. Roduner, I. D. Reid, *Israel J. Chem.*, **29**, (1989), 102.

134. L. E. Sutton, *Tables of Interatomic Distances and Configurations in Molecules and Ions*, Special Publication no.11, The Chemical Society, London, 1958.

135. W. Strub, E. Roduner, H. Fischer, *J. Phys. Chem.*, **91**, (1987), 4379.

136. I. D. Reid, personal communication.

137. M. F. Guest, J. Kendrick, *An Introductory Guide to GAMESS*, UMRCC, Manchester, 1986.

138. D. Moncrieff, V. R. Saunders, *ATMOL Manual*, UMRCC, Manchester, 1986.

139. A. D. McLean, G. S. Chandler, *J. Chem. Phys.*, **72**, (1980), 5639.

140. R. Ahlrichs, P. R. Taylor, *J. Chem. Phys.*, **78**, (1981), 315.

141. J. Heicklen, *Atmospheric Chemistry*, Academic Press, New York, 1976.

142. A. C. Aikin, J. R. Herman, E. J. Maier, *Proc. NATO ASI on Atmospheric Ozone*, (1979), 191.

143. S. Saebø, L. Radom, H. F. Schaefer III, *J. Chem. Phys.*, **78**, (1983), 845.

144. D. Solgadi, J.- P. Flament, *Chem. Phys.*, **98**, (1985), 387.

145. E. Kean, Thesis, Glasgow, 1987.

146. R. S. Mulliken, *J. Chem. Phys.*, **23**, (1955), 1833.

147. R. S. Mulliken, *J. Chem. Phys.*, **23**, (1955), 1841.

148. R. S. Mulliken, *J. Chem. Phys.*, **36**, (1962), 3428.

149. I. Carmichael, *J. Phys. Chem.*, **89**, (1985), 4727.

150. I. Carmichael, *Chem. Phys.*, **116**, (1987), 351.

151. M. H. Lien, A. C. Hopkinson, *J. Comput. Chem.*, **6**, (1985), 274.

152. I. G. Csizmadia, *Theory and Practice of MO Calculations on Organic Molecules*, Elsevier, Amsterdam, 1976.

153. M. G. Evans, M. Polanyi, *Trans. Faraday Soc.*, **32**, (1936), 1333.

154. M. G. Evans, M. Polanyi, *Trans. Faraday Soc.*, **34**, (1938), 22.

155. E. L. Eliel, *Stereochemistry of Carbon Compounds*, McGraw-Hill, New York, 1962.

156. W. F. Forbes, R. Shilton, A. Balasubramanian, *J. Org. Chem.*, **29**, (1964), 3527.

157. H. Dodziuk, *J. Mol. Struct.*, **14**, (1972), 343.

158. H. Dodziuk, *J. Mol. Struct.*, **20**, (1974), 317.

159. C. J. Rhodes, E. Roduner, *Tet. Letters*, **29**, (1988), 1437.

160. E. Roduner, M. J. Ramos, personal communication.

161. R. F. Kiefl, S. Kreitzmann, R. Keitel, G. M. Luke, J. H. Brewer, D. R. Noakes, P. W. Percival, T. Matsuzaki, K. Nishiyama, *Phys. Rev. A*, **34**, (1986), 681.

162. G. M. Marshall, J. B. Warren, D. M. Garner, G. S. Clark, J. H. Brewer, D. G. Fleming, *Phys. Rev. A*, **65**, (1978), 351.

163. R. F. Kiefl, J. B. Warren, C. J. Oram, G. M. Marshall, J. H. Brewer, D. R. Harshman, *Phys. Rev. B*, **26**, (1982), 2432.

164. M. Heming, E. Roduner, *Surface Science*, **189/190**, (1989), 535.

165. G. C. Bond, P. B. Wells, *Applied Catalysis*, **18**, (1985), 225.

166. J. W. Geus, P. B. Wells, *Applied Catalysis*, **18**, (1985), 231.

PUBLICATIONS

(1) On the interpretation of muon spin rotation and level crossing resonance observations on the muonic ethyl radical.

B.C. Webster and R.Macrae, Chemical Physics Letters **150** (1988) 18.

(2) Muonium-substituted organic free radicals produced in carbonyl compounds in the liquid phase.

R.M. Macrae, B.C. Webster and E. Roduner, Muon Studies in Solid State Physics, IOP Short Meetings Series No 22, 95.

(3) Competitive muonium addition to 3-methylbut-2-enal.

D. Buttar, R.M. Macrae, B.C. Webster and E. Roduner, Journal of the Chemical Society Faraday Transactions, **86**, (1990), 220.